Beathe Sitter

Tissue characterization by high resolution magic angle spinning MR spectroscopy

Trondheim, January 2004

Doctoral thesis for the degree of doctor philosophiae

Norwegian University of Science and Technology
Faculty of Medicine
Department of Neuroscience

NTNU

URN:NBN:no-3463

Tissue characterization by high resolution magic angle spinning MR spectroscopy

by

Beathe Sitter

Thesis submitted for the partial fulfillment of the degree of
Dr. Philos.

Department of Neuroscience
Faculty of Medicine
The Norwegian University of Science and Technology
Trondheim

Trondheim January 2004

URN:NBN:no-3463

Preface and Acknowledgments

The work presented in this thesis has been carried out at the MR Center in Trondheim in the period January 2000 to December 2003. Grant was provided by the Norwegian research council through the SINTEF Unimed strategic institute program (SIP) "MR technology in cancer diagnosis". In this period, I also received a scholarship for two months of salary from "Wenche Johansens minnefond", administered by Namsos Kommune (Namsos Township).

Help and support have been provided me in many ways from many persons. I am especially grateful to the breast and cervical cancer patients in Norway and families of NCL patients in Finland who agreed to contribute to the research projects. Thank you! This thesis depended on your efforts.

In particular I want to thank my supervisors, Senior Researcher Ingrid S. Gribbestad and Professor Ursula Sonnewald for all their support. This project came to life because of Ingrid S. Gribbestad and her ideas and visions. Your unique enthusiasm and your ability to see results when I see failure are most impressive. Ursula Sonnewald has been a major support in the periods of writing. Just thinking of you Ursula makes me hear you say: "how is the writing going?". I sincerely appreciated all help!

I am also very grateful to Dr. Hans Fjøsne, who has coordinated all biopsy excisions from breast cancer patients, and the rest of the staff at the Department of Surgery who has been involved in this project the last years. Dr. Steinar Lundgren at the Cancer Department has been in charge of finding clinical data from patient journals. Both Hans and Steinar have patiently answered all my questions about any topic related to cancer. Dr. Jostein Halgunset at Dept. of Histology, NTNU has performed the histopathological evaluation of all breast cancer samples, and Engineer Eli Johannesen has prepared the biopsy material for microscopy. Your contributions were crucial for this thesis. Thank you!

Dr. Tone Bathen has performed many of the multivariate analysis, and is a very supportive friend and colleague. Engineer Trond E. Singstad has provided brilliant technical support. Your good mood makes it easy to ask for your help Trond. Engineer Tina Bugge Pedersen has helped me with the storing of samples in liquid nitrogen, and is an important provider of order in the lab. Dr. David Axelson performed the multivariate analysis in the study on extracts from breast cancer tissue, and has always helped me out when I struggled with different topics in multivariate analysis. Thank you all for making my work easier and for providing a cheerful and positive working environment.

Dr. Manfred Spraul in Bruker Biospin, Germany gave valuable and much appreciated help in the initial phase when MAS was first applied in our lab. Dr. Anna Maija Häkkinen and her group at HCUH in Helsinki, Finland provided *in vivo* results and autopsy material for the NCL study as well as essential contributions throughout the project. Thank you for a fulfilling cooperation. Dr. Bjørn Hagen at institute of laboratory medicine, children and womens disease, NTNU recruited patients and collected tissue samples for the cervical

cancer project, whereas Dr. Finn Egil Skjeldestad at section of epidemiological research, SINTEF Unimed was one of the initiators of the project. Both have patiently contributed at all stages of this project, which I sincerely appreciated. I would also thank Cecilie Arentz for her contribution and good company during many long hours in the MR lab during the cervical cancer project.

I also want to thank my colleagues at the MR Center during these years, for creating an atmosphere I like and appreciate. A warm thanks to my friends and family who always are there for me, giving me the best of reasons for not being at work. And last, but not least, I want to thank Øyvind for his support and patience.

Preface and Acknowledgments 1

Abbreviations 4

1. List of papers 5

2. Background 6

2.1 Cancer 6

2.2 Breast cancer 6

2.3 Cervical cancer 7

2.4 Neuronal ceroid lipofuscinoses 7

2.5 Metabolism in human cells 8
Metabolism of tumors 10
Neurochemistry 11

2.6 MR spectroscopy 12

2.7 High-resolution magic angle spinning (HR MAS) 12

2.8 Spectral analysis 14

3. Objectives 15

4. Summary of papers 16

5. Discussion 19

5.1 Establishing a HR MAS protocol 19

5.2 MAS spectra of intact tissue compared to spectra of extracts 23

5.3 Chemical profiles connected to biological processes 24

5.4 HR MAS spectral profiles compared to clinical parameters 27

6. Conclusion 30

7. References 31

Paper I - V

Abbreviations

ADP	adenosine diphosphate
ATP	adenosine triphosphate
CIN	cervical intraepithelial neoplasia
CLN1	infantile neuronal ceroid lipofuscinosis
CLN3	juvenile neuronal ceroid lipofuscinosis
CNS	central nervous system
CDP	cytidine diphosphate
Cho	choline
CoA	coenzyme A
Cr	creatine
1,2 DAG	1,2-diacylglycerol
FAD	flavine adenine dinucleotide
$FADH_2$	flavine adenine dinucleotide (reduced form)
G-3-P	glycerol-3-phosphate
GABA	gamma-aminobutyric acid
GMP	guanosine monophosphate
GPC	glycerophosphocholine
Glc	glucose
HPV	human papillomavirus
HR	high-resolution
Lac	lactate
MAS	magic angle spinning
MR	magnetic resonance
MRI	magnetic resonance imaging
MRS	magnetic resonance spectroscopy
NAA	*N*-acetyl-L-aspartate
NAD	nicotinamide adenine dinucleotide
NADH	nicotinamide adenine dinucleotide (reduced form)
NCL	neuronal ceroid lipofuscinosis
m-Ino	*myo*-inositol
PA	phosphatic acid
PC	phosphocholine
PCA	principal component analysis
PE	phsphoethanolamine
PNN	probabilistic neural networks
ppm	parts per million
PtdCho	phosphatidylcholine
S/N	signal to noise
s-Ino	*scyllo*-inositol
Tau	taurine
TCA	tricarboxylic acid
TMAO	trimethylamine *N*-oxide

1. List of papers

I Gribbestad IS, Sitter B, Lundgren S, Krane J, Axelson D. *Metabolite composition in breast tumors examined by proton nuclear magnetic resonance spectroscopy*. Anticancer Research (1999) **19**: 1737-1746.

II Sitter B, Sonnewald U, Spraul M, Fjösne HE, Gribbestad IS. *High-resolution magic angle spinning MRS of breast cancer tissue*. NMR in Biomedicine (2002) **15**: 327 – 338.

III Sitter B, Lundgren S, Bathen TF, Halgunset J, Fjosne HE, Gribbestad IS. *Comparison of HR MAS MR spectroscopic profiles of breast cancer tissue to clinical parameters*. Submitted to NMR in Biomedicine.

IV Sitter B, Bathen T, Hagen B, Arentz C, Skjeldestad FE and Gribbestad IS. *Cervical cancer tissue characterized by high-resolution magic angle spinning MR spectroscopy*. MAGMA, in press.

V Sitter B, Autti T, Tyynelä J, Sonnewald U, Bathen TF, Puranen J, Santavuori P, Haltia MJ, Paetau A, Polvikoski T, Gribbestad IS, Häkkinen A-M. *HR MAS ^{1}H MR spectroscopy reveal significantly altered neuronal metabolite profiles in CLN1 but not in CLN3*. Accepted for publication in Journal of Neuroscience Research.

2. Background

2.1 Cancer

Cancer is an increasing cause of death globally. More than ten million people are diagnosed with cancer worldwide and more than six million die from the disease each year (1). The forms of cancer with the highest incidence are lung, breast and colon, while highest mortality is associated with cancer of the lungs, stomach and liver (2). Cancer is a term covering more than 100 different diseases that vary in age of onset, invasiveness, metastatic potential, response to treatment and prognosis (3, 4). Although tumors are different in site and origin, malignancies have some common features. They all affect the body's basic unit, the cell, and occur when cells become abnormal and divide without control or order. Cancer cells are less differentiated than their normal counterparts. They have the ability to invade and destroy adjacent normal tissue and to metastasize through lymphatic channels or the blood. Cell proliferation is usually elevated in a tumor compared to normal tissue, and tumors tend to grow despite starvation of the host. Tumor cells can replicate an infinite number of times and evade apoptosis (programmed cell death) (5).

The principles of therapy are surgery, chemotherapy and radiotherapy, often in combination. A patient treatment plan is determined by an increasing amount of markers, where tumor size and metastatic potential are the most fundamental (2).

2.2 Breast cancer

Breast cancer is the most common type of cancer affecting women, with more than one million new cases globally each year (1). In Norway, more than 2500 women are diagnosed with breast cancer and about 800 die from the disease every year (6). Early detection is important for successful treatment, and screening programs have been effected in most western countries (2). The incidence is increasing, but mortality rates are declining in developed countries. The enhanced perspectives for breast cancer patients have been attributed to improvements in breast cancer diagnosis and treatment.

The majority of breast cancers originate from the ducts, and 70-80% of breast cancer patients are diagnosed with invasive ductal carcinoma (7). Other common types of breast cancer are invasive lobular carcinomas, medullary carcinomas, colloid carcinomas and tubular carcinomas. Non-invasive cancers of the ducts or lobules are called ductal and lobular carcinomas in situ (DCIS and LCIS). About one third of the women with in situ cancers will develop invasive cancers if untreated.

The strongest prognostic factor for breast cancer patients is their axillary lymph node status (8). About one third of the breast cancer patients die because of metastasis (9). The most common sites of secondary tumors in breast cancer patients are bone, lung, liver and brain (10). A patient treatment plan is based upon the patients age, axillary lymph node status, steroid receptor status, tumor size and histologic grade (11). Conservative local

surgery has proven equally effective as mastectomy in prolonging survival (10). Sentinel lymph node biopsy has led to reduced morbidity in selected patients compared to axillary lymph node resection. Adjuvant systemic treatment as chemotherapy and/or hormone therapy has led to prolonged lives for patients with early detected breast cancer.

2.3 Cervical cancer

Screening for cervical cancer by smear test has contributed to a decline in incidence and mortality over the last 50 years in western countries (2). The incidence of cervical cancer in Norway has been decreasing over the last 30 years. In 2000, close to 300 women were diagnosed with cervical cancer in Norway, and 99 died from the disease (6). In less developed countries however, screening has often not been established and cervical cancer is the most frequent form of cancer in many developing countries (2).

The most common type of cervical cancer by far is squamous cell carcinoma, representing 75-90% of all cases (7, 12). Squamous cell carcinomas generally evolve from precursor cervical intraepithelial neoplasia (CIN) (7). Adenocarcinomas, arising from mucus producing glands in the cervix, and variants of adenocarcinomas are the other types of cervical cancers. Human papillomaviruses (HPV) are responsible for the majority of malignancies in the cervix (13). More than 100 types of HPV have been identified, of which 13 are considered oncogenic and infect the genital tract (14). Other coexisting risk factor are smoking, nutrition, number of live births and long-term use of oral contraceptives.

The choice of treatment for cervical cancer depends on the location and size of the tumor, the stage (extent) of the disease, the woman's age and general health, and other factors (14). Most often, treatment for cervical cancer involves surgery and radiation therapy (2).

2.4 Neuronal ceroid lipofuscinoses

Neuronal ceroid lipofuscinoses (NCL) comprise a group of progressive neurological diseases of childhood. All forms of the disease are recessively inherited and characterized by lysosomal storage of autofluorescent lipopigments in several types of tissues, in particular in neurons of the central nervous system (CNS) (15). Storing of lipopigments is possibly caused by an enzyme deficiency (16). Progressive neurodegeneration is also characteristic for NCLs, in particular loss of neurons in the frontal cortex in the infantile forms (15). It is not known if the lipopigment storage causes the neuronal death (16).

The first sign of the disease is often loss of vision (17). Over time, affected children suffer mental impairment, worsening seizures, and progressive loss of sight and motor skills. Eventually, children become blind, bedridden, and unable to communicate. Treatment is focused on reducing seizures and other symptoms. All forms are fatal.

The forms of NCL are classified by age of onset, and eight underlying genes (CLN1 – CLN8) have been defined (18). Infantile NCL (CLN1, INCL or Santavuori disease) is a

rapidly progressing form. Onset is typically before two years of age, with extreme brain atrophy and a life expectancy of 9-11 years (19). Juvenile NCL (CLN3, JNCL or Battens disease) onsets before eight years of age, is associated with moderate brain atrophy and a life expectancy of 25-35 years (19).

2.5 Metabolism in human cells

All cells are concerned with synthesis of macromolecules needed for cell structure and function and energy requirements for biosynthesis, active transport over the cell membrane and some have specialized functions (3). Although most cells contain the enzymes needed for the various metabolic pathways, the level of expression is differently regulated in different tissues.

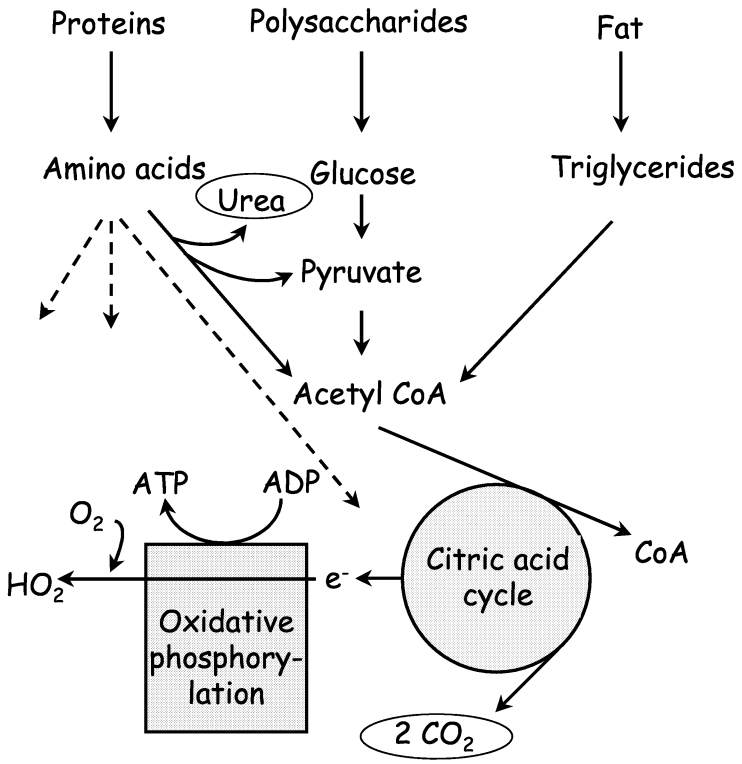

Figure 1 Simplified, schematic presentation of the metabolism of nutrients for energy generation in the citric acid cycle and subsequent oxidative phosphorylation. Modified from Stryer, page 325 (20).

Dietary proteins, lipids and carbohydrates are digested and transported from the intestines with the blood to distant tissues. Excess glucose can be stored as glycogen in the liver, whereas surplus lipids are stored as neutral fat or triglycerides in adipose tissue.

Cells receive nutrients from the blood as short peptides and amino acids, triglycerides, fatty acids and glycerol, and glucose and other disaccharides. Exergonic reactions are used for the synthesis of adenosine triphosphate (ATP), and the chemical bond energy of ATP drives the energy dependent processes. A simplified overview of the generation of cellular energy as ATP from nutrients is presented in Figure 1.

Proteins are broken down to amino acids, carbohydrates to glucose and lipids to triglycerides. Glucose is converted to pyruvate in the process called glycolysis. This reaction takes place in the cell cytoplasm and generates small amounts of ATP and NADH. Pyruvate is transported to mitochondria, where it is oxidatively decarboxylated and connected to coenzyme A (CoA), forming acetyl CoA. Fatty acids are degraded to acetyl CoA by β-oxidation in mitochondria. Some surplus amino acids can be converted to pyruvate, acetyl CoA, acetoacetate or intermediates of the citric acid cycle (TCA or Krebs cycle). The amino group is usually removed initially in the amino acid catabolism to an α-keto acid and further to urea which is excreted. The urea cycle is not active in the brain.

Acetyl CoA enters the citric acid cycle by a reaction of the acetyl group with oxaloacetate to form citric acid. Citric acid is converted to oxaloacetate through a series of reactions, generating two molecules of CO_2 and reducing nicotinamide adenine dinucleotide (NAD) and flavine adenine dinucleotide (FAD) to NADH and $FADH_2$ respectively. The electrons from the hydrogen atoms in NADH and $FADH_2$ are passed to molecular oxygen to form water, after being passed through a complex chain of membrane-bound carriers in the inner mitochondrial membrane. The energy released in these electron transfer steps provides transport of hydrogen ions out of the mitochondria. The resulting electrochemical proton gradient across the inner mitochondrial membrane drives the synthesis of most of the cells ATP (3).

Biosynthesis of macromolecules in a cell is concerned with proteins, nucelotides and membrane constituents. Amino acids can be precursors of a variety of molecules as proteins, nucleotides and polysaccharides (20). Protein synthesis takes place on the ribosomes, which are free in the cytoplasm or bound to the membranes of endoplasmatic reticulum. All important properties of living cells depend on proteins, as oxygen transport (hemoglobin) and membrane transport of ions and molecules (21).

Nucleic acids and nucleotides from the diet are poorly absorbed and we depend on biosynthesis of purines and pyrimidines (21). Pyrimidine is synthesized in the cytosol from aspartate and carbamoyl phosphate. The ribose is added in the final steps, leading to uridine-5'-phosphate from which the other pyrimidine nucleotides can be converted (22). The components of the purine ring are added stepwise to ribose, synthesizing inosine monophosphate (IMP), which is converted to adenosine and guanosine monophosphate (AMP and GMP) (22). The atoms in the synthesized purine ring originate from the amino acids aspartate, glycine and glutamine, from CO_2 and from folates.

Cell membranes consist of a double layer of lipid molecules, embedded with various membrane proteins. The most important types of membrane lipids are phospholipids, sphingolipids and cholesterol (21). Most cells can synthesize these components themselves.

The enzymes involved in the phosphoglyceride synthesis are located in the cytoplasm or are associated with endoplasmatic reticulum membranes. The most common hydrophilic ends in phosphoglycerides are phosphoethanolamine (PE), phosphocholine (PC), phosphoserine and phosphoinositol.

Metabolism of tumors

The increased proliferation of tumors has as a consequent an increased biochemical activity. One of the established theories of altered tumor metabolism is the increased glycolytic activity in tumors first reported by Warburg (23). This high rate is believed to depend on the glucose membrane transporters and overexpression of the respective genes (24). The increased glucose flux and capacity of tumors to metabolize glucose in hypoxic environments have been supported by numerous studies (25).

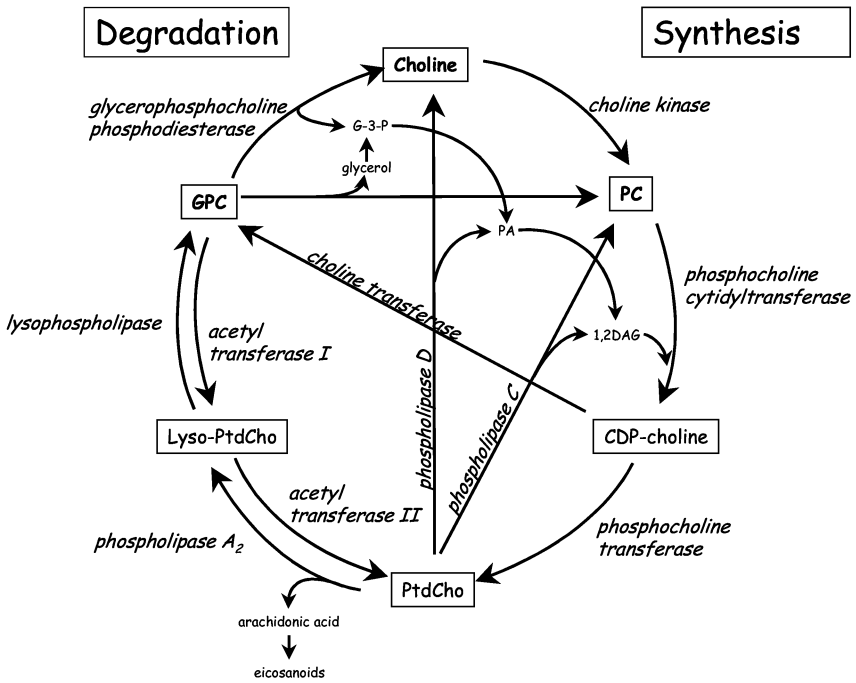

Figure 2 Pathways for synthesis and degradation of the phospholipid phosphatidylcholine. From Ruiz-Cabello and Cohen (26). The following abbreviations are used: GPC; glycerophosphocholine, PC; phosphocholine, CDP; cytidine diphosphate, PtdCho; phosphatidylcholine, G-3-P; glycerol-3-phosphate, PA; phosphatic acid, 1,2 DAG; 1,2-diacylglycerol. Enzymes regulating the major pathways are in italics.

MR spectroscopic studies of different cancers have focused on altered phospholipid metabolism (26, 27). *In vivo* studies of breast tumors (28-30) and astrocytomas (31) have reported increased total choline in tumors compared to normal tissue. Studies of malignant mammary cell lines have proven increased choline phospholipid metabolite levels (32). *Ex vivo* studies have shown that PC and PE increase in tumors (26, 27). This increased pool of PC and PE in many tumors is believed to be due to both biosynthesis and catabolism of phospholipids (26, 27). It has also been shown that phospholipid metabolism is altered when the patient receives successful tumor reducing treatment (33). Metabolic and catabolic pathways of phospholipids are shown in Figure 2.

Figure 2 illustrates that choline acts as a substrate for phosphatidylcholine (PtdCho) and is also a degradation product. PC is an intermediate in the PtdCho synthesis as well as a product of catabolism. Glycerophosphocholine (GPC) is a degradation product of CDP-choline and PtdCho. GPC can be utilized in PtdCho synthesis after conversion to choline, glycerol-3-phosphate (G-3-P) or PC. The elevated levels of PC found in tumor cells cannot result from increased PtdCho synthesis alone, but is likely to result from biosynthetic and catabolic interactions (27). The biochemical mechanisms responsible for elevated PC levels in tumor cells are not fully understood. Increased transport of choline to the cell, increased choline phosphorylation and growth factor-mediated activation of PtdCho-specific phospholipases have been found (27).

Neurochemistry

There are two different types of brain cells: neurons and glial cells. Furthermore there are three types of glial cells: astrocytes, oligodendrocytes and microglia (34). Neurons receive, process and transmit information using biochemical or bioelectrical changes in the cell. The primary function of glial cells is to shuttle nutrients to the neurons, remove waste products and maintain the electrochemical surroundings of the neurons. Nerve cells maintain almost no reserves of glycogen or fatty acids and rely almost entirely on a supply of glucose from the bloodstream. The oligodendrocytes form the myelin sheets around CNS axons, and surround CNS neuronal cell bodies. The microglia are the brain immune effector cells. Astrocytes are important for several functions, as they maintain extra-cellular ionic environment, secrete growth factors and support the neurons - structurally and metabolically.

The human brain contains approximately 10^{14} to 10^{15} connections between neurons, and communication at most of these is mediated by chemical messengers (35). The majority of signaling within the nervous system is performed by amino acid transmitters, specifically glutamate and gamma-aminobutyric acid (GABA). Astrocytes play an important role in regulation of glutamate and GABA neuro-transmission. Glutamate is synthesized from glutamine or α-ketoglutarate in the neuron. Much of the glutamate within the synaptic cleft is transported into astrocytes where it is converted to glutamine. The glutamine is transported to the presynaptic terminal and reconverted to glutamate. GABA released from GABAergic neurons can be partially accumulated into astrocytes. However, most of the GABA is taken back into the presynaptic neuron (34).

Other examples of small molecules that act as chemical messengers are the amino acids glycine and taurine, the biogenic amines acetylcholine and dopamine and adenosine (nucleotide) and ATP (nucleoside) (35). Several neuropeptides are also probable messengers, as oxytocin and angiotensin II.

2.6 MR spectroscopy

MR imaging and spectroscopy both exploit the magnetic properties exhibited by nuclei with nuclear spin ($I \neq 0$) when placed in a uniform magnetic field. The nuclear spins are then oriented in $2I+1$ different energy levels by equilibrium processes, and a radio frequency (rf) energy is applied to induce transmission between the different energy states. The excited nuclei return to equilibrium via longitudinal (T_1) and transversal (T_2) relaxation processes. This time dependent decay is acquired and Fourier transformed into a frequency dependent spectrum. The appearance of a specific peak depends on the molecular environments of the originating nuclei and physical, chemical, and biological properties of the studied sample can be revealed from MR spectra (36).

Metabolic characteristics of various human diseases have been explored by MR spectroscopy for 20 years (37). MR spectroscopy applied on cultured cells (38), animal models (38), intact human tissue (39) and extracts of tissue (40) has contributed to the understanding of different biological processes in conditions of health and disease.

Correlation of MR spectra to patient diagnosis and histopathology have been established by conventional MR spectroscopy of intact tissue samples (39, 41, 42). Spectral resolution in such spectra is however low and the biochemical information thereby limited. MR spectra of cell or tissue extracts provide detailed information on chemical composition, but at the cost of tissue destruction and possibly modified composition.

2.7 High-resolution magic angle spinning (HR MAS)

Tissue can be considered as a semisolid and broad lines are achieved in *ex vivo* spectra obtained by conventional MR spectroscopy. The lack of molecular mobility leads to anisotropic interactions, imposing a spin orientation dependence on the MR frequency (43). Anisotropic interactions are direct homonuclear and heteronuclear magnetic dipolar interactions, indirect electron coupled interactions, electric quadrupolar interactions and electron shielding interactions.

Andrew *et al.* (44) and Lowe (45) first described the narrowing of MR lines when solids were spun at the magic angle. Line broadening in solids can be reduced by spinning the sample rapidly about an axis inclined 54.7° to the direction of the static magnetic field (Figure 3). The spinning splits the broad resonance into a narrow line at the isotropic resonance frequency and spinning sidebands (46). All spin interactions become time-dependent and sidebands appear at integer multiples of the spinning rate. The time independent part of the anisotropic interactions is dependent on $(3\cos^2\theta-1)$ and cancelled

by the choice of angle. The time dependent anisotropic interactions average over a rotor period. If the spinning rate is much larger than the anisotropic spin interaction the sidebands are well separated from the central line and their intensity decrease with increasing spinning rate. As a consequence, anisotropic interactions are averaged to their isotropic value, resulting in substantial line narrowing.

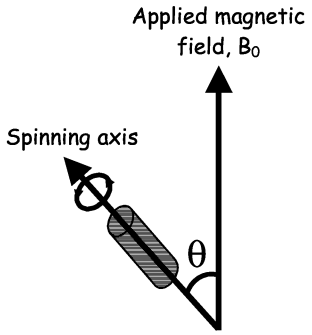

Figure 3 Schematic presentation of a sample in a magic angle spinning probe. θ is the magic angle, 54.7 °, B_0 is the static magnetic field.

Although narrower lines are obtained because of the MAS effect, large molecules like proteins and lipids appear as broad signals in the MAS spectrum. A common method to reduce these broad signals is by utilizing their short T_2 values. This can be performed by a spin-echo sequence for acquisition (47).

One of the pioneer publication on HR MAS of human tissue was a study of human lymph nodes presented by Cheng in 1996 (48). The HR MAS technique was shown to provide highly resolved spectra from intact tissue samples. In addition to studies of animal and human tissue, the MAS technique has been used in studies of cells (49) and bio-membranes (50, 51).

MAS has been applied in numerous types of tissue, and provided detailed descriptions of the chemical composition of healthy and affected tissue from, for instance, kidney (52, 53), brain (54, 55) and prostate (56). A study of human kidney has provided classification of renal carcinomas (57) while MAS studies of brain tissue have shown that specific metabolites and metabolite ratios correlate to density of specific cell types (58) and fraction of cancerous and necrotic areas (59). Also in MAS studies of prostate tissue, metabolite concentration has been found to correlate to tissue composition (60, 61). MAS MR spectra could also discriminate malignant prostate from healthy glandular tissue (61). One study on breast cancer tissue has previously been performed using HR MAS MR spectroscopy (62). The study showed that breast carcinomas could be distinguished from non-involved breast tissue based on intensities and T_2 relaxation values of cellular metabolites. The HR MAS technique gives the opportunity to investigate the same sample

by microscopy after MR analysis, providing direct comparisons of morphological and chemical characteristics (59-61).

2.8 Spectral analysis

Biological samples, such as blood, urine and tissue, comprise a vast amount of MR detectable compounds and the resulting high field proton MR spectra can be very complex. Different approaches are used to investigate MR spectra. Spectral characteristics can be explored by examining peak intensities or peak areas. Peak areas can be obtained by integration or, in spectra where peaks are overlapping, by deconvolution (63). Metabolites of interest can be quantified by comparing peak areas to an internal reference like water (60, 64) or to an added reference (63). Peak-by-peak investigations to extract information have been useful in many studies, and makes direct comparison between chemical and biological features possible (29, 65-68).

MR spectra from biological samples are often investigated with respect to a specific disease. Characterization of spectral findings from the disease can be attempted by comparisons between samples from different stages or to controls. Several MR spectroscopic studies have shown that almost all resonances influence the spectral patterns (69, 70) and visual inspection of such spectra yield limited information from the available data. In recent years multivariate analysis has gained a lot of interest in MR data handling. Multivariate spectral analyses can be applied to entire data sets. They can be used to reduce the complexity in the data and generate and test scientific hypotheses (71).

An often used unsupervised method for analyses of MR spectroscopic data, is principal component analysis (PCA) (69-72). The objective of PCA is to convert the multiple and possibly correlated parameters from the measurements to a non-correlated and much smaller set of parameters (69). PCA creates linear combinations from the original spectra based on the variance, leading to a reduced set of independent variables describing the original data set. A set of MR spectra can be considered as a D-dimensional vector **x**, consisting of possibly correlated elements. D corresponds to the number of points describing the spectra. PCA then transforms the vector **x** into another D-dimensional vector **y**, whose elements are not correlated. From the resulting **y**-vector, d variables (d is smaller than D) are selected that approximately represent the original measured vector **x**. These variables are called principal components. The first principal component (PC1) contains the largest part of the variance in the data set, and correspondingly smaller amounts of the variance are contained in the following principal components (71). In general, there are no reasons for large variances to indicate discrimination and PCA is merely considered as a method for visualization of complex data and to reduce data input before classification (69). However, PCA has been applied on MR spectra resulting in sample grouping based on score values for the principal components (57, 73, 74).

3. Objectives

Morphologically visible changes in tissue are believed to have parallel biochemical changes, possibly detectable by MRS. The main objective of this study was to establish HR MAS as a method to study biochemical properties of human tissue, in particular breast cancer. The more specific aims of this thesis were to:

1. Establish a protocol for HR MAS analysis of tissue samples, preserving the specimens for histopathologic evaluation.

2. Compare obtained information on tissue properties from HR MAS to findings from extract studies.

3. Investigate the chemical profiles from intact tissue samples in order to obtain increased understanding of biological processes in affected tissue.

4. Investigate correlation of the biochemical profiles of tissue specimens to clinical parameters using multivariate analysis.

4. Summary of papers

Paper I

Gribbestad IS, **Sitter B**, Lundgren S, Krane J, Axelson D. *Metabolite composition in breast tumors examined by proton nuclear magnetic resonance spectroscopy*. Anticancer Research (1999) **19**: 1737-1746.

The aim of this study was to use MR spectra of perchloric acid extracts to characterize the biochemical composition of breast tumors and non-involved breast tissue. Involved and non-involved breast tissue specimens were excised from 16 patients undergoing scheduled surgery for breast cancer. Tissue specimens were extracted using perchloric acid and the extracts were analyzed by ^{1}H MR spectroscopy on a BRUKER DRX 600 spectrometer operating at 600 MHz for protons. Metabolic concentrations were calculated from peak areas obtained by curve fitting (PeakFit from Jandel Scientific) relative to TSP as an internal reference. PCA and probabilistic neural networks (PNNs) were applied on the calculated concentrations. In addition PNNs were applied to the raw data (spectra). The spectra from the cancerous samples differed from the non-involved samples by absence of glucose in half of the spectra, but higher (10-20 times) content of cholines, PE, alanine, lactate and taurine. The PCA performed on the calculated values of the nine metabolites almost enabled classification of tumor and non-involved samples (three malignant samples overlapping the non-involved group of samples). The same result was found by PNNs.

Paper II

Sitter B, Sonnewald U, Spraul M, Fjösne HE, Gribbestad IS. *High-resolution magic angle spinning MRS of breast cancer tissue*. NMR in Biomedicine (2002) **15**: 327 – 338.

The main objective of this paper was to compare HR MAS spectra from intact breast cancer specimens with previously obtained high-resolution spectrum of a perchloric acid extract from the same kind of tissue. Breast cancer specimens and non-involved adjacent tissue were excised from 10 patients and examined using HR MAS spectroscopy. Spin-echo acquisitions of spectra were performed to reduce the appearance of broad signals, leading to a relative increase in signals from small molecules. The spectral resolution was found to be comparable to the presented spectrum from a perchloric acid extract. Two-dimensional techniques combined with literature values of chemical shifts led to assignment of 99 peaks from 30 different metabolites. The largest observed difference from perchloric acid extract spectra were the absence of nucleotide signals in the low field region (9.0 – 6.0 ppm). Resonance peaks from choline, PC and GPC were found to be individually separable in the MAS spectra. The paper also describes reduced S/N ratios in two samples after flushing the samples in solvent as compared to the exact same specimens immersed in solvent demonstrating extraction of metabolites from the tissue.

Paper III

Sitter B, Lundgren S, Bathen TF, Halgunset J, Fjosne HE, Gribbestad IS. *Comparison of HR MAS MR spectroscopic profiles of breast cancer tissue to clinical parameters*. Submitted to NMR in Biomedicine.

Tumor samples from 85 patients and adjacent non-involved tissue from 18 of these patients were analyzed by water suppressed and spin-echo HR MAS MR spectroscopy. Tumor samples could be distinguished from non-involved samples (82% sensitivity, 100% specificity) based on relative intensities of signals from GPC, PC and choline in spin echo spectra. Tissue concentrations were estimated from water suppressed spectra for eight metabolites: β-glucose, glycine, taurine, myo-inositol, GPC, PC, choline and creatine. Non-involved spectra showed low content of water-soluble metabolites, and metabolite estimations from these spectra could generally not be performed. The tissue metabolite estimates were compared to patient diagnosis, tumor grading, tumor size, patient lymph node status and microscopic evaluation of tissue composition for each sample. Significant higher tissue concentrations of choline and glycine were found for tumors larger than 2 cm compared to smaller tumors. Principal component analysis was used to compare the MR spectra to the same parameters as metabolite concentrations. Metabolite estimates and PCA of MAS spectra indicate that the spectral patterns depend on sample tissue composition. A possible prediction of spread to axillary lymph nodes was found in PCA of samples without fat tissue from patients with invasive ductal carcinomas.

Paper IV

Sitter B, Bathen T, Hagen B, Arentz C, Skjeldestad FE and Gribbestad IS. *Cervical cancer tissue characterized by high-resolution magic angle spinning MR spectroscopy*. MAGMA, in press.

Cervical specimens from patients in surgery for cervical cancer (n=8) and for non-malignant diseases of the uterus (n=8) were analyzed using HR MAS spectroscopy. MAS spectra were acquired using water suppression as well as a spin-echo sequence. The two sets of MR spectra served as inputs in two separate matrices for principal component analysis. Both resulting score plots of principal components one and two (PC1 versus PC2) classified malignant from non-malignant cervical biopsy specimens. The separation of malignant from non-malignant was better from spin-echo spectra where signals from lipids and macromolecules were reduced, leaving the smaller water-soluble metabolites to dominate the MR spectrum. Higher levels of cholines and amino acid residues distinguished malignant from non-malignant cervical tissue in addition to lower glucose content. The principal component analysis of spectra containing lipids led to positioning of adenocarcinomas (n=2) and squamous cell carinomas with lymphatic spread (n=2) in two distinct groups. Methyl and methylene signals from lipids, lactate and cholines gave the largest contribution to the separation from remaining samples. The tissue specimens had been subject to room temperatures for more than 1.5 hours when the MAS spectra were

recorded. Sample score values and the time period each sample had experienced room temperature were not correlated. Although providing detailed biochemical information, a study performed at lower temperature to reduce biochemical degradation on a larger patient group ought to be performed to verify the findings.

Paper V

Sitter B, Autti T, Tyynelä J, Sonnewald U, Bathen TF, Puranen J, Santavuori P, Haltia MJ, Paetau A, Polvikoski T, Gribbestad IS, Häkkinen A-M. *HR MAS ^{1}H MR spectroscopy reveal significantly altered neuronal metabolite profiles in CLN1 but not in CLN3*. Accepted for publication in Journal of Neuroscience Research.

In this study, *in vivo* ^{1}H magnetic resonance (MR) brain spectra of patients with neuronal ceroid lipofuscinosis (NCL) and controls, were compared to *ex vivo* ^{1}H high-resolution magic angle spinning (HR MAS) MR spectra of brain autopsy tissue from similar patients. The purpose was to investigate if the *ex vivo* HR MAS technique could provide information about altered neuronal metabolites in NCL brain tissue. The tissue material for MAS analysis was autopsy samples.

In vivo spectra of late stage patients with CLN1 (n=3) revealed marked decrease in all metabolites compared to control subjects, except *myo*-inositol and lipids. NAA was especially strongly decreased. The spectra of patients with CLN3 (n =13) did not differ from those of controls (n =15). *Ex vivo* spectra from CLN1 autopsy brain tissue (n=10) were clearly different from the other two groups, while no differences were found in metabolite levels between CLN3 (n=5) and control autopsy tissue (n=9). Principal component analysis showed that decreased levels of GABA, NAA, glutamine and glutamate and increased levels of inositols characterized the CLN1 spectra. Also, the methylene/methyl ratio of lipids in CLN1 patients was decreased compared to CLN3 patients and controls.

In conclusion, the *ex vivo* spectroscopic findings were in strong agreement with the *in vivo* findings. Furthermore, HR MAS spectra facilitated refined detection of numerous neuronal metabolites, including GABA and composition of lipids, in autopsy brain tissue.

5. Discussion

5.1 Establishing a HR MAS protocol

Implementation of a new method for metabolite studies also introduces the risk of unforeseen errors into the measurements. When applying HR MAS as a tool for human tissue characterization, it was attempted to preserve the metabolic information from the living tissue. The treatment of specimens from sample collection to MR analysis will influence the chemical composition of specimens because of chemical processes after tissue excision. Storing, additives, MAS conditions and temperature affect the extent of these reactions.

In the HR MAS studies of this thesis (paper II-V), tissue specimens have been put in cryogenic vials without any additives and stored in liquid nitrogen (except for the brain specimens (paper IV) that were stored at -80°C) as soon as possible after surgical removal. In previous studies, the freezing of kidney tissue has reportedly led to increased amounts of amino acids and decreased contents of choline, GPC, glucose, *myo*-inositol, trimethylamine *N*-oxide (TMAO) and taurine (75, 76). A storage buffer has been added before cryo storage of sample (41, 62), presumably to increase heat transfer and thereby minimize formation of ice crystals and the consequent damage of cells and cell components (77). We held the risk of metabolite leakage to the storage buffer, as described by Bourne *et al.* (78), as far more of a disadvantage than the risk of increased tissue damage by a slower freezing process. The long-time storage in liquid nitrogen is assumed to not affect the chemical composition. In paper III, sample storage periods and metabolic profiles were compared. No obvious correlation could be found, and degradation during liquid nitrogen storing was assumed insignificant.

Sample treatments for MAS analyses have been performed by two different procedures. The breast tissue specimens studied in paper III were analyzed at temperature-controlled conditions (5.8 °C). Samples were immersed in phosphate buffered saline in a MAS rotor with inserts providing a 50 μL sample volume. All other samples (specimens from breast, cervix and brain in paper II, IV and V respectively) were examined using rotors of about 100 μL and added D_2O. These samples were analyzed using a MAS probe without the possibility of air cooling, leading to sample temperatures of 25-28°C (paper IV). There are a few publications on HR MAS of tissue specimens where D_2O is added (56, 79, 80). Addition of water to cells or a tissue sample cause osmotic pressure (3), and saline or a saline buffer is preferred to limit tissue damage. Attempts were made on packing MAS rotors without adding any fluid. This procedure for sample preparation introduced air bubbles in the sample volume, and the large susceptibility differences made it very difficult to obtain highly resolved MR spectra. In the protocol for MAS studies established by the work presented in paper III, saline PBS was used in sample preparations.

Tissue rinsing prior to HR MAS analysis is reported in numerous publications (48, 61, 74, 80-83), sometimes stated as necessary to remove residual blood (74, 76, 83, 84) and improved water suppression (55, 56). Effects on resulting spectra have been examined by Waters *et al.* (76) and Bourne *et al.* (78). Waters *et al.* found enhanced resolution in HR MAS spectra from rat kidney tissue after saline D_2O perfusion, but the spectra also showed a profound loss of glycine. Prostate samples rinsed with D_2O were described by Bourne *et al.* to have 40-50% of measured metabolites in the storage buffer (78). Tissue perfusion by an aqueous solution lead to a washout of water-soluble metabolites. The degree will probably depend on the tissue, and so will the spectral benefits of tissue perfusion (76). We reported a reduced S/N ratio when breast cancer tissue was subject to rinsing in D_2O prior to MAS analysis, and could not find improvements in resolution (paper II).

Sample preparation for HR MAS analysis is simple and fast. There are however continuing biochemical processes in the tissue during analysis. Such processes are reduced by low temperatures, and 2-5 °C are commonly used during HR MAS acquisitions (54, 58, 64, 85-87). High-energy phosphate compounds are readily decomposed after tissue excision. As presented in paper II, the high-energy compounds ATP, adenosine diphosphate (ADP) and PCr were detectable in the spectrum from extract but not in MAS spectra of intact specimens analyzed at room temperature. Neither could these compounds be detected in spectra of breast cancer specimens acquired at low temperature (paper III).

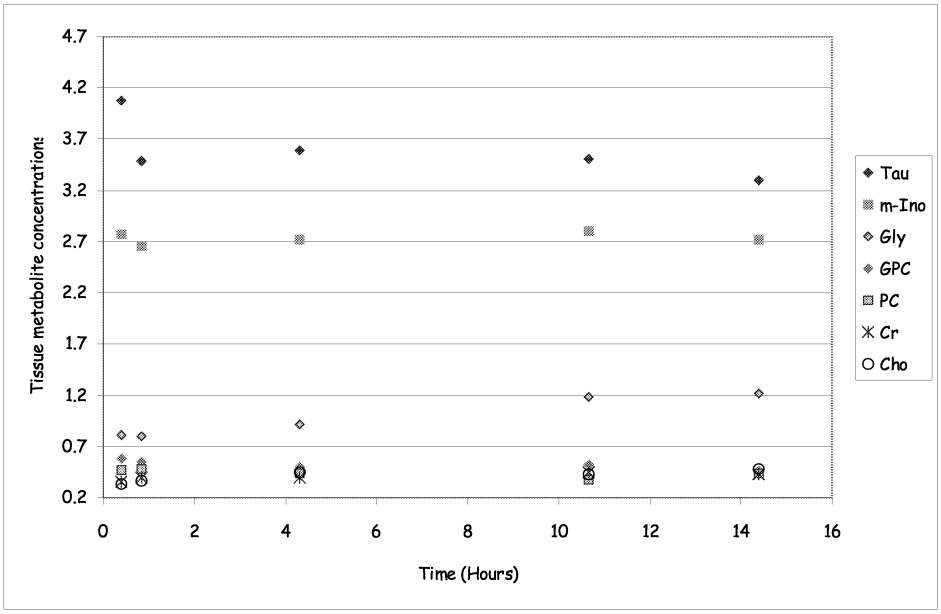

Figure 4 Changes in metabolite concentration in one breast cancer tissue specimen from patient diagnosed with invasive ductal carcinoma grade III, analyzed by HR MAS at 1.5 °C over a 14 hours time span.

The concentration of selected metabolites (glycine, *myo*-inositol, taurine, GPC, PC, choline and creatine) in breast cancer specimens analyzed at 1.5 °C (calculated from glucose and water signals as described by Farrant *et al.* (88)), were estimated at different time periods after sample thawing. Results obtained from one sample are presented in Figure 4. Changes in tissue metabolite levels after 4.3 hours were less than 15% for all metabolites except choline (33% increase). The metabolite levels were further changed 14.5 hours after thawing in this sample, especially for glycine and choline. Spectra were recorded within 1 hour and 40 minutes for all samples in paper III, and the observed tissue metabolite profiles were assumed to not be significantly altered by tissue degradation.

Breast tissue specimens analyzed by HR MAS, presented in paper II and paper III were analyzed at 30 °C and 5.8 °C respectively. In the spectra in paper II, the amino acids aspargine, isoleucine, leucine, lysine and valine are more dominant than in spectra in paper III, indicating that elevated amino acid levels partly result from protein degradation. Waters *et al.* have explored how spectra are affected by biochemical changes in rat liver and kidney with time (76). MAS spectra from rat liver tissue were not found to be significantly altered after several hours at 30°C. They registered an increase in GPC in kidney after four hours at 0°C, and reduced triglycerides and TMAO after four hours at 30°C. There are obviously large variations between various tissue types in compound stability. Metabolites in human breast tissue appear to be less stable than in human cervical tissue.

Cervical samples (paper IV) and brain autopsy samples (paper V) were analyzed at room temperature, with presumable faster degradation rates than in Figure 4. It is assumed that for cervical cancer samples analyzed at 27°C after 1.6 hours, metabolite degradation has been significant. In addition, the one-hour difference samples were exposed to 27°C which might have a large impact on spectral patterns. That the two groups can be identified based on the spectral pattern after such treatment indicates that the differences between malignant and non-malignant samples are so distinct that degradation processes do not mask the variation between the groups (paper IV). In the brain autopsy study (paper V), analyses were performed on samples that were dissected at various times after death. The HR MAS analyses were performed at room temperature approximately the same time after thawing. HR MAS provided separation of the most severe lipofuscinosis (CNL1), implying that the brain tissue specimens were metabolically different after probable severe tissue degradation.

In the outer part of a 4 mm MAS rotor spun at 5 kHz, tissue will experience centrifugal forces of about 5100 g (m/s^2). The analyses presented in this thesis have all been performed at high spinning rates (3.5 - 6 kHz), and tissues are likely to be influenced by this. The high spin-rates were used to avoid spinning sidebands in the spectra. Garrod *et al.* presented a HR MAS study on rat renal cortex and medulla (74). They found that spinning speeds of 12 kHz increased resolution in spectra of renal cortex compared to spectra recorded at spin rate 4.2 kHz, and furthermore, that the changes were reversible. Cheng *et al.* reported that the histopathologic characteristics of a sample were not disturbed by HR MAS analysis after 2.3 kHz brain sample spinning (85). Increased spectral resolution by increasing spinning rates has been reported by Cheng *et al.* (48) and

Garrod *et al.* (74). Wind *et al.* (79) however state that spinning at high speed like 4.3 kHz led to sample deformation. Several studies report MAS experiments of tissue specimens where rotor spinning speed is low (40 - 700 Hz) to avoid sample damage from centrifugal forces (79, 87, 89). Taylor *et al.* demonstrated the better preservation of tissue for histopathological evaluation of low speed spinning (700 Hz) compared to high (3 kHz) (87). A disadvantage of slow magic angle spinning is that spectral sidebands must be removed by the pulse sequence (89). For our purposes, simple acquisition procedures and high spectral resolution were preferred over improved tissue preservation for histopathology. In our study of breast cancer samples analyzed at low temperatures and 5 kHz spinning rates (paper III), 82 of 85 tumor samples could be evaluated by microscopy after HR MAS analysis.

It has been demonstrated by Waters *et al.* (76) that MAS rotors of small sample volumes (12 μL) increased the spectral resolution due to increased sample homogeneity and optimized localization in the MAS probe. We have performed experiments with three types of MAS rotors. MAS rotors without inserts contain a sample volume of approximately 100 μL, and were used in the MAS experiments presented in paper II, IV and V. Because of the limited detection area of the coil, parts of the sample volume are possibly not detected in such rotors. In addition, it was difficult to obtain stable rotor spinning in the MAS probe with cooling possibilities. MAS rotors with small spherical volumes (12 μL) have also been used in MAS experiments. The small sample volumes led to longer acquisition times in order to obtain satisfactory S/N. MAS rotors with spherical inserts of 50 μL provided sufficient S/N within five minutes of acquisition (paper III) and spinning was stable.

Many papers on MAS MR spectroscopy of tissue specimens describe the use of a spin-echo sequence for suppression of broad signals (section 2.6), for instance (59, 61, 62, 64, 81). T_2 values have been measured for various metabolites and suggested to differ in accordance with clinical state (62). Diffusion parameters have also been recorded, enabling separation of large molecules and smaller metabolites (86). We chose to focus on MR sequences which were easy to apply, such as water suppression acquisitions in combination with spin-echo suppression of broad signals (paper II - V). For the HR MAS protocol to become a routine clinical tool, the analysis should be fast and kept as simple as possible. The protocol we have established requires 1 to 1.5 hours spectrometer time per sample, which can be shortened to approximately 30 minutes by reducing the number of MR experiments per sample.

The use of a standard for metabolite quantification is more complicated in MAS experiments than in conventional high-resolution MRS. Addition of the standard with the sample or buffer within the rotor volume involves a probable loss of standard in MAS rotor assembling due to excess fluid removal. In addition, the conventional standard TSP has the ability to bind to proteins (90). Protein binding leads to shorter T_2 values and a reduction of the TSP signal in spin-echo spectra, which depends on the degree of binding to proteins. We tested if TSP could be used as an external standard by adding it above the 50 μL inserts. HR MAS spectra acquired from these samples contained no signal from the TSP due to the restricted detection area of the coil. Attempts on internal and external referencing for quantitative measures of tissue metabolites from MAS spectra

have been described in the literature. In HR MAS studies of brain specimens, tissue water has been used as an internal standard to estimate brain metabolite concentrations (54). A method using silicone rubber sample as external standard has been described by Taylor *et al.* (87). As described in paper III, we chose to use TSP as an internal reference for quantification. Inaccuracy due to standard loss in rotor assembling was assumed to be similar for all samples and loss of TSP with the buffer was corrected for in the metabolite estimations. In further studies, we will attempt to use other standards like formate (90) and quantify metabolites from spin-echo spectra.

5.2 MAS spectra of intact tissue compared to spectra of extracts

MR spectra from tissue extracts show high resolution (paper I). The extraction process is however laborious, time consuming and it destroys the specimens. Direct comparison to histopathology is impossible. Compounds that are MR visible when analyzing the intact tissue may not pass into extracts and tissue compounds may undergo chemical changes during the extraction procedure. Askenasy *et al.* (91) showed by $^{1}H/^{31}P$ spectroscopy that signals observable from intact tissue were absent in spectra from extracts, and that new signals were introduced in extract spectra from hydrolysis of RNA. In our comparison of extract and MAS spectra of breast cancer tissue (paper II), we found the major differences to be the presence of signals from lipids and reduced number of signals in the low-field region in MAS spectra of intact breast cancer specimens. UDP-hexoses, NADH, ATP and ADP identified in the extract spectra from breast tissue (paper II) are possible hydrolysis products since they only are observed in spectra from extracts. Breast tissue can contain large amounts of fat, and lipid signals may dominate a MAS spectrum of breast cancer tissue (paper III). The dominating lipid signals can mask smaller signals from metabolites like lactate (paper III). This problem can be reduced by using a spin-echo sequence for acquisition of spectra (paragraph 2.7).

As can be seen in Figure 5, the spectral resolution in spin-echo acquired HR MAS spectrum (B) is close to the resolution found in the MR spectrum of a tissue extract (C). Lipid signals at 4.1 and 4.3 ppm in (A) are completely removed by the spin-echo sequence, and lactate can clearly be detected in (B) at 4.11 ppm.

The effectiveness of the extraction procedure is probably incomplete and differs for different compounds. Cheng compared neuronal metabolites studied in intact specimens and extracts, and found choline and PC to be remarkably less intense in spectra from extracts (64). HR MAS spectroscopy of intact specimens provides high resolution compared to spectra of perchloric acid extracts (paper II). A specimen analyzed by HR MAS is practically untreated, and tissue architecture and relative cellular composition are maintained. Tissue samples analyzed by the MAS technique can be examined by microscopy after MR analysis, and the spectral profile can be compared to tissue composition (paper III).

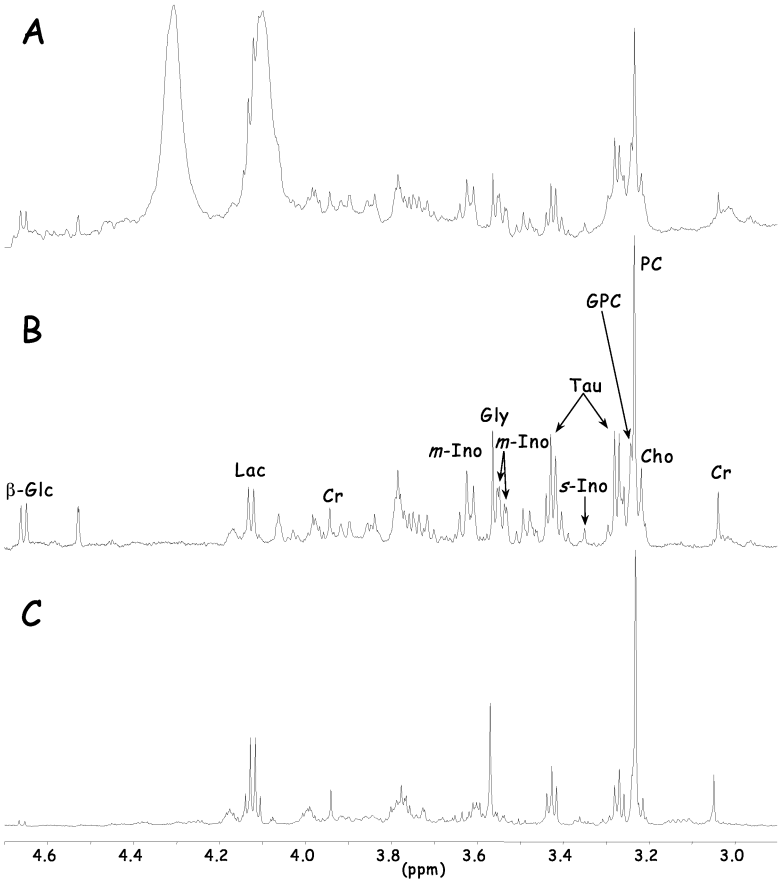

Figure 5 Spectral region 4.70 to 2.90 ppm from three different spectra from breast cancer tissue. A: MAS spectrum acquired using a water suppression sequence, B: MAS spectrum from the same sample as in A recorded using a spin-echo sequence with 285 ms total echo time and C: spectrum of an extract of breast cancer tissue acquired using water suppression. Some peak assignments are given in B, the following abbreviations are used: β-Glc; β-glucose, Lac; lactate, Cr; creatine, *m*-Ino; *myo*-inositol, Gly; glycine, Tau; taurine, *s*-Ino; *scyllo*-inositol, GPC; glycerophosphocholine, PC; phosphocholine and Cho; choline.

5.3 Chemical profiles connected to biological processes

HR MAS spectra of human tissues show an extensive picture of MR detectable metabolites, which are related to biochemical processes. The spin-echo HR MAS spectra

of cervix and breast cancer specimens (paper II, III and IV) were dominated by the same metabolites amino acids (taurine and glycine), cholines (GPC, PC and choline), *myo*-inositol, creatine and lactate. The spectra from brain autopsy samples (paper V) also contained substantial amounts of amino acids, cholines, *myo*-inositol and lactate, but in addition neuron specific molecules (GABA and NAA) were important contributors to the spectral profiles.

All compounds we can study in cancerous tissues are intermediates in processes where oncogenes play a part. Cancer cells in primary tumors mainly differ from their normal counterparts by elevated cell proliferation. As stated by B. D. Ross: *It is likely that we are looking for the same metabolites as normally present, but in abnormal proportions* (92). Another possible contribution to observed differences between cancerous and normal tissue is the altered physiology. Alterations in blood and substrate supply, tumor necrosis and nutritional disturbances in the host are all factors likely to contribute.

The increased glycolytic activity in solid tumors was expected to be reflected in spectra of cancer tissue, possibly as reduced glucose concentration compared to non-involved tissue. In paper I, glucose was undetectable in eight of 15 malignant breast samples analyzed after perchloric acid extraction. The average glucose concentration in tumor tissue was 0.32 μmol/gram, compared to 0.52 μmol/gram in non-involved tissue. The difference was statistically non-significant (student t-test, p=0.159). In a study of breast tissue extracts by Beckonert *et al.* (93), glucose levels were found to be higher in control tissue compared to tumor tissue.

In the cervical cancer study (paper IV), glucose levels were found to contribute to cervical cancer classification based on PCA. Glucose levels estimated from HR MAS spectra of breast cancer samples (paper III) varied within each group, and non-involved samples (0.62 μmol/gram tissue) was not significantly different from glucose in tumor tissue (1.34 μmol/gram tissue). Glucose was undetectable in several of the spectra from adjacent non-involved breast specimens. The high content of fat tissue in non-involved samples is a probable reason for non-measurable levels of selected metabolites (choline, creatine, β-glucose, GPC, glycine, *myo*-inositol, PC and taurine) as well as glucose. This finding of low glucose content in non-involved tissue is not yet understood, and should be looked into further. In our study of extracts of breast cancer tissue (paper I), lactate concentration was significantly higher (student t-test, $p < 0.001$) in tumor tissue (1.23 μmol/gram tissue) than in adjacent non-involved breast tissue (0.58 μmol/gram tissue). Lactate has previously been found to correlate to metastasis in cervical cancer, which might be related to hypoxia (94). Roslin *et al.* measured metabolites in astrocytes using microdialysis and found weakly lower glucose levels in tumor compared to control tissue, whereas lactate levels were significantly higher in tumor (95). Elevated lactate might be a better measure of increased glycolytic activity in tissue from tumors than reduced glucose, as glucose flux also is increased in cancerous tissue (96).

Higher content of choline compounds in cancerous tissue compared to control tissue was found to contribute to classification of cervical cancer samples (paper IV). Choline was found to correlate to tumor size in the MAS study on samples from breast cancer patients (paper III). Perchloric acid extracts of breast cancer samples showed a tenfold higher

level of cholines than non-involved samples (Paper I). The elevated cholines in breast and cervical cancer tissue correspond to findings in other studies on breast (27), prostate (61), colon (97) and brain cancers (98). In cancer studies using MRS, the altered pattern of choline-compounds have added important diagnostic information (99).

In our studies of cervical cancer (paper IV) and breast cancer (paper III) where PCA was performed and compared to clinical evaluations, the cholines, and PC in particular, were found to influence tumor sample characteristics. Numerous studies confirm the altered pattern of choline metabolites in tumors (27), but the mechanisms are not fully understood. Studies of malignant and benign brain cells have shown that relative proportions of PC and GPC vary in different types of tumors (100). Studies on prostate cell lines verify that increased total choline concentration found in prostate cancer is due to altered phospholipid metabolism (101). Enhanced choline transport and increased synthesis of betaine and PC were found to dominate increased levels of cholines in malignant mammary cell lines (102). Choline kinase activity is increased in lung, prostate, colon (97, 103) and breast carcinomas (104).

Glycine has been found to be increased in accordance to degree of malignancy in glioblastomas (105). Altered glycolysis in tumors has been suggested as a source of elevated glycine (106). Increased glycine levels contributed to cancer tissue classification in cervical tissue (paper IV). Glycine was elevated in samples from large breast tumors (paper III) and was furthermore important in characterization of samples from lymph node positive breast cancer patients (paper III). Glycine is also a substrate in nucleotide synthesis (section 2.5) and as most amino acids, a substrate in protein synthesis. It constitutes one third of the most common type of collagen in connective tissue (20). Ductal carcinomas are in part characterized by large fractions of connective tissue (7), and high levels of glycine in tissue from such tumors might be connected to collagen synthesis.

Taurine represents one of the dominant peaks in spectra from both cervical and breast tissue. In the cervical cancer study (paper IV) taurine was elevated in cancerous tissue, and when comparing MAS spectra of breast cancer samples (paper III), taurine was slightly increased with tumor grade for invasive ductal carcinomas. It was also found to be important in the possible discrimination of samples from lymph node positive patients (paper III). The roles of taurine are not fully understood, and it appears to have different functions in different tissues (107). It is an osmolyte and antioxidant and stimulates glycolysis and glucogenesis. Increased taurine levels have been found in malignant compared to non-involved tissue studies of breast (93), pancreatic (108), colon (109) and prostate cancer (61).

Similar to taurine, the role of *myo*-inositol is not fully understood. The role of inositol-phosphates as second messengers have gained significant attention in recent years (110). However, since it is essential that the concentration of these messengers is small, it is unlikely that they influence the spectra. *Myo*-inositol can be the polar group on membrane phospholipids (paragraph 2.5) and its levels might reflect membrane phospholipid composition. *Myo*-inositol did not contribute to characterization of cervical cancer (paper IV) and was not found to be important in the first principal components in PCA of breast

cancer samples (paper III). Tissue metabolite estimates in breast cancer samples (paper III) showed slightly higher levels of *myo*-inositol in samples from patients with positive lymph nodes. In our study of extracts from breast cancer (paper I), the level of *myo*-inositol was not significantly higher in tumor tissue (0.90 μmol/gram tissue) compared to non-involved (0.36 μmol/gram tissue) (student t-test, p=0.101). Beckonert *et al.* found *myo*-inositol to be elevated in healthy tissue in a study of breast tissue extracts (93). *Myo*-inositol is not significantly altered in malignant tissue of the cervix and breast compared to non-involved tissue of the same origin.

The MR lipid profiles of breast cancer tissue, obtained by water suppressed spectra, did not provide correlation to patient diagnoses (paper III). Parts of spin echo spectra, strictly dominated by small, water-soluble metabolites, were found to provide sample grouping in relation to clinical parameters. Lipid profiles have been reported to be different in malignant breast tissue compared to healthy (111). The lipid signals in the HR MAS spectra of breast tissue (paper III) probably merely reflect fat tissue content. Lipid profiles in cervical cancers are associated with viral infections (112, 113). Although lipid-containing spectra from cervical tissue were examined, a direct comparison to viral infection could not be performed, as the HPV status of patients was unknown.

In the study of brain autopsy samples (paper V), there was a clear difference between spectra from CLN1 patients compared to controls and CLN3 patients. The neurotransmitter GABA was undetectable in most CNL1 spectra. Also NAA was undetectable in these spectra, and glutamine and glutamate were reduced. These findings reflect neuronal death (64) and astrocyte dysfunction. As described in paragraph 2.5, GABA and glutamate are neurotransmitters, whereas glutamine is synthesized by astrocytes and connected to glutamate and GABA synthesis. NAA is synthesized and stored primarily in the neurons, but catabolized in oligodendrocytes. Recent evidence shows that one important role of the NAA intercompartmental cycle is osmoregulation, by removing intracellular water from myelinated neurons (114).

Increased inositol levels were found to strongly contribute in the classification of CLN1 samples in the MAS study of brain autopsy samples (paper V). *Myo*-inositol is a glial marker (115). The neuronal death in CLN1 leads to progressive axonal degeneration and gliosis (116). An increased number of glial cells might cause increased levels of *myo*-inositol (116, 117). However, the reverse was observed for glutamine and might point to altered astrocyte metabolism. Furthermore, an increased lipid CH_2/CH_3 ratio of CLN1 patients was found, supporting a previous study suggesting shorter fatty acids in CLN1 brain (118). The mechanism for this is not yet understood.

5.4 HR MAS spectral profiles compared to clinical parameters

The main purpose of the MR spectroscopic studies presented in this thesis was to investigate if MR spectral profiles correlated to clinical parameters. Tissue from cancerous breast and cervix (paper I-IV) and pathological brain (paper V) have been compared to non-involved tissue of the same origin (brain and cervix) or adjacent tissue (breast). This should provide the opportunity to compare metabolic patterns of unaltered

tissue to that of affected tissue. The MAS spectra presented in paper II were not directly compared to clinical parameters.

Cervical cancer samples could be separated from non-involved cervical samples based on the MR spectral profiles from spin-echo experiments (paper IV). The separation of cancerous and non-cancerous samples were poorer when water suppressed spectra were used as input in the principal component analysis, but led to a grouping of samples from patients with adenocarcinomas and patients with spread to lymph nodes. The MAS MR spectral profiles showed clear relationships to patient diagnosis. Previous MR spectroscopic studies on cervical cancers have been performed using conventional spectroscopy on intact tissue samples (39, 65, 119). The correlation to patient diagnosis in these studies has been good, but the biochemical information has been limited by low spectral resolution.

The MAS study of brain autopsy samples (paper V) showed that spectra of samples from patients with CLN1 were different from spectra obtained from patients with CLN3 and controls. MAS MR spectroscopy of the brain autopsy samples were applied in order to investigate if this technique could contribute to an increased understanding of altered biochemical processes in the brains of children affected by this neurodegenerative disease. The detected differences were caused by neuronal loss in the frontal cortex in CLN1 patients, as lower levels of NAA and GABA dominated the principal component separating CLN1 from CLN3 and controls. Our findings confirmed previous knowledge of severe neuronal loss in the frontal cortex of CLN1 patients and a moderate loss of frontal cortex neurons in patients affected by CLN3.

The impact of breast cancer tissue heterogeneity on MAS spectra was demonstrated in paper III as the percentage of tumor cells in the specimens was found to influence the spectral profiles. Similar effects on MAS spectra from cell type composition of specimens has been reported by other groups in studies on cancers of other organs (59, 85). It was also shown in paper III that MAS spectral profiles enabled correlation to clinical parameters in spite of heterogeneous tissue samples. The same finding was reported by Swanson *et al.* in a MAS study of prostate tissue (61). Early on it was suggested by Smith *et al.* that other types of tissue dilute the information from cancer cells metabolism (120). As reported by Jagannathan *et al.*, breast tissue from controls and non-involved tissue from patients are dominated by lipid signals (28). In paper I, where samples have been extracted, tissue origin is not verified by microscopy on the same sample.

Several correlations could be found between MAS spectral profiles of breast cancer tissue and clinical descriptions of the tumors (paper III). Relative intensities of cholines were different in tumor tissue compared to non-involved, and tissue concentrations of choline and glycine were elevated in large tumors (> 2 cm). Cheng *et al.* possibly found a method to discriminate invasive ductal carcinomas of different grading (62). In our study however, we could not find apparent correlation between spectral patterns and tissue samples from patients with different histologic type of breast cancer. However, the MAS spectra were found to possibly predict patient lymph node status. A previous study on breast cancer tissue by Smith *et al.* also found a possible connection between breast tumor biochemical profile and lymph node status (121). Both these possible methods of

lymph node prediction are restricted to samples without fat tissue. The high fat content in breast tissue limits such a method, and attempts should be made to include samples of all possible tissue compositions.

The correlation of MAS spectral profiles to patient diagnosis (paper IV and V), verify that the biochemical profiles obtained by the HR MAS technique correspond to pathological changes. MAS spectra of autopsy samples from NCL patients could not provide new information about the deficits, but discriminated the most severe type of the diseases by characterizing neuron loss. However, the potential of HR MAS as a clinical tool for NCL patients is limited. Screening programs and successful treatment have led to high survival rates of cervical cancer in western countries (2). MAS spectra of cervical tissue clearly distinguished cancerous from non-involved samples, and MAS MR spectroscopy under temperature controlled conditions might provide biochemical information about the altered metabolism of tumors.

Negative findings of tumor spread in the axillary lymph nodes of breast cancer patients are associated with good prognosis for the patient. Still, about 25% of these patients experience recurrence or spread of their breast cancer (8). A method that could provide a higher level of confidence in predicting patients with high probability of recurrence or metastasis would make a profound effect for the large number of women affected by the disease. Eight of the 19 samples from negative lymph node patients showed principal component scores values comparable to samples from patients with lymph node spread (paper III). In future studies we would like to compare the possible correlation between MAS spectral profiles of breast tumor tissue and lymph node status to patient outcome after 5 and possibly 10 years. Also, a larger number of samples should be analyzed and compared to these preliminary findings.

6. Conclusion

The HR MAS spectra presented in this thesis provide detailed information about the molecular composition of breast, cervical and brain tissue specimens. HR MAS analysis of intact tissue specimens should be performed at low temperatures to reduce degradation of sample components and minimize the influence from sample treatment on the detected metabolic profiles. Most breast cancer specimens analyzed by HR MAS could be examined by microscopy after HR MAS analysis for a direct comparison to tissue anatomy.

Spectra obtained by HR MAS spectroscopy are highly resolved, and provide detailed information about tissue components at the same level as spectra from tissue extracts. MAS spectroscopy also has the advantage of omitting the possible disturbance of metabolic findings from the extraction procedure.

The detailed chemical profiles of neurodegenerated brain and cancerous cervical and breast tissue were in accordance to patient diagnoses. Brain autopsy spectra showed metabolic features connected to neuronal loss. Cervical and breast tissue showed elevated levels of numerous metabolites, probably connected to general increased cellular activity. MAS spectra from breast cancer samples also provided correlation to clinical findings. A promising result was the possible correlation between the MR spectral profile from breast cancer specimens and patient lymph node status.

7. References

1. Parkin DM, Bray F, Ferlay J, Pisani P. *Estimating the world cancer burden: Globocan 2000*. Int J Cancer (2001) **94**: 153-156.

2. Kleihues P, Stewart BW, World Health Organization. *World cancer report*. 1st edition. Lyon, WHO, IARC Press. (2003)

3. Alberts B, Bray D, Lewis J, Raff M, Roberts K, Watson JD. *Molecular biology of the cell*. 2nd edition. New York, Garland Publishing. (1998)

4. Ruddon RW. *Nature of malignant tumors*. In Cancer Biology. New York: Oxford University Press (1995) 3-18.

5. Hanahan D, Weinberg RA. *The hallmarks of cancer*. Cell (2000) **100**: 57-70.

6. *Cancer in Norway 2000*. 2002. Cancer registry of Norway.

7. Crum CP, Lester SC, Cotran RS. *The female genital system and breast*. In Robbins basic pathology. Editors: V Kumar, RS Cotran, SL Robbins. Philadelphia: Saunders (2003) 679-718.

8. Noguchi M. *Therapeutic relevance of breast cancer micrometastases in sentinel lymph nodes*. Brit J Surg (2002) **89**: 1505-1515.

9. Jones A, McAdam K. *Medical therapy of advanced disease*. In Medical therapy of breast cancer. Editors: Z Rayter, J Mansi. Cambridge: Cambridge University Press (2003) 283-308.

10. Campos SM, Hayes DF. *Breast cancer*. In Atlas of diagnostic oncology. Editors: K Shaffer, T Wieczorek, AT Skarin. Edinburgh: Mosby (2003) 243-281.

11. Eifel P, Axelson JA, Costa J, Crowley J, Curran WJ, Jr., Deshler A, Fulton S, Hendricks CB, Kemeny M, Kornblith AB, Louis TA, Markman M, Mayer R, Roter D. *National Institutes of Health Consensus Development Conference Statement: adjuvant therapy for breast cancer, November 1-3, 2000*. J Natl Cancer Inst (2001) **93**: 979-989.

12. Vizcaino AP, Moreno V, Bosch FX, Munoz N, Barros-Dios XM, Borras J, Parkin DM. *International trends in incidence of cervical cancer: II. Squamous-cell carcinoma*. Int J Cancer (2000) **86**: 429-435.

13. Franco EL, Schlecht NF, Saslow D. *The epidemiology of cervical cancer*. Cancer J (2003) **9**: 348-359.

14. Franco EL, Duarte-Franco E, Ferenczy A. *Cervical cancer: epidemiology, prevention and the role of human papillomavirus infection*. Can Med Assoc J (2001) **164**: 1017-1025.

15. Goebel HH. *The neuronal ceroid-lipofuscinoses*. J Child Neurol (1995) **10**: 424-437.

16. Jolly RD. *Comparative Biology of the Neuronal Ceroid-Lipofuscinosis (NCL): An Overview*. Am J Med Genet (1995) **57**: 307-311.

17. Mitchison HM, Mole SE. *Neurodegenerative disease: the neuronal ceroid lipofuscinoses (Batten disease)*. Curr Opin Neurol (2001) **14**: 795-803.

18. Mole SE. *Batten's disease: eight genes and still counting?* Lancet (1999) **354**: 443-445.

19. Santavuori P, Lauronen L, Kirveskari E, Åberg L, Sainio K, Autti T. *Neuronal ceroid lipofuscinoses in childhood*. Neurological Sciences (2000) **21**: S35-S41.

20. Stryer L. *Biochemistry*. 3rd edition. New York, Freeman. (1988)

21. Meisenberg G, Simmons WHS. *Principles of medical biochemistry*. 1st edition. St. Louis, Mosby. (1998)

22. Michal G. *Biochemical pathways. An atlas of biochemistry and molecular biology*. 1st edition. New York, Wiley. (1999)

23. Warburg O. *The metabolism of tumors*. 1st edition. London, Constable and Co. (1930)

24. Smith TA. *Facilitative glucose transporter expression in human cancer tissue*. Brit J Biomed Sci (1999) **56**: 285-292.

25. Dang CV, Semenza GL. *Oncogenic alterations of metabolism*. Trends Biochem Sci (1999) **24**: 68-72.

26. Ruiz-Cabello J, Cohen JS. *Phospholipid metabolites as indicators of cancer cell function*. NMR Biomed (1992) **5**: 226-233.

27. Podo F. *Tumour phospholipid metabolism*. NMR Biomed (1999) **12**: 413-439.

28. Jagannathan NR, Kumar M, Seenu V, Coshic O, Dwivedi SN, Julka PK, Srivastava A, Rath GK. *Evaluation of total choline from in-vivo volume localized proton MR spectroscopy and its response to neoadjuvant chemotherapy in locally advanced breast cancer*. Brit J Cancer (2001) **84**: 1016-1022.

29. Negendank W. *Studies of human tumors by MRS: a review*. NMR Biomed (1992) **5**: 303-324.

30. Gribbestad IS, Singstad TE, Nilsen G, Fjosne HE, Engan T, Haugen OA, Rinck PA. *In Vivo ^{1}H MRS of Normal Breast and Breast Tumors Using a Dedicated Double Breast Coil*. J Magn Reson Imaging (1998) **8**: 1191-1197.

31. Speck O, Thiel T, Hennig J. *Grading and Therapy Monitoring of Astrocytomas with ^{1}H-Spectroscopy: Preliminary Study*. Anticancer Res (1996) **16**: 1581-1586.

32. Ting Y-LT, Sherr D, Degani H. *Variations in Energy and Phospholipid Metabolism in Normal and Cancer Human Mammary Epithelial Cells*. Anticancer Res (1996) **16**: 1381-1388.

33. Natarajan K, Mori N, Artemov D, Aboagye EO, Chacko VP, Bhujwalla ZM. *Phospholipid profiles of invasive human breast cancer cells are altered towards a less invasive phospholipid profile by the anti-inflammatory agent indomethacin*. Adv Enzyme Regul (2000) **40**: 271-284.

34. Hutchins JB, Naftel JP, Ard MD. *The cell biology of neurons and glia*. In Fundamental neuroscience. Editor: DE Haines. New York: Churchill Livingstone (2002) 15-36.

35. Rockhold RW. *The chemical basis for neuronal communication*. In Fundamental neuroscience. Editor: DE Haines. New York: Churchill Livingstone (2002) 57-70.

36. Derome AE. *Modern NMR techniques for Chemistry research*. 1st edition. Exeter, Pergamon Press. (1991)

37. Podo F, Bovée WMMJ, Certaines JD. *Magnetic resonance spectroscopy in biology and medicinefunctional and pathological tissue characterization* Oxford, Pergamon Press. (1992)

38. Kandel J, Bossy-Wetzel E, Radvanyi F, Klagsbrun M, Folkman J, Hanahan D. *Neovascularization is associated with a switch to the export of bFGF in the multistep development of fibrosarcoma*. Cell (1991) **66**: 1095-1104.

39. Mountford CE, Delikatny EJ, Dyne M, Holmes KT, Mackinnon WB, Ford R, Hunter JC, Truskett ID, Russell P. *Uterine cervical punch biopsy specimens can be analyzed by 1H MRS*. Magn Reson Med (1990) **13**: 324-331.

40. Merchant TE, Gierke LW, Meneses P, Glonek T. *^{31}P magnetic resonance spectroscopic profiles of neoplastic human breast tissue*. Cancer Res (1988) **48**: 5112-5118.

41. Mackinnon WB, Barry PA, Malycha PL, Gillett DJ, Russell P, Lean CL, Doran ST, Barraclough BH, Bilous M, Mountford CE. *Fine-Needle Biopsy Specimens of Benign Breast Lesions Distinguished from Invasive Cancer ex Vivo with Proton NMR Spectroscopy*. Radiol (1997) **204**: 661-666.

42. Mountford CE, Saunders JK, May GL, Holmes KT, Williams PG, Fox RM, Tattersall MH, Barr JR, Russell P, Smith IC. *Classification of human tumours by high-resolution magnetic resonance spectroscopy*. Lancet (1986) **1**: 651-653.

43. Andrew ER. *Magic angle spinning*. In Encyclopedia of nuclear magnetic resonance. Editors: DM Grant, RK Harris. Chichester: Wiley (1996) 2891-2901.

44. Andrew ER, Newing RA. *The Narrowing of Nuclear Magnetic Resonance Spectra by Molecular Rotation in Solids*. The Proceedings of the Physical Society (1958) **72**: 959-972.

45. Lowe IJ. *Free induction decays of rotating solids*. Phys Rev Lett (1959) **2**: 285-287.

46. Mehring M. *Nuclear spin interactions in solids*. In Principles of high resolution NMR in solids. Berlin: Springer (1983) 8-62.

47. Mountford CE, Lean CL, Hancock R, Dowd S, Mackinnon WB, Tattersall MHN, Russell P. *Magnetic Resonance Spectroscopy Detects Cancer in Draining Lymph Nodes*. Invasion Metastasis (1993) **13**: 57-71.

48. Cheng LL, Lean CL, Bogdanova A, Wright SCJr, Ackerman JL, Brady TJ, Garrido L. *Enhanced Resolution of Proton NMR Spectra of Malignant Lymph Nodes Using Magic-Angle Spinning*. Magn Reson Med (1996) **36**: 653-658.

49. Griffin JL, Bollard M, Nicholson JK, Bhakoo K. *Spectral profiles of cultured neuronal and glial cells derived from HRMAS (1)H NMR spectroscopy*. NMR Biomed (2002) **15**: 375-384.

50. Pampel A, Volke F, Engelke F. *Biomembrane Research Using High-Resolution MAS NMR at 750 MHz*. Bruker Report (1998) **145**: 23-26.

51. Gawrisch K, Eldho NV, Polozov IV. *Novel NMR tools to study structure and dynamics of biomembranes*. Chem Phys Lipids (2002) **116**: 135-151.

52. Moka D, Vorreuther R, Schicha H, Spraul M, Humpfer E, Lipinski M, Foxall PJD, Nicholson JK, Lindon JC. *Magic Angle Spinning Proton Nuclear Magnetic Resonance Spectroscopic Analysis of Intact Kidney Tissue Samples*. Anal Commun (1997) **34**: 107-109.

53. Moka D, Vorreuther R, Schicha H, Spraul M, Humpfer E, Lipinski M, Foxall PJD, Nicholson JK, Lindon JC. *Biochemical Classification of Kidney Carcinoma Biopsy Samples Using Magic-Angle-Spinning ^{1}H Nuclear Magnetic Resonance Spectroscopy*. J Pharm Biomed Anal (1998) **17**: 125-132.

54. Cheng LL, Chang I-W, Louis DN, González RG. *Correlation of High-Resolution Magic Angle Spinning Proton Magnetic Resonance Spectroscopy with Histopathology of Intact Human Brain Tumor Specimens*. Cancer Res (1998) **58**: 1825-1832.

55. Barton SJ, Howe FA, Tomlins AM, Cudlip SA, Nicholson JK, Bell BA, Griffiths JR. *Comparison of in vivo 1H MRS of human brain tumours with 1H HR-MAS spectroscopy of intact biopsy samples in vitro*. MAGMA (1999) **8**: 121-128.

56. Tomlins AM, Foxall PJD, Lindon JC, Lynch MJ, Spraul M, Everett JR, Nicholson JK. *High Resolution Magic Angle Spinning ^1H Nuclear Magnetic Resonance Analysis of Intact Prostatic Hyperplastic and Tumour Tissues*. Anal Commun (1998) **35**: 113-115.

57. Tate AR, Foxall PJD, Holmes E, Moka D, Spraul M, Nicholson JK, Lindon JC. *Distinction between normal and renal carcinoma kidney cortical biopsy samples using pattern recognition of ^1H magic angle spinning (MAS) NMR spectra*. NMR Biomed (2000) **13**: 64-71.

58. Cheng LL, Newell K, Mallory AE, Hyman BT, Gonzalez RG. *Quantification of neurons in Alzheimer and control brains with ex vivo high resolution magic angle spinning proton magnetic resonance spectroscopy and stereology*. Magn Reson Im (2002) **20**: 527-533.

59. Tzika AA, Cheng LL, Goumnerova L, Madsen JR, Zurakowski D, Astrakas LG, Zarifi MK, Scott RM, Anthony DC, Gonzalez RG, Black PM. *Biochemical characterization of pediatric brain tumors by using in vivo and ex vivo magnetic resonance spectroscopy*. J Neurosurg (2002) **96**: 1023-1031.

60. Cheng LL, Wu C, Smith MR, González RG. *Non-destructive quantification of spermine in human prostate tissue samples using HR MAS ^1H NMR spectroscopy at 9.4 T*. FEBS Lett (2001) **494**: 112-116.

61. Swanson MG, Vigneron DB, Tabatabai ZL, Males RG, Schmitt L, Carroll PR, James JK, Hurd RE, Kurhanewicz J. *Proton HR-MAS spectroscopy and quantitative pathologic analysis of MRI/3D-MRSI-targeted postsurgical prostate tissues*. Magn Reson Med (2003) **50**: 944-954.

62. Cheng LL, Chang I-W, Smith BL, González RG. *Evaluating human breast ductal carcinomas with high-resolution magic-angle spinning proton magnetic resonance spectroscopy*. J Magn Reson (1998) **135**: 194-202.

63. Ala-Korpela M, Posio P, Mattila S, Korhonen A, Williams SR. *Absolute Quantification of Phospholipid Metabolites in Brain-Tissue Extracts by ^1H NMR Spectroscopy*. J Magn Reson B (1996) **113**: 184-189.

64. Cheng LL, Ma MJ, Becerra L, Ptak T, Tracey I, Lackner A, González RG. *Quantitative neuropathology by high resolution magic angle spinning proton nuclear magnetic resonance spectroscopy*. Proc Natl Acad Sci USA (1997) **94**: 6408-6413.

65. Delikatny EJ, Russell P, Hunter JC, Hancock R, Atkinson K.H., van Haaften-Day C., Mountford CE. *Proton MR and human cervical neoplasia: ex vivo spectroscopy allows*

distinction of invasive carcinoma of the cervix from carcinoma in situ and other preinvasive lesions. Radiol (1993) **188**: 791-796.

66. Rutter A, Hugenholtz H, Saunders JK, Smith ICP. *Classification of Brain Tumors by Ex Vivo ^{1}H NMR Spectroscopy.* J Neurochem (1995) **64**: 1655-1661.

67. Lean CL, Newland RC, Ende DA, Bokey EL, Smith IC, Mountford CE. *Assessment of Human Colorectal Biopsies by ^{1}H MRS: Correlation with Histopathology.* Magn Reson Med (1993) **30**: 525-533.

68. Leach MO, Verrill M, Glaholm J, Smith TA, Collins DJ, Payne GS, Sharp JC, Ronen SM, McCready VR, Powles TJ, Smith IE. *Measurements of human breast cancer using magnetic resonance spectroscopy: a review of clinical measurements and a report of localized 31P measurements of response to treatment.* NMR Biomed (1998) **11**: 314-340.

69. el Deredy W. *Pattern recognition approaches in biomedical and clinical magnetic resonance spectroscopy: a review.* NMR Biomed (1997) **10**: 99-124.

70. Hagberg G. *From magnetic resonance spectroscopy to classification of tumors. A review of pattern recognition methods.* NMR Biomed (1998) **11**: 148-156.

71. Lindon JC, Holmes E, Nicholson JK. *Pattern recognition methods and applications in biomedical magnetic resonance.* Prog Nucl Magn Reson Spectrosc (2001) **39**: 1-40.

72. Bollard ME, Xu J, Purcell W, Griffin JL, Quirk C, Holmes E, Nicholson JK. *Metabolic profiling of the effects of D-galactosamine in liver spheroids using ^{1}H NMR and MAS-NMR spectroscopy.* Chemical Research in Toxicology 15, 1351-1359. 2002.

73. Anthony ML, Sweatman BC, Beddell CR, Lindon JC, Nicholson JK. *Pattern Recognition Classification of the Site of nephrotoxicity Based on metabolic Data derived from Proton Nuclear Magnetic Resonance Spectra of Urine.* Mol Parmacol (1994) **46**: 199-211.

74. Garrod S, Humpfer E, Spraul M, Connor SC, Polley S, Connelly J, Lindon JC, Nicholson JK, Holmes E. *High-Resolution Magic Angle Spinning ^{1}H NMR Spectroscopic Studies on Intact Rat Renal Cortex and Medulla.* Magn Reson Med (1999) **41**: 1108-1118.

75. Middleton DA, Bradley DP, Connor SC, Mullins PG, Reid DG. *The effect of Sample Freezing on Proton Magic-Angle Spinning NMR Spectra of Biological Tissue.* Magn Reson Med (1998) **40**: 166-169.

76. Waters NJ, Garrod S, Farrant RD, Haselden JN, Connor SC, Connelly J, Lindon JC, Holmes E, Nicholson JK. *High-resolution magic angle spinning ^{1}H NMR spectroscopy of intact liver and kidney: optimization of sample preparation procedures and*

biochemical stability of tissue during spectral acquisition. Anal Biochem (2000) **282**: 16-23.

77. Isachenko E, Isachenko V, Katkov II, Dessole S, Nawroth F. *Vitrification of mammalian spermatozoa in the absence of cryoprotectants: from past practical difficulties to present success*. Reprod Biomed Online (2003) **6**: 191-200.

78. Bourne R, Dzendrowskyj T, Mountford C. *Leakage of metabolites from tissue biopsies can result in large errors in quantitation by MRS*. NMR Biomed (2003) **16**: 96-101.

79. Wind RA, Hu JZ, Rommereim DN. *High-resolution ^{1}H NMR spectroscopy in organs and tissues using slow magic angle spinning*. Magn Reson Med (2001) **46**: 213-218.

80. Rooney OM, Troke J, Nicholson JK, Griffin JL. *High-resolution diffusion and relaxation-edited magic angle spinning 1H NMR spectroscopy of intact liver tissue*. Magn Reson Med (2003) **50**: 925-930.

81. Waters NJ, Holmes E, Waterfield CJ, Farrant RD, Nicholson JK. *NMR and pattern recognition studies on liver extracts and intact livers from rats treated with alpha-naphthylisothiocyanate*. Biochem Pharmacol (2002) **64**: 67-77.

82. Millis K, Weybright P, Campbell N, Fletcher JA, Fletcher CD, Cory DG, Singer S. *Classification of Human Liposarcoma and Lipoma Using Ex Vivo NMR Spectroscopy*. Magn Reson Med (1999) **41**: 257-267.

83. Garrod S, Humpfer E, Connor SC, Connelly JC, Spraul M, Nicholson JK, Holmes E. *High-resolution ^{1}H NMR and magic angle spinning NMR spectroscopic investigation of the biochemical effects of 2-bromoethanoamine in intact renal and hepatic tissue*. Magn Reson Med (2001) **45**: 781-790.

84. Bollard ME, Garrod S, Holmes E, Lindon JC, Humpfer E, Spraul M, Nicholson JK. *High-Resolution ^{1}H and ^{1}H-^{13}C Magic Angle Spinning NMR Spectroscopy of Rat Liver*. Magn Reson Med (2000) **44**: 201-207.

85. Cheng LL, Anthony DC, Comite AR, Black PM, Tzika AA, González RG. *Quantification of microheterogeneity in glioblastoma multiforme with ex vivo high-resolution magic-angle spinning (HRMAS) proton magnetic resonance spectroscopy*. Neuro-Oncology (2000) **2**: 87-95.

86. Griffin JL, Troke J, Walker LA, Shore RF, Lindon JC, Nicholson JK. *The biochemical profile of rat testicular tissue as measured by magic angle spinning 1H NMR spectroscopy*. FEBS Lett (2000) **486**: 225-229.

87. Taylor JL, Wu CL, Cory D, Gonzalez RG, Bielecki A, Cheng LL. *High-resolution magic angle spinning proton NMR analysis of human prostate tissue with slow spinning rates*. Magn Reson Med (2003) **50**: 627-632.

88. Farrant RD, Lindon JC, Nicholson JK. *Internal Temperature Calibration for ^1H NMR Spectroscopy Studies of Blood Plasma and other Biofluids*. NMR Biomed (1994) **7**: 243-247.

89. Ernst M, Kentgens APM, Meier BH. *2D Exchange NMR Spectra under Slow MAS: A Simplified Scheme to Obtain Pure-Phase Spectra without Unwanted Cross Peaks*. J Magn Reson (1999) **138**: 66-73.

90. Kriat M, Confort-Gouny S, Vion-Dury J, Sciaky M, Viout P, Cozzone PJ. *Quantitation of Metabolites in Human Blood Serum by Proton Magnetic Resonance Spectroscopy. A Comparative Study of the Use of Formate and TSP as Concentration Standards*. NMR Biomed (1992) **5**: 179-184.

91. Askenasy N, Kushnir T, Navon G, Kaplan O. *Differences in metabolite content between intact pancreases and their perchloric acid extracts. A 2D 1H/31P correlation NMR study*. NMR Biomed (1990) **3**: 220-226.

92. Ross BD. *The biochemistry of living tissues: examination by MRS*. NMR Biomed (1992) **5**: 215-219.

93. Beckonert O, Monnerjahn J, Bonk U, Leibfritz D. *Visualizing metabolic changes in breast-cancer tissue using 1H-NMR spectroscopy and self-organizing maps*. NMR Biomed (2003) **16**: 1-11.

94. Walenta S, Wetterling M, Lehrke M, Schwickert G, Sundfor K, Rofstad EK, Mueller-Klieser W. *High lactate levels predict likelihood of metastases, tumor recurrence, and restricted patient survival in human cervical cancers*. Cancer Res (2000) **60**: 916-921.

95. Roslin M, Henriksson R, Bergstrom P, Ungerstedt U, Bergenheim AT. *Baseline levels of glucose metabolites, glutamate and glycerol in malignant glioma assessed by stereotactic microdialysis*. J Neurooncol (2003) **61**: 151-160.

96. Dang CV, Lewis BC, Dolde C, Dang G, Shim H. *Oncogenes in tumor metabolism, tumorigenesis, and apoptosis*. J Bioenerg Biomembr (1997) **29**: 345-354.

97. Nakagami K, Uchida T, Ohwada S, Koibuchi Y, Suda Y, Sekine T, Morishita Y. *Increased Choline Kinase Activity and Elevated Phosphocholine Levels in Human Colon Cancer*. Jpn J Cancer Res (1999) **90**: 419-424.

98. Herminghaus S, Pilatus U, Moller-Hartmann W, Raab P, Lanfermann H, Schlote W, Zanella FE. *Increased choline levels coincide with enhanced proliferative activity of human neuroepithelial brain tumors*. NMR Biomed (2002) **15**: 385-392.

99. Nelson SJ. *Multivoxel magnetic resonance spectroscopy of brain tumors*. Mol Cancer Ther (2003) **2**: 497-507.

100. Florian CL, Preece NE, Bhakoo KK, Williams SR, Noble M. *Characteristic metabolic profiles revealed by 1H NMR spectroscopy for three types of human brain and nervous system tumours*. NMR Biomed (1995) **8**: 253-264.

101. Ackerstaff E, Pflug BR, Nelson JB, Bhujwalla ZM. *Detection of increased choline compounds with proton nuclear magnetic resonance spectroscopy subsequent to malignant transformation of human prostatic epithelial cells*. Cancer Res (2001) **61**: 3599-3603.

102. Katz-Brull R, Seger D, Rivenzon-Segal D, Rushkin E, Degani H. *Metabolic markers of breast cancer: enhanced choline metabolism and reduced choline-ether-phospholipid synthesis*. Cancer Res (2002) **62**: 1966-1970.

103. Ramirez de Molina, Rodriguez-Gonzalez A, Gutierrez R, Martinez-Pineiro L, Sanchez J, Bonilla F, Rosell R, Lacal J. *Overexpression of choline kinase is a frequent feature in human tumor-derived cell lines and in lung, prostate, and colorectal human cancers*. Biochem Biophys Res Commun (2002) **296**: 580-583.

104. Ramirez de Molina, Gutierrez R, Ramos MA, Silva JM, Silva J, Bonilla F, Sanchez JJ, Lacal JC. *Increased choline kinase activity in human breast carcinomas: clinical evidence for a potential novel antitumor strategy*. Oncogene (2002) **21**: 4317-4322.

105. Kinoshita Y, Yokota A. *Absolute concentrations of metabolites in human brain tumors using in vitro proton magnetic resonance spectroscopy*. NMR Biomed (1997) **10**: 2-12.

106. Peeling J, Sutherland G. *High-resolution ^{1}H NMR spectroscopy studies of extracts of human cerebral neoplasm*. Magn Reson Med (1992) **24**: 123-136.

107. Stapleton PP, O'Flaherty L, Redmond HP, Bouchier-Hayes DJ. *Host defense--a role for the amino acid taurine?* JPEN J Parenter Enteral Nutr (1998) **22**: 42-48.

108. Kaplan O, Kushnir T, Askenazy N, Knubovets T, Navon G. *Role of nuclear magnetic resonance spectroscopy (MRS) in cancer diagnosis and treatment: 31P, 23Na, and 1H MRS studies of three models of pancreatic cancer*. Cancer Res (1997) **57**: 1452-1459.

109. Moreno A, Rey M, Montane JM, Alonso J, Arus C. *1H NMR spectroscopy of colon tumors and normal mucosal biopsies; elevated taurine levels and reduced polyethyleneglycol absorption in tumors may have diagnostic significance*. NMR Biomed (1993) **6**: 111-118.

110. Shears SB. *The versatility of inositol phosphates as cellular signals*. Biochim Biophys Acta (1998) **1436**: 49-67.

111. Punnonen K, Hietanen E, Auvinen O, Punnonen R. *Phospholipids and fatty acids in breast cancer tissue*. J Cancer Res Clin Oncol (1989) **115**: 575-578.

112. Louw L, Engelbrecht AM, Cloete F. *Comparison of the fatty acid compositions in intraepithelial and infiltrating lesions of the cervix: part I, total fatty acid profiles*. Prostaglandins Leukot Essent Fatty Acid (1998) **59**: 247-251.

113. Engelbrecht AM, Louw L, Cloete F. *Comparison of the fatty acid compositions in intraepithelial and infiltrating lesions of the cervix: part II, free fatty acid profiles*. Prostaglandins Leukot Essent Fatty Acid (1998) **59**: 253-257.

114. Baslow MH. *N-acetylaspartate in the vertebrate brain: metabolism and function*. Neurochem Res (2003) **28**: 941-953.

115. Brand A, Richter-Landsberg C, Leibfritz D. *Multinuclear NMR studies on the energy metabolism of glial and neuronal cells*. Dev Neurosci (1993) **15**: 289-298.

116. Seitz D, Grodd W, Schwab A, Seeger U, Klose U, Nagele T. *MR imaging and localized proton MR spectroscopy in late infantile neuronal ceroid lipofuscinosis*. Am J Neuroradiol (1998) **19**: 1373-1377.

117. Brockmann K, Pouwels PJ, Christen HJ, Frahm J, Hanefeld F. *Localized proton magnetic resonance spectroscopy of cerebral metabolic disturbances in children with neuronal ceroid lipofuscinosis*. Neuropediatrics (1996) **27**: 242-248.

118. Kakela R, Somerharju P, Tyynela J. *Analysis of phospholipid molecular species in brains from patients with infantile and juvenile neuronal-ceroid lipofuscinosis using liquid chromatography-electrospray ionization mass spectrometry*. J Neurochem (2003) **84**: 1051-1065.

119. Künnecke B, Delikatny EJ, Russell P, Hunter JC, Mountford CE. *Proton Magnetic Resonance and Human Cervical Neoplasia. II. Ex Vivo Chemical-Shift Microimaging*. J Magn Reson B (1994) **104**: 135-142.

120. Smith TA, Glaholm J, Leach MO, Machin L, McCready VR. *The effect of intra-tumour heterogeneity on the distribution of phosphorus-containing metabolites within human breast tumours: an in vitro study using 31P NMR spectroscopy*. NMR Biomed (1991) **4**: 262-267.

121. Mountford CE, Somorjai RL, Malycha PL, Gluch L, Lean CL, Russell P, Barraclough BH, Gillett DJ, Himmelreich U, Dolenko B, Nikulin AK, Smith ICP. *Diagnosis and prognosis of breast cancer by magnetic resonance spectroscopy of fine-needle aspirates analysed using a statistical classification strategy*. Brit J Surg (2001) **88**: 1234-1240.

Paper I

URN:NBN:no-3463

ANTICANCER RESEARCH *19:* 1737-1746 (1999)

Metabolite Composition in Breast Tumors Examined by Proton Nuclear Magnetic Resonance Spectroscopy

I.S. GRIBBESTAD[1], B. SITTER[1], S. LUNDGREN[2], J. KRANE[3] and D. AXELSON [1,4]

[1]*SINTEF Unimed MR Center, N-7034 Trondheim;* [2]*Department of Oncology, University Hospital, N-7006 Trondheim;*
[3]*NTNU, Department of Chemistry, N-7034 Trondheim, Norway;*
[4]*Queen's University, Department of Chemistry, Kingston, Ontario, Canada*

Abstract. *Background: In vivo characterisation of breast tumors using proton (^{1}H) MR spectroscopy relies upon in vitro interpretation of tissue samples. The present study has investigated metabolite composition in extracts from breast tumors and non-involved breast tissue. Multivariate data analysis was used to determinate combinations of metabolites important for differentiation. Materials and Methods: Tumor and non-involved breast tissue were obtained from 16 patients undergoing surgical treatment. ^{1}H NMR spectra of perchloric acid tissue extracts were obtained at a BRUKER Avance DRX600 spectrometer. The data was analysed using principal component analysis and probabilistic neural networks. Results: Low levels of glucose and high content of choline compounds were dominant findings in the tumor spectra. Principal component loadings demonstrated this strong association. The spectra were correctly classified using neural network analysis. Conclusions: Large differences in the metabolite composition of breast tumors and surrounding breast tissues have been documented.*

In Norway breast cancer is the leading cause of cancer-related death among women and the incidence is strongly increasing (1). Improved diagnostic methods for early detection, for better differentiation, and for evaluation of therapeutic effects are important in trying to gain control of the increase. Dynamic contrast enhanced T1- weighted MR imaging is established as an important diagnostic tool (2) but differentiation between malignant and benign tumors is often difficult. Recently, new methods such as $T2^*$-weighted first pass perfusion MRI have been shown to increase the specificity for differentiating breast tumors (3; 4).

Correspondence to: Ingrid S. Gribbestad, SINTEF Unimed, MR Center, N-7034 Trondheim, Norway. Phone: +4773590493; Telefax+4773867708. E-mail: Ingrid.S.Gribbestad@.unimed.sintef.no

Key Words: MR spectroscopy, breast cancer, tumor metabolism, perchloric acid extracts, phosphocholine, choline.

MR spectroscopy (MRS) has a unique role in clinical research as a technique for non- invasive monitoring of body metabolism. *In vivo* applications of MRS have reached the point where clinical trials are underway for a number of different applications (5). Preul and co-workers have shown that using *in vivo* ^{1}H chemical shift imaging (CSI) on human brain tumors improves the preoperative clinical diagnosis from 77% to 99% accuracy when combined with pattern ented that ^{1}H MRS can be utilised for identification of brain tumors not detectable with contrast enhanced MRI, and that this technique might be important for better definition of tumor borders (7). Furthermore, addition of MR spectroscopic imaging to MRI significantly improves the specificity of prostate cancer diagnostics (8). In a recent *in vivo* ^{1}H MRS study, we demonstrated high concentrations of choline compounds in breast carcinomas (9). The ability of *in vivo* ^{1}H MRS for differentiation of benign and malignant tumors is now being investigated (10).

Several studies have shown that *ex vivo* MR spectroscopy of biopsies taken from suspicious thyroid, cervix, ovarian and colon tissue can be used for discriminating benign tumors from malignant (11; 12). *Ex vivo* ^{1}H MRS could also be used for distinguishing malignant from benign prostatic tissue with high sensitivity and specificity, and might be useful for discriminating fast and slow growing prostate tumors (13). Recently, a study using *ex vivo* MR spectroscopy to investigate fine- needle biopsy specimens of benign and invasive breast cancer reported a sensitivity of 95% and a specificity of 96% in distinguishing benign lesions from invasive breast cancer. This result was based upon the ratio of the signal at 3.25 ppm to the signal at 3.05 ppm, calculated from measured peak heights in the spectra (14).

In an approach aimed at characterisation of breast tumors *in vivo* we have reported ^{1}H NMR studies of perchloric acid (PCA) extracts of breast carcinomas and non-involved breast tissue (15). Better resolved spectra obtained from tissue extracts allow for more precise assignment of resonances and identification of components

0250-7005/99 $2.00+.40

seen in the low-resolution *in vivo* ^{1}H spectra of breast tissue. This information is also of crucial importance in interpretation of *ex vivo* MR spectra of tissue biopsies. In accordance with other reports (16), our studies demonstrated variations in phosphocholine (PC) and phosphoethanolamine (PE) content in malignant and non-involved breast tissue from the same origin (15). Differences in levels of other metabolites like amino acids, sugars, lactate, inositols and phosphocreatine were also observed (15).

Multivariate data analysis has been applied for classification of NMR spectra using a number of different methods (17). Examples of such supervised learning techniques are principal component analysis and artificial neural networks. Automated classification of human brain tumors by neural network analysis using *in vivo* ^{1}H magnetic resonance spectroscopic metabolite data was successful even if there was no simple statistically significant metabolite concentration differences between the tissue groups (18). MRS allows for observation of a large number of metabolites simultaneously and without preselection. Combined with the development of a suitable multivariate data analysis, the user is not required to make objective assumptions regarding which spectral factors are most relevant to the problem under investigation.

The purpose of the present study was to investigate metabolite composition and concentration of selected metabolites in extracts from breast tumors and non-involved breast tissue. Multivariate data analysis was used for determination of metabolites or combinations of metabolites important for distinguishing the two types of tissues.

Materials and Methods

Patient selection/Tissue preparation. Tumor and non-involved tissue were obtained from patients undergoing surgical treatment. A total of 16 patients were included in this study, with samples from tumor tissue and non-involved tissue in the same breast. Patient data including histology are listed in Table I. All specimens were immediately immersed in liquid nitrogen and stored at -80°C until perchloric acid extraction. Preparation of PCA extracts was performed according to previously described procedure (19). Before NMR analysis, the samples were dissolved in 600 µl phosphate buffer (0.055 M KH_2PO_4 and 0.045 M NaOD, uncorrected pH of 7.50), containing 0.05 mM TSPA-d*4* (3-(trimethylsilyl-) 3,3,2,2-tetradeutero-propionic acid) for internal reference.

NMR measurements. All experiments were performed on a BRUKER Avance DRX600 spectrometer (BRUKER, Germany) using a 5 mm QXI probe (H, X inverse) with triple gradients. The spectra were acquired at 25°C. The lD-proton spectra were obtained using a water presaturation period of 10 seconds followed by a 90° excitation pulse, 128 free induction decays of an accumulated spectral width of 12 kHz were collected into 64 K data points. The acquisition time was 2.7 seconds, giving a total repetition time of 12.7 seconds.

Data analysis. The concentration of selected metabolites was estimated by curve fitting using an internal standard (TSP). The areas of selected signals in the spectra were calculated using PeakFit (Jandel Scientific). The curve fitting function used was Voigt area, which is a combination of Lorentian and Gaussian lineshapes. The correlation factor (r^2) was better than 0.995 for all calculations.

For the principal component analysis, the estimated concentrations of selected metabolites given in Table II were used as input values. The first eigenvalue accounts for 66% of the total variance in the data, the second and third account for 16.8% and 6.1%, respectively. Thus, the first three eigenvalues account for almost 90% of the total variance in the data.

Probabilistic Neural Networks (PNN) were used to categorise the samples in two classes, each sample was assigned to either [1,0] for non-infiltrated tissue or [0,1] for tumor tissue. Three different approaches for network analysis were applied. First, the concentrations of selected metabolites were used as input values. Then two methods using raw data from the spectrum region 2.80–3.50 ppm were tested as input without regard to detailed assignments or preselection of peaks. One method employed all chemical shifts within the stated range and in the other principal component scores was first calculated. In the former case the analysis involved 1000 input values and the latter only 17. Output values represent probability density estimates and add up to 1. Highest output corresponds to the most probable category and the minimum value for classification was set to 0.501.

Results

Assignment of the metabolites in the spectra of tumors and non-involved breast tissue was done according to published data (20), spiking with authentic compounds and two-dimensional NMR spectroscopy (*i.e.* COSY, J-resolved and HSQC). The ^{1}H NMR spectra of extracts of breast specimens provided a comprehensive window into the metabolic activities of the tissue. Identified metabolites included glucose (Glc), lactate, amino acids, phosphocholine (PC), phosphoethanolamine (PE) and polyamines (Figure 1).

Several differences in the metabolite content of extracts are obvious when comparing spectra from tumors and non-involved breast tissue. As we have reported earlier, the spectra from non-involved breast tissue are dominated by signals from glucose and other carbohydrates, while most tumors have very low levels of Glc (15). This can also be seen from the calculated concentrations for Glc given in Table I. It was not possible to quantify Glc in 8 of 14 tumor samples, while the concentration ranged from 0.12 to 1.1 µmol /g wet weight in non-involved breast tissue (Table II). The concentration of selected metabolites was estimated by curve fitting using an internal standard (TSP). The correlation factor (r^2) was better than 0.995 for all calculations.

The spectrum region 3.19 ppm to 3.31 ppm from a carcinoma and non-involved breast tissue is plotted in Figure 2. The major metabolites in this spectral region are choline (Cho), PE, PC, glycerophosphocholine (GPC), taurine (Tau), *myo*-inositol (*myo*-Ino) and ß-Glc. The sum of choline compounds, tCho (Cho+PC+GPC) is a factor 10-15 times larger in tumor extracts compared to non-infiltrated tissue extracts. In extracts from non-infiltrated

Table I. *Clinical and pathological characteristics.*

no	Age (years)	T (mm)	Regional lymph nodes	pT (mm)	p(x/y)	Histopathology	Grade	DNA analysis	Receptor status
1	47	30	N0	25	1/11	DC	III	Tetraploid	neg
2	70	80	N0	45	2/13	DC	III	Aneuploid	pos
3	73	15	N0	10	0/7	DC	I	NA	pos
4	62	95	N1	NA	0/15	Low differentiated carcinoma	-	NA	neg
5	33	75	N1	NA	NA	DC	III	NA	pos
6	66	55	N0	35	0/7	DC	I	Aneuploid	pos
7	80	30	N0	20	NA	LC +LCIS	-	Aneuploid	NA
8	78	21	N0	25	0/8	DC	II	Tetraploid	pos
9	83	80	N1	NA	NA	Medullary carcinoma	-	NA	neg
10	76	22	N0	20	1/7	DC	III	Aneuploid	pos
11	79	60	N0	50	NA	DC	II	NA	pos
12	70	60	N0	33	0/13	Mucinous carcinoma	-	Diploid	pos
13	48	45	N0	32	1/11	DC	II	Diploid	neg
14	50	44	N0	30	1/14	DC	III	Diploid	pos
15	53	T0	N0	14	NA	Fibroadenoma	-	NA	NA
16	47	30	N0	35	0/7	DC	II	Aneuploid	pos

Abbreviations used: N0: no palpable lymph nodes, N1: solitary palpable lymph nodes, DC: infiltatring ductal carcinoma, LC: infiltrating lobular carcinoma, LCIS: lobular carcinoma in situ, NA: not analyzed, T: clinical tumor size, pT: pathological tumor size, p(x/y): number of positive lymph nodes/number of analysed lymph nodes.

breast tissue, the GPC content is on average higher than the PC content (0.042 vs. 0.029 μmol/g wet weight tissue), while the level of Cho is approximately half the PC content. All choline-containing compounds were increased in tumor extracts and the relative composition of the metabolites was altered. The PC concentration is 3 times higher than GPC, which again is twice the concentration of Cho (Table II). The PE /tCho ratio is within the same range (1.8) in the two groups, due to a strong increase also in PE in tumor extracts (Table II).

Glc is dominant in spectra from non-involved breast tissue, whereas the content of *myo*-Ino is much more variable. In five out of the 16 spectra of tumor tissue, quantification of the *myo*-Ino peak at 3.28 ppm was not possible. In the remaining 11 spectra, the contribution of myo-Ino was larger than in spectra of non-involved tissue extracts. Taurine had much higher values in the tumor extracts, except for the samples from the mucinous carcinoma and the lobular carcinoma with a large proportion of in situ cancer.

The score plot of the two groups using the principal component analysis is shown in Figure 3. The first group comprises most of the tumor samples while the second includes most of non-infiltrated tissue samples. In the first region all samples belong to a single class, the spread in the points reflects the normal biochemical variation in components of malignant tissues. The second region, dominated by samples characteristic of the non-involved tissue, also contain two samples (patient 7 and 15) which do not belong in this category.

The relationship between the score plot positioning and the metabolite composition can be explored by considering loadings of eigenvectors in the principal component analysis (Figure 3). A negative first principal component (PC1) loading is strongly associated with the value of the ß-Glc metabolite. Thus, this is a feature that separates the two classes of tissue samples. A positive loading on PCl is dominated in similar proportions by a combination of metabolites PC, choline, GPC, taurine, PE, lactate and alanine. Negative PC2 positioning of scores is related mostly to *myo*-inositol and positive PC2 correlation by phosphocholine.

Table II. *Calculated concentrations (μmol/g wet weight) using curve fitting for a selected number of metabolites in non-infiltrated (A) and tumor (B) extracts, using the resonances at: Choline (Cho) 3.21 ppm, phosphocholine (PC) 3.22 ppm, glycerophosphocholine (GPC) 3.23 ppm, phosphoetanolamine (PE) 3.22 ppm, alanine (Ala) 1.47 ppm, lactate (Lac) 1.33 ppm, ß-glucose (ß-Glc) 3.25 ppm, myo-inositol (m-Ino) 3.28 ppm and taurine (Tau) 3.27 ppm. For some of the patients, two samples of the same tissue type were analysed. *Patient 5 had received tamoxifen treatment prior to operation.*

A

Patient no.	Histology	Cho	GPC	PC	tCho	PE	Ala	Lac	ß-GIC	m-Ino	Tau
3	N	0.024	0.066	0.035	0.124	0.136	0.119	0.855	0.432	0.259	0.191
4	N	0.005	0.014	0.005	0.024	0.033	0.016	0.119	0.070	0.184	0.016
5	N	0.008	0.028	0.016	0.053	0.037	0.034	0.437	0.145	0.218	0.040
6	N	0.020	0.025	0.021	0.066	0.076	0.090	1.044	0.832	0.256	0.112
7	N	0.015	0.018	0.013	0.046	0.084	0.085	0.319	0.354	0.195	0.118
8	N	0.022	0.035	0.030	0.087	0.317	0.117	0.585	0.677	0.363	0.202
10	N	0.025	0.143	0.075	0.243	0.304	0.129	0.571	1.062	0.762	0.448
12	N	0.008	0.039	0.017	0.064	0.084	0.054	0.281	0.468	0.313	0.139
13	N	0.008	0.005	0.004	0.017	0.206	0.054	0.321	0.224	0.183	0.100
14	N	0.007	0.050	0.010	0.067	0.122	0.037	0.250	0.293	0.468	0.126
15	N	0.019	0.047	0.065	0.131	0.191	0.098	1.031	0.996	0.448	0.338
16	N	0.032	0.029	0.062	0.123	0.334	0.136	1.105	0.745	0.697	0.291
Average		0.016	0.042	0.029	0.087	0.160	0.081	0.577	0.525	0.362	0.177
Standard deviation		0.009	0.036	0.025	0.062	0.109	0.041	0.349	0.332	0.197	0.126

continued

In the neural network analysis of spectra using concentrations of selected metabolites all spectra were correctly classified. The lowest category probabilities were 0.572 (lobular/LCIS) and 0.615 for one control sample. All samples were also correctly predicted when using raw data from a defined spectrum region. Reducing the number of input variables by principal component analysis give faster calculations with the same high predictions (100 % correct). The response was the same regardless of the choice of test/training samples.

Discussion

One major focus for in vivo MRS in cancer diagnostics has been differentiating tumor lesions and discriminating these from surrounding tissue. The tissue types must have different metabolic characteristics to obtain such differentiation. In the present study, samples of non-involved tissue surrounding the tumor were used as controls. The major part of the non-involved specimens consisted of fatty tissue (adipose cells) and glandular tissue (epithelial and myoepithelial cells), with contribution from small vessels. Thus, the metabolite composition expressed in the spectrum represents several cell types. The fact that tissue specimen contain different cell types and possibly also different fractions of these in each sample, must be considered when interpreting the MR spectra. Most tumor samples were excised from carcinomas and one fibroadenoma, which orginate from epithelial cells. Furthermore, the tumor samples might also contain fatty and glandular breast tissue.

Elevated levels of phosphomonoesters (PME) have been found in most human cancers when comparing to corresponding normal tissue (21; 22). This has also been shown in animal tumor models as well as cell cultures (23; 24). PC and PE are derived from either uptake of exogenous choline and ethanolamine, or produced by phospholipase action on phosphatidylcholine and -ethanolamine, respectively (25). The interests of non-invasively observe PME levels are the unique opportunity to monitor these metabolites in patients during treatment. Decrease in PME has been observed in response to treatment for different types of tumors (21). PME can also in conjunction with other tumor metabolites detected with

Table II. *continued.*

B

Patient no.	Histology	Cho	GPC	PC	PE	tCho	Ala	Lac	ß-GlC	m-Ino	Tau
3	DC.I	0.103	0.278	0.414	1.358	0.794	0.409	7.738	ND	0.891	2.607
4	DC.II	0.381	0.200	0.506	1.063	1.086	0.980	7.176	0.581	2.386	2.541
6	DC.I	0.106	0.070	1.400	1.406	1.576	0.967	10.441	ND	0.453	2.107
7	DC+LCIS	0.046	0.025	0.061	0.283	0.132	0.164	1.737	0.487	0.426	0.315
8	DC.II	0.123	0.174	1.538	4.190	1.835	0.925	8.426	ND	ND	8.278
9	Medullary carcinoma	0.162	0.363	0.855	2.853	1.380	1.632	9.083	ND	ND	5.222
10	DC.III	0.094	0.268	1.327	1.988	1.689	0.733	7.811	ND	ND	3.930
11	DC.II	0.117	0.621	1.263	3.348	2.001	0.927	10.461	ND	ND	5.549
12	Mucinous carcinoma	0.047	0.104	0.249	0.510	0.400	0.253	1.916	0.816	0.615	0.701
12	Mucinous carcinoma	0.067	0.134	0.148	1.685	0.349	0.290	2.328	0.662	0.874	0.759
13	DC.II	0.097	0.195	0.452	1.900	0.745	0.577	5.245	0.779	1.269	1.861
13	DC.II	0.202	0.676	0.455	3.441	1.333	0.845	8.693	ND	3.860	5.822
14	DC.III	0.120	0.304	0.718	2.459	1.141	0.692	8.555	1.098	1.853	3.171
16	DC.II	0.134	0.442	1.640	2.362	2.216	0.985	11.636	ND	ND	2.984
Average		0.128	0.275	0.788	2.060	1.191	0.741	7.232	0.737	1.403	3.275
SD		0.084	0.195	0.545	1.131	0.644	0.388	3.233	0.215	1.132	2.271
15	Fibroadenoma	0.022	0.069	0.108	0.369	0.199	0.110	1.482	0.978	0.465	0.338
5	DC.III*	0.0046	0.134	0.105	0.839	0.245	0.357	1.433	1.149	1.938	1.203

MRS discriminate among different type and grade of tumors (6). Despite all these observations, there is no clear explanation for the variation of phospholipid metabolites in tumor tissue (26).

The level of PC shows a significant variability in the present study (Table II). Many studies have recently focused upon parameters that might regulate the MR visibility of these peaks. Aiken and Gillies (23) suggest from their studies of different breast cancer cells that the PME level is regulated by a combination of extrinsic (such as necrosis, perfusion, availibility of nutrients) and intrinsic (such as proliferative status) factors. They found that PE was more under intrinsic control than PC (23). Ting *et al* (26) have compared the metabolism of human mammary epithelial cells and human breast cancer cells (MCF7 and T47D) which proliferate at approximately same rate. The results demonstrated significant lower levels of PC, PE and glycerol derivatives in normal cells compared to cancer cells. These results suggest that variations in phospholipid metabolism are associated with malignancy, and not with proliferation rate. The same group (24) demonstrated enhanced choline transport and choline kinase activity in breast cancer cells. They concluded that these two factors are responsible for the presence of high PC in breast cancer cells (24).

Previous *in vitro* MR spectroscopy studies of perchloric acid extracts of excised breast cancer tissue and fine needle specimens have demonstrated high levels of choline compounds in malignant breast tissue, but low levels in normal breast tissue (15). Recently, we published *in vivo* ^{1}H MR spectroscopy investigations of breast tumor and normal breast tissue. Typically, such spectra show signals from lipids (1.0-1.4 ppm) and in malignant lesions also signals from choline containing compounds (3.2-3.3 ppm) (9).

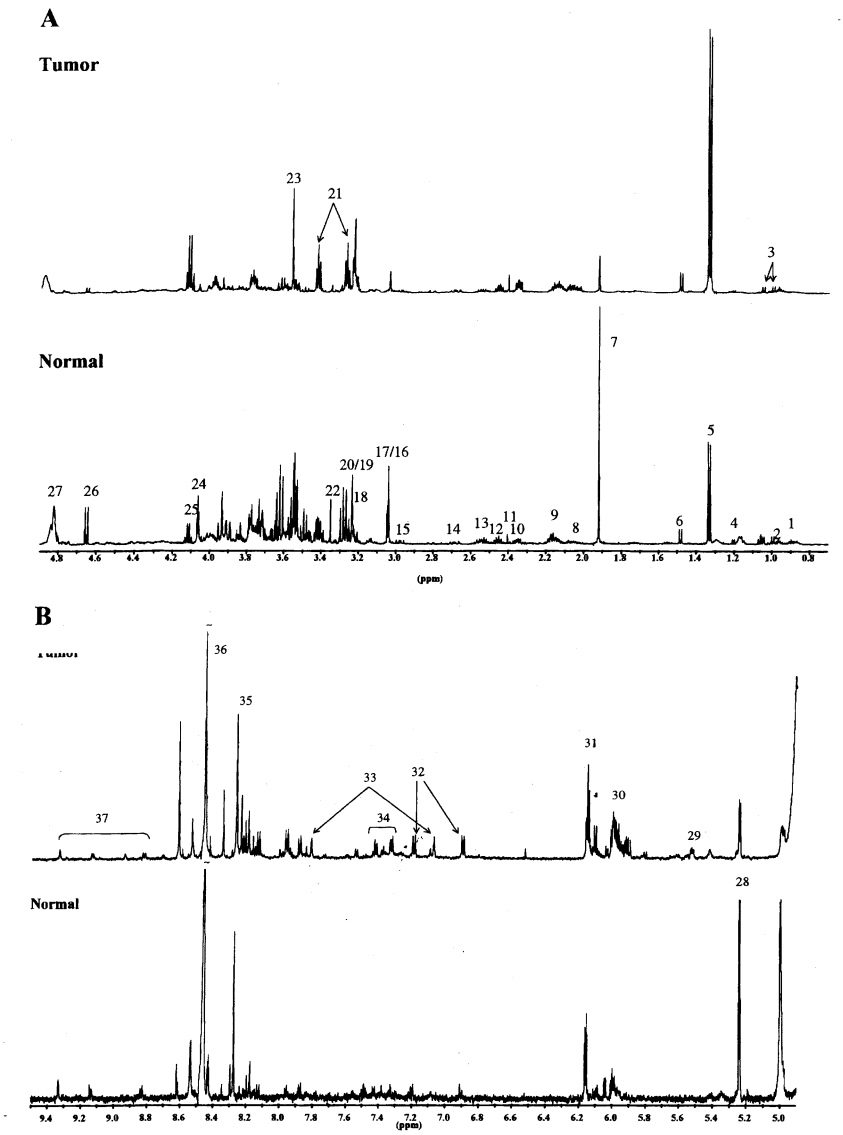

Figure 1. *Representative 600 MHz ^1H NMR spectra of PCA extracts from a ductal carcinoma (upper part) and non-involved breast tissue (lower part). In the low frequency region of the spectra (A) signals from the following metabolites can be identified (numbers in ( ) indicate which proton): 1 Leucine, 2 Isoleucine, 3 Valine CH_3, 4 3-hydroxybutyrate CH_3, 5 Lactate CH_3, 6 Alanine CH_3, 7 Acetate, 8 Glutamate $CH_2(3)$, 9 Glutamine $CH_2(3)$ and glutamyl CH_2 (3) in Glutathione disulfide (GSSG), 10 Glutamate $CH_2(4)$, 11 Succinate, 12 Glutamine $CH_2(4)$, 13 Glutathione disulfide (GSSG), glutamyl CH_2 (4), 14 Aspartate, CH_2 (4), 15 Glutathione disulfide (GSSG), cystine CH_2 (3), 16 Creatine CH_3, 17 Phosphocreatine CH_3, 18 Phosphoetanolamine (N), 19 Phosphocholine $N(CH_3)_3$, 20 Glycerophosphocholine $N(CH_3)_3$, 21 Taurine (N), 22 scyllo-Ino, 23 Glycine, 24 myo-Inositol (2), 25 Lactate CH, 26 β-GIucose (1), 27 Residual water. The high frequency region of the spectra (B) show signals from: 28 β- Glucose (1), 29 Uridine diphospho-N-acetylglucosamine UDP-GlcNAc (1) and galactosamine UDP-GalNAc (1), 30 Uridine diphosphate hexoses, 31 Ribonucleotide signals ribose (1), 32 Tyrosine (6 and 5), 33 Histidine (8 and 6), 34 Phenylalanine (5, 7 and 6), 35 Adenosine triphosphate, adenosine diphosphate, 36 Formate and 37 Nicotine adenine dinucleotide.*

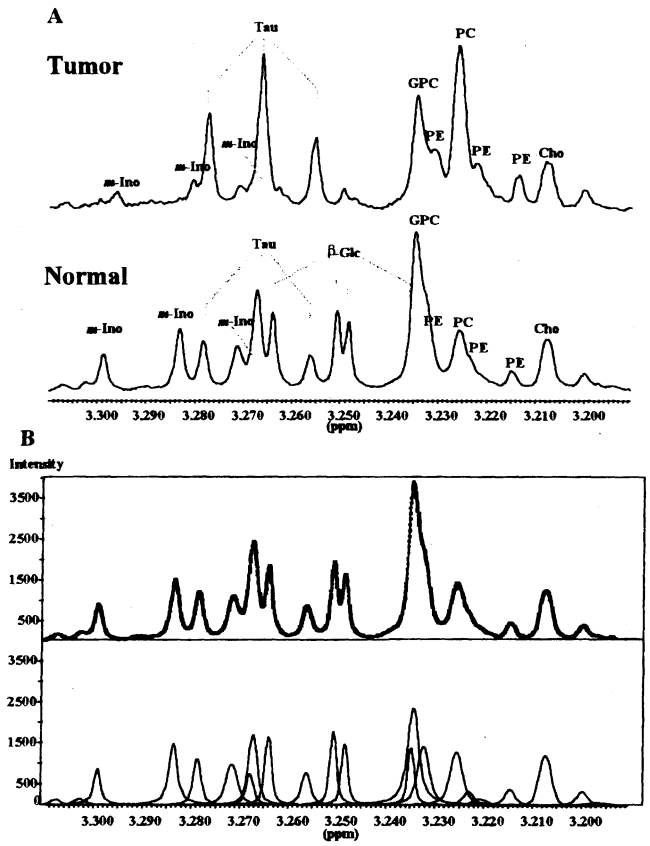

Figure 2. *A) High-resolution ^{1}H NMR spectra of a tumor and non-infiltrated breast tissue from the same patient, the spectrum region 3.19 ppm to 3.31 ppm is shown. The assignments are as follows: PE, phosphoetanolamine; Cho, choline; PC, phosphocholine; GPC, glycerophospocholine; β-Glc, β-Glucose; Tau, taurine; m-Ino, myo-inositol. The spectra are scaled according to wet weight of the tissue and internal standard TSP. B) Calculated (bottom) and experimental (top) spectra of a sample from non-involved breast tissue. A non-linear curve fitting program using least square minimisation method was used for calculating the theoretical spectrum. The correlation factor r^2 was better than 0.995 for all the calculations. The calculated relative areas are shown in the theoretical spectrum.*

Together these studies indicate that *in vivo* ^{1}H MRS can be utilized for detection of malignant breast lesions based on the presence or absence of choline related compounds. However, in a recent study from our laboratory, choline was detected in 2 out of 10 benign lesions, and also in normal breast tissue of lactating women (10). Thus, the presence of a choline related peak in an *in vivo* MR spectrum is not sufficient for the identification of malignancy.

A recent study has examined whether invasive breast cancer can be distinguished from benign lesions based on *ex vivo* ^{1}H MR spectra (14). Based on the ratio of peak height intensities of the signals at 3.25 ppm to 3.05 ppm, a sensitivity of 95% and a specificity of 96 % for differentiation of benign and invasive cancer were obtained. The increased Cho/Cr ratio found in carcinomas was explained by elevated choline metabolite levels (14). In the present study, we have examined closer the contribution to the spectrum region 2.95-3.35 ppm. The major contribution to the 3.25 ppm peak is from PC and GPC in the invasive cancers. PE and taurine might also provide a significant contribution, due to the high levels found in the tumors. Our study documented that these metabolites are elevated in malignant tumors compared to non- involved breast tissue (Figure 2 and Table I). Glucose contributes to the 3.25 ppm signal in non-involved breast tissue. Due to J-modulation of these dublets and triplets in the ^{1}H *in vivo*

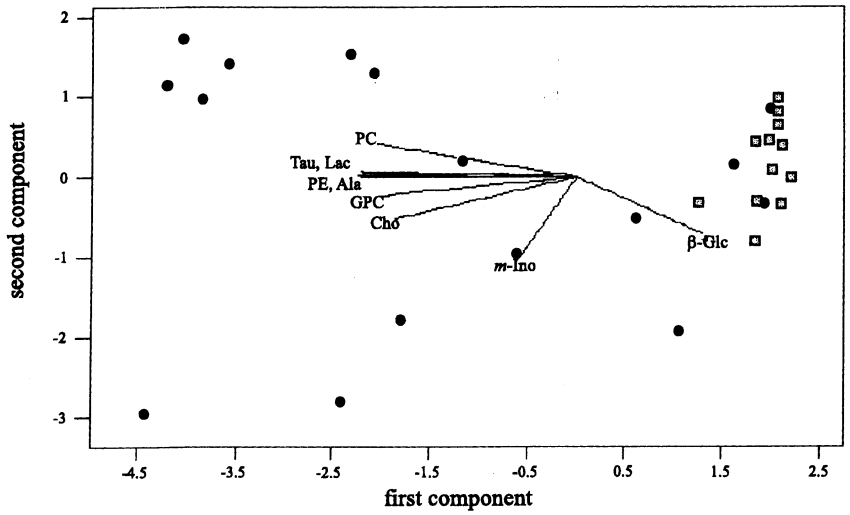

Figure 3. *Principal components biplot. Solid squares denote scores for non-involved breast tissue samples and circles denote scores for tumor samples. Relative contributions to the loadings of each principal component are denoted by the length and direction of the variables noted in the overlaid plot.*

spectra the relative contribution will be less than from the choline singlets due to spin echo experiments with relative long echo times. Mackinnon *et al* (14) obtained high sensitivity and specificity using peak height measurements for determining Cho/Cr ratio, demonstrating the diagnostic potential of MRS for breast tumor differentiation.

High concentration of PC in cells has also been linked to energy metabolism. Roby *et al* (27) observed accumulation of PC in cytoplasm of plant cells during a long period of sucrose starvation. They explained this by utilization of fatty acids from membrane lipids as a carbon source for respiratory purposes. Similar mechanisms have been discussed for the variation in the level of PC in differentiated and undifferentiated human colon adenocarcinoma cells (28) and it is well known that tumors have a high rate of aerobic glycolysis. Our results have shown that malignant breast tumors have low levels of glucose (Table I). In the multivariate analysis (Figure 3) glucose gives one of the heaviest loadings. Glucose was not quantified in 8 of the malignant tumor extracts. Six of these tumors had the highest PC levels found in the study. This result might be interpreted as a connection between low glucose level and high PC content, but more data are certainly needed to establish the significance of the finding. With little or no glucose left, there is a demand for other types of energy supply and degradation of lipids is a likely alternative energy source.

PE gives a large contribution to the signal at 3.2 ppm. In non-involved breast tissue the average PE content is 0.145 ±0.1 compared to 2.06 ±1.13 μmol/g wet weight tissue in the tumor group. Possible metabolic pathways to explain this large difference can be the same route as for PC. The average content of total Cho in the tumor group is about half of the PE content, which is also the case for PE in non-infiltrated breast tissue compared to the tumors.

The relationship between the score plot positioning and the metabolite composition can be explored by considering loadings of the eigenvectors in the principal component analysis. A negative PCl loading is strongly associated with the value of the ß-Glc metabolite; this is one feature that separates the two classes of tissue samples. A positive loading on PCl is dominated in similar proportions by a combination of metabolites: PC, choline, GPC, taurine, PE, lactate, and alanine. This behaviour indicates that numerous simultaneous variations in metabolite concentrations occur in malignant tissue. This is also a reason why simple linear regression analyses may be incapable of quantifying/modelling such data. Non-linearity may be significant. Negative PC2 positioning of scores is most related to myo-inositol concentration and positive PC2 correlation by PC.

The second region was dominated by samples of non-involved tissue, but also contained two samples that should be categorised otherwise. In the case of patient 15, a fibroadenoma, there is reason to believe that the metabolite distribution should not be that associated with malignant tissue. However, it would be desirable for such samples to be better discriminated from the other classes. Finally, patient 7, with a lobular carcinoma with a large in situ component, is associated with the normal tissue region.

Clearly, discrimination fails for this sample with this methodology. The overall variation in metabolite composition in the score appears to be smaller for the normal tissues than for the malignant tissues. This reflects the variability of the metabolite concentrations for the two populations of samples (*i.e.*, tumors versus non- infiltrated breast tissue).

For differentiating the two tissue groups, curve fitting and calculation of concentrations are a time demanding process. Using the spectrum region from 3.0 to 3.35 ppm, correct classifications of the spectra were obtained using probabilistic neural network analysis. Two methods were tested, one employing all chemical shifts within the stated range (1000) and another whereby principal component scores were calculated in a pre-processing step to reduce the dimensionality of the calculations (to 17) and to improve the speed of the calculations. The choice of the number of eigenvalues to keep was based on accounting for approximately 90% of the variance in the original data set. However, it was noted that a smaller number might also lead to equally acceptable results. By retaining only such linear combinations corresponding to some subset of the largest eigenvalues, it is assumed that the effect of noisy or correlated variables in the original data matrix has been removed. A potential danger is that the effects of interest in the data may account for only a small proportion of the total variance in the data. In this case information related to these small effects would be lost along with some of the smaller eigenvalues. By using the dimensionality-reduced data set generated by the PCA pre-processing step, predictions of similar quality as those obtained using the complete chemical shift range were obtained. Compared with the analyses performed using the pre-selected metabolite components, the present data are of similar quality.

In conclusion, this study has documented large differences in the metabolite composition of breast tumors and surrounding breast tissue. These findings encourage in vivo MRS studies of breast tumors. It has also been shown that composition and amount of metabolites in breast tumors can be analysed by multivariate data analysis, which might provide a fast data analysis of complex high resolution NMR spectroscopy data set. Future work need to document the metabolic composition of tumors related to histopathology, in order to explore the potentials of MR spectroscopy as a tool in breast cancer diagnostics.

Acknowledgements

This work was supported by the Norwegian Cancer Society and the Program for Medical Technology at the University of Trondheim. We want to thank Professor Bjoern Larsen, Institute of Biotechnology, University of Trondheim, for helpful discussions during this work.

References

1 The Cancer Registry of Norway. Cancer in Norway 1995. Institute for epidemiological cancer research, Oslo. 1998.

2 Gribbestad IS, Nilsen G, Fjosne HE, Fougner R, Haugen OA, Petersen SB, Rinck PA and Kvinnsland S: Contrast-enhanced magnetic resonance imaging of the breast. Acta Oncol *31:* 833-842, 1992.

3 Kuhl CK, Bieling H, Gieseke J, Ebel T, Mielcarek P, Far F, Folkers P, Elevelt A and Schild HH: Breast neoplasms: T2* susceptibility-contrast, first pass perfusion MR imaging. Radiology *202:* 87-92, 1997.

4 Kvistad KA, Lundgren S, Fjosne HE, Smenes E, Smethurst HE and Haraldseth O: Differentiating benign and malignant breast lesions with T2*- weighted first pass perfusion imaging. Acta Radiologica *40:* 45-51, 1999.

5 Nelson S, Vigneron DB, Star-Lack J and Kurhanewicz J: High spatial resolution and speed in MRSI. NMR Biomed *10:* 411-422, 1997.

6 Preul MC, Caramanos Z Collins DL, Villemure JG, Leblanc R, Olivier A, Pokrupa R and Arnold D: Accurate, noninvasive diagnosis of human brain tumors by using proton magnetic resonance spectroscopy. Nature Medicine *2:* 323-325, 1996.

7 Wald LL, Nelson SJ, Day MR, Noworolski SE, Henry RG, Huhn S.L, Chang S, Prados MD, Sneed PK, Larson DA, Wara WM, McDermott M, Dillon, W.P, Gutin PH and Vigneron DB: Serial proton magnetic resonance spectroscopy imaging of glioblastoma multiforme after brachytherapy. J Neurosurg *87:* 525-534, 1997.

8 Kaji Y, Kurhanewicz J, Hricak H, Sokolov DL, Huang LR, Nelson SJ and Vigneron DB: Localizing prostate cancer in the presence of postbiopsy changes on MR images: Role of proton MR spectroscopic imaging. Radiology *206:* 785-790, 1998.

9 Gribbestad IS, Singstad TE, Nilsen G, Fjosne HE, Engan T, Haugen OA and Rinck PA: *In vivo* ^{1}H MRS of normal breast and breast tumors using a dedicated double breast coil. J Magn Reson. Imaging, *8:* 1191-1197, 1998.

10 Kvistad KA, Bakken IJ, Gribbestad IS, Ehrnholm B, Lundgren S, Fjosne HE and Haraldseth O: Characterization of neoplastic and normal human breast tissues with *in vivo* ^{1}H MR spectroscopy. Submitted, 1998.

11 Mountford CE, Lean CL and Mackinnon WB: The use of proton MR in cancer pathology. In: G.A. Webb (ed.), Annual Reports on NMR spectroscopy, pp. 173-215, London, England: Academic Press 1993.

12 Wallace JC, Raaphorst GP, Somorjai RL, Ng CE, Fung Kee Fung M, Senterman M and Smith ICP: Classification of ^{1}H MR spectra of biopsies from untreated and recurrent ovarian cancer using linear discriminant analysis. Magn Reson Med *38:* 569-576, 1997.

13 Hahn P Smith, ICP, Leboldus L, Littman C, Somorjai RL and Bezabeh T: The classification of benign and malignant human prostate tissue by multivariate analysis of lH magnetic resonance spectra. Cancer Res*57:* 3398- 3401, 1997.

14 Mackinnon WB, Barry PA, Malycha PL, Gillett DJ, Russell P, Lean CL, Doran ST, Barraclough BH, Bilous M and Mountford CE: Fine- needle biopsy specimens of benign breast lesions distinguished from invasive cancer ex vivo with proton MR spectroscopy. Radiology *204:* 661-666, 1997.

15 Gribbestad IS, Fjosne HE, Haugen OA, Nilsen G, Krane J, Petersen SB and Kvinnsland S: *In vitro* proton NMR spectroscopy of extracts from human breast-tumors and non-involved breast-tissue. Anticancer Res *13:* 1973- 1980, 1993.

16 Smith TAD, Glaholm J, Leach MO and *et al:* A comparison of *in vivo* and *in vitro* ^{31}p NMR spectra from human breast tumours: variations in phospholipid metabolism. Br J Cancer *63:* 210-216, 1991.

17 Hagberg G: From magnetic resonance spectroscopy to classification of tumors. A review of pattern recognition methods. NMR Biomed *11:* 148-156, 1998.

18 Usenius JP, Tuohimetsa S, Vainio P, AlaKorpela M, Hiltunen Y and Kauppinen RA: Automated classification of human brain tumours by neural network analysis using *in vivo* H-1 magnetic resonance spectroscopic metabolite phenotypes. NeuroReport *7:* 1597- 1600, 1996.

19 Glonek T, Kopp SJ, Kot E, Pettegrew JW, Harrison WH and Cohen MM: P-31 nuclear magnetic analysis of brain, the perchloric acid extract spectrum. J Neurochem *39:* 1210-1219, 1982.

20 Behar KL and Ogino T: Assignment of resonances in the 1 H spectrum of rat brain by two-dimensional shift correlated and J-resolved NMR spectroscopy. Magn Reson Med *17:* 285-303, 1991.

21 Negendank WG: Studies of human tumors by MRS: a review. NMR Biomed *5:* 303-324, 1992.

22 Robinson SP, Barton SJ, McSheehy PMJ and Griffiths JR: Nuclear magnetic resonance spectroscopy of cancer. Br J Radiology, *70:* 60-69, 1997.

23 Aiken NR and Gillies RJ: Phosphomonoester metabolism as a function of cell proliferative status and exogenous precursors. Anticancer Res *16:* 1393- 1398, 1996.

24 KatzBrull R and Degani H: Kinetics of choline transport and phosphorylation in human breast cancer cells; NMR application of the zero trans method. Anticancer Res *16:* 1375-1379, 1996.

25 Ruiz-Cabello J and Cohen JS: Phospholipid metabolites as indicators of cancer cell function. NMRBiomed *5:* 226-233, 1992.

26 Ting YLT, Sherr D and Degani H: Variations in energy and phospholipid metabolism in normal and cancer human mammary epithelial cells. Anticancer Res 16: 1381-1388, 1996.

27 Roby C, Martin JB, Blingny R and Douce R: Biochemical changes during sucrose deprivation in higher plant cells. J Biol Chem *262:* 5000-5007, 1987.

28 Galons JP, Fantini J, Vion-Dury J, Cozzone PJ and Caniom P: Metabolic changes in undifferentiated and differentiated human colon adenocarcinoma cells studied by multinuclear magnetic resonance spectroscopy. Biochimies *71:* 949-961, 1989.

Received February 26, 1999
Accepted March 26, 1999

Paper II

URN:NBN:no-3463

NMR IN BIOMEDICINE
NMR Biomed. 2002;**15**:327–337
Published online 1 August 2002 in Wiley InterScience (www.interscience.wiley.com). DOI:10.1002/nbm.775

High-resolution magic angle spinning MRS of breast cancer tissue

Beathe Sitter,[1,2]* Ursula Sonnewald,[2] Manfred Spraul,[3] Hans E. Fjösne[4] and Ingrid S. Gribbestad[1]

[1]SINTEF Unimed, MR-Center, N-7465 Trondheim, Norway
[2]NTNU, Department of Clinical Neurosciences, N-7489 Trondheim, Norway
[3]Bruker Analytik GmbH, Rheinstetten, Germany
[4]University Hospital, Department of Surgery, N-7006 Trondheim, Norway

Received 9 October 2001; revised 28 February 2002; accepted 9 May 2002

ABSTRACT: High-resolution magic angle spinning (HR MAS) may develop into a new diagnostic tool for studying intact tissue samples, and several types of cancer have been investigated with promising results. In this study HR MAS spectra of breast cancer tissue from 10 patients have been compared to conventional high-resolution spectra of perchloric acid extracts of the same tissue type. The HR MAS spectra show resolution comparable to spectra of extracts, and two-dimensional techniques lead to identification of a majority of the constituents. More than 30 different metabolites have been detected and assigned. To our knowledge this is the most detailed assignment of biochemical components in intact human breast tissue. The spectra of intact breast cancer tissue differ from perchloric acid extracts by the presence of lipids and fewer signals in the low field region. HR MAS analysis of intact breast tissue specimens is a rapid method, providing spectra with resolution where relative quantification of the majority of the detected metabolites is possible. Copyright © 2002 John Wiley & Sons, Ltd.

KEYWORDS: HR MAS; breast cancer; tissue; PCA extract

INTRODUCTION

Breast cancer is one of the major causes of death among women in the Western world. The incidence is increasing, but a slight decline in mortality has been registered from the mid 1980s.[1] In Norway, more than 2200 women were diagnosed with the disease in 1995 and nearly 800 died.[2,3] Much research has been done to increase the understanding of the causes of breast cancer, and to develop new methods for diagnosis and treatment evaluation. Early diagnosis is believed to be an important factor for reducing breast cancer deaths.[4] Screening X-ray mammography of defined age groups has been started in most Western countries, even though the benefit of screening is a much debated topic.[5–10] The pursuit of improved diagnosis has also resulted in development of new methods for magnetic resonance imaging (MRI). MRI has so far proven useful in differentiating malignant and benign tumors,[11,12] as well as evaluating breast cancer treatment.[13] In addition to early detection and good characterization of the tumors, predicting severity of the disease in each patient might be an important factor for choosing the optimal treatment.

MR spectroscopy of extracts from human tissue has been discussed as an additional method to histopathological analysis for many years.[14–17] Biochemical alterations in cancerous tissue are expected to be detectable before any visible morphological changes, and MR spectroscopy of extracts could yield substantial information. Spectra of extracts contain detailed information on different components in tissue and have contributed to an increased understanding of biochemical changes in cancer. Extraction of either the water- or fat-soluble fractions yields spectra with narrow lines and good separation of signals arising from different metabolites. The extraction procedure is, however, time-consuming and labor-intensive. Also, large tissue samples (typically 0.5–2.0 g) are required to assure a reasonable S/N ratio.[18] MR analyses of extracts from breast tissue have documented a relative increase in phosphocholine compared with other choline compounds in cancerous tissue.[18,19] Other findings were the lowered glucose and carbohydrate levels in tumor tissue. Furthermore, the *myo*-inositol profile follows the lowered levels of

**Correspondence to:* B. Sitter, SINTEF Unimed, MR Center, N-7465 Trondheim, Norway.
Email: Beathe.Sitter@unimed.sintef.no
Contract/grant sponsor: The Norwegian Research Council; *contract grant number:* 133673/420.

Abbreviations used: Cho, choline; Cr, creatine; CPMG, Carr–Purcell–Meiboom–Gill; DCIS, ductal carcinoma *in situ*; GPC, glycerophosphocholine; IDC, infiltrating ductal carcinoma, MAS, magic angle spinning; PCA, perchloric acid; PC, phosphocholine; *s*-Ino, *scyllo*-inositol; Tau, taurine.

glucose, while metabolites such as lactate, taurine and succinate were found to be increased.[19,20]

Analysis of intact tissue specimens omits the extraction. A traditional MR spectrum of a tissue sample consists of broad overlapping peaks due to unresolved anisotropic interactions, both intra- and intermolecular. In spite of this, conventional MR spectroscopic studies of tissue samples have shown high sensitivity and specificity in differentiating malignant and benign tumors. In a study on breast cancer biopsies from 191 patients it was shown that the MR spectra could be used to separate benign from malignant tumors with a high degree of sensitivity and specificity (95 and 96%, respectively).[21] A study of a total of 159 cervical biopsies showed that MR spectroscopy differentiated pre-invasive lesions and invasive cancer with a high degree of sensitivity using conventional MR spectroscopy.[22] Smith *et al.*[23,24] have in several reports shown good classification of different cancer tissue samples like ovarian, prostate and brain tumors, using conventional spectroscopy and multivariate analysis.

High-resolution magic angle spinning (HR-MAS) is a method where broadening due to anisotropic interactions in solid material is reduced by spinning the sample about its own axis at a 54.7° angle to the static magnetic field.[25,26] An angular factor $(3\cos^2\theta - 1)$ contributes to anisotropic broadening in solids, where θ corresponds to the angle between the sample spinning axis and the static magnetic field. Under MAS conditions the term $\cos^2\theta - 1$ equals 0 and fast spinning leads to narrowed lines. Spectra with narrow lines are obtained with more detailed information than conventional MR spectra of tissue samples. The extraction procedure is omitted, and spectra with acceptable signal-to-noise ratios are achieved from small tissue specimens (~20 mg).[27] Millis *et al.*[28] have classified human liposarcoma and lipoma based on lipid profiles in HR-MAS spectra. The lipid profile in renal carcinoma has been found to correlate with malignancy of kidney tissue.[29] Kidney tissue has also been studied using HR MAS by Garrod *et al.*,[30] who identified numerous metabolites and found differences in the metabolic profile in the medulla and cortex. Cheng *et al.*[31] have shown that HR MAS spectra of tissue biopsies from breast cancer patients correlate well with histopathological examinations and that it is possible to separate the different choline metabolites. In healthy breast only small amounts of phosphocholine are detected, while it is the dominant contributor to the choline signals in ductal carcinoma.[32]

Histopathological evaluation of breast tumor specimens is, in combination with lymph node status, the basis for the patient treatment plan. These evaluations are performed on a small fraction of the surgically excised tumors, raising the issue of sample handling and the reliability of observer interpretation.[31] Additional methods for diagnosis and prediction of the disease development using tissue samples could be important for better treatment strategies.

Table 1. Pathological patient characteristics

Patient	Age (years)	Histopathology	Grade
1	68	IDC	I
2	54	IDC	III
3	63	IDC	II
4	49	IDC	III
5	32	IDC	III
6	91	IDC	II
7	59	IDC	II
8	33	IDC	II
9	72	IDC	II
10	78	DCIS	—

IDC; infiltrating ductal carcinoma, DCIS; ductal carcinoma *in situ*.

The lipid content in breast tissue is often high, concealing water-soluble metabolites in MR spectra. In this work, experimental conditions were explored to achieve profiles of low-concentration water-soluble metabolites in intact breast tissue specimens. Metabolite composition in PCA extracts of breast cancer tissue and healthy breast tissue has previously been explored in detail.[18,19,32] The purpose of the present study was to establish the metabolic profile of breast tumor and non-involved breast tissue in HR MAS spectra compared with previously obtained results from extracts. Two-dimensional HR MAS experiments were performed to support identification of individual metabolites.

EXPERIMENTAL

Tissue samples

Specimens of breast cancer tissue and adjacent non-involved tissue were excised from patients ($n = 10$) undergoing scheduled surgery for breast cancer. Patient data are presented in Table 1. All subjects provided informed written consent and the local independent ethics committee approved the study protocol. The tissue samples (96.4 ± 13.7 mg) were put in liquid nitrogen immediately after dissection and stored until MR analysis. Before HR MAS analysis, all samples were cut to fit a MAS rotor (4 mm o.d.). Two of the breast cancer samples were flushed with D_2O prior to HR MAS analysis. The other eight breast cancer specimens were put in the MAS rotor and D_2O added before HR MAS analysis. Two of these tumor samples were taken out of the rotor and flushed in D_2O before repeated HR MAS analysis. Non-involved breast tissue specimens also had D_2O added before MR spectroscopic analysis. Sample and instrument preparation took one hour or more for all samples. The MAS data were compared with previously obtained results on PCA extracts.[18,19,32]

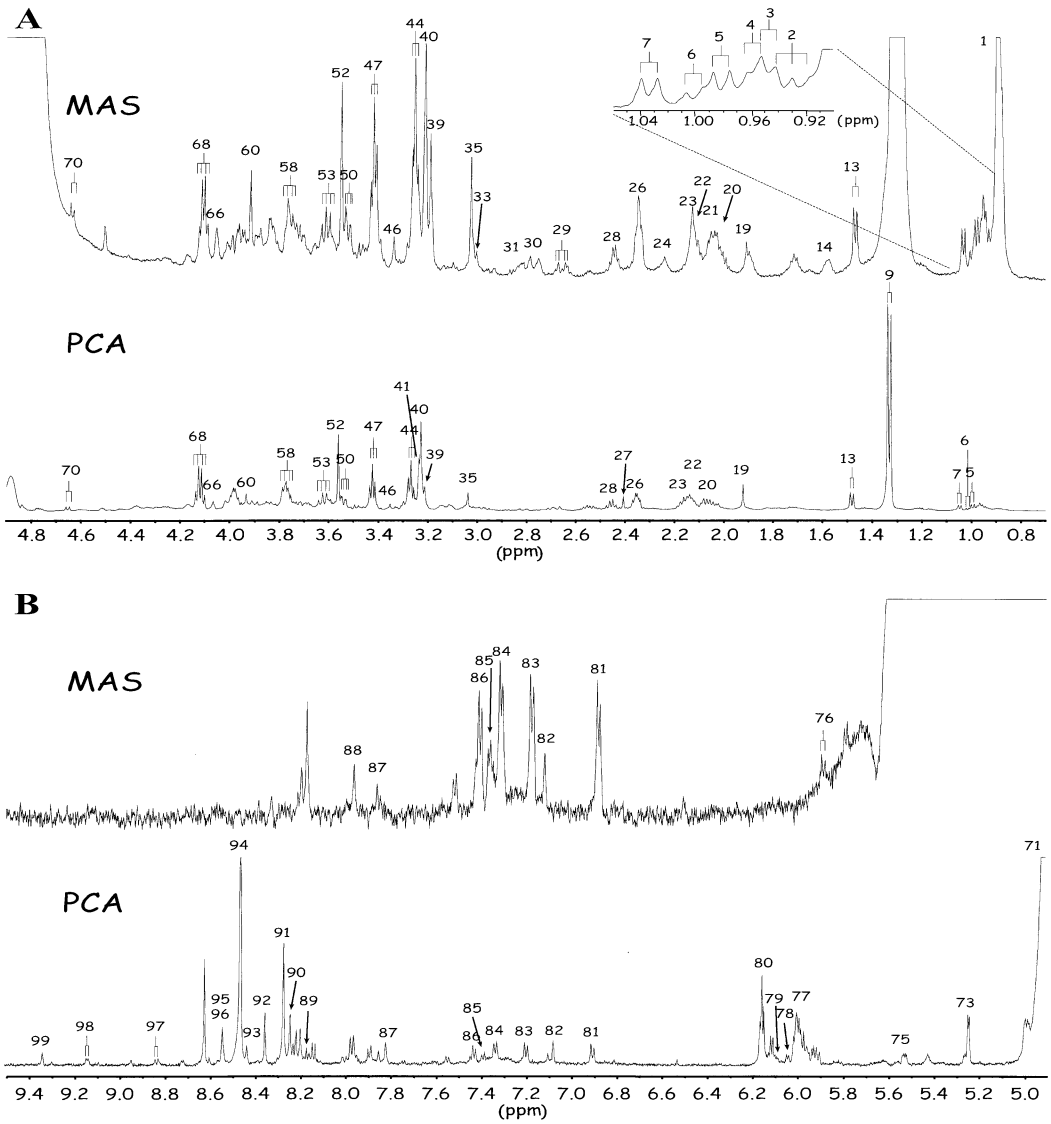

Figure 1. High-resolution proton spectra of breast cancer tissues, showing (A) the high-field region, 4.9–0.7 ppm, and (B) low-field region, 9.5–4.9 ppm. The MAS spectrum (top) of an intact breast cancer specimen (invasive ductal carcinoma grade II) is compared with a high-resolution spectrum of PCA extract (bottom) of tumor tissue (invasive ductal carcinoma grade III). Scaling of the spectra led to cutting the residual water signal at 4.7 ppm. In the high field region (A) of the MAS spectrum (top) the lactate doublet at 1.33 ppm and lipid signals at 1.3 and 0.9 ppm have been cut. Assignments are given in Table 2

MR experiments

High-resolution proton MAS spectra were recorded using a Bruker Avance DRX600 spectrometer equipped with a $^{1}H/^{13}C$ MAS probe able to provide a magnetic field gradient along the magic angle axis (Bruker Spectrospin, Germany). Samples were spun at 6 kHz and acquisitions obtained using a one-dimensional spin-echo sequence with water presaturation (cpmgpr, Bruker). One-hundred and twenty-eight transients over a spectral region of

Table 2. Tentative ^{1}H chemical shift assignment on HR MAS spectra of human breast cancer tissue. Chemical shift referencing is relative to alanine doublet (CH_3) at 1.47 ppm downfield of TSP in MAS spectrum

Metabolite		Assigned number	^{1}H multiplet	MAS	PCA
Fatty acids	—CH_3	1	t	0.89	ND
Isoleucine	δCH_3	2	t	0.95	0.94
Leucine	$\delta' CH_3$	3	d	0.96	0.96
Leucine	δCH_3	4	d	0.97	0.97
Valine	$\gamma' CH_3$	5	d	0.98	0.99
Isoleucine	γCH_3	6	d	1.00	1.02
Valine	$\gamma' CH_3$	7	d	1.03	1.05
Fatty acids	—$(CH_2)_n$	8	m	1.30	ND
Lactate	CH_3	9	d	1.32	1.33
Fatty acids	—CH_2—CH_3	10	m	1.35	ND
Isoleucine	$\gamma' CH$	11	m	1.45	1.45
Lysine	γCH_2	12	m	1.45	1.45
Alanine	CH_3	13	d	1.47	1.48
Fatty acids	—CH_2—CH_2—CO—	14	m	1.58	ND
Leucine	γCH	15	m	1.68	ND
Lysine	δCH_2	16	m	1.68	1.69
Leucine	βCH_2	17	m	1.72	1.72
Lysine	βCH_2	18	m	1.90	1.89
Acetate	(CH_3)	19	s	1.91	1.92
Isoleucine	βCH	20	m	1.97	1.96
Fatty acids	—CH=CH—CH_2—CH_2—	21	m	2.02	ND
Glutamate	βCH_2	22	dt	2.07	2.09
Glutamine	βCH_2	23	c	2.13	2.14
Fatty acids	—CH_2—CH_2—CO—	24	m	2.25	ND
Valine	βCH	25	m	2.27	2.27
Glutamate	γCH_2	26	t	2.34	2.34
Succinate	$(\alpha,\beta CH_2)$	27	s	2.41	2.41
Glutamine	γCH_2	28	c	2.44	2.45
Aspartate	βCH	29	dd	2.67	2.68
Fatty acids	—CH=CH—CH_2—CH=CH—	30	m	2.75	ND
Aspartate	$\beta' CH$	31	dd	2.81	2.79
Aspargine	βCH	32	dd	2.85	2.87
Aspargine	$\beta' CH$	33	dd	2.95	2.95
Lysine	εCH_2	34	t	3.02	3.01
Creatine	CH_3	35	s	3.03	3.04
Phosphocreatine	CH_3	36	s	ND	3.05
Tyrosine	1/2 β-CH_2	37	dd	3.03	3.05
Tyrosine	1/2 β-CH_2	38	dd	3.11	3.15
Choline	$N(CH_3)_3$	39	s	3.19	3.21
Phosphocholine	$N(CH_3)_3$	40	s	3.21	3.23
Glycerophosphocholine	$N(CH_3)_3$	41	s	3.22	3.24
Phosphoethanolamine	N—CH_2	42	t	3.23	3.24
β-Glucose	C2H	43	dd	3.24	3.26
Taurine	N—CH_2	44	t	3.25	3.27
myo-Inositol	C5H	45	t	3.27	3.28
scyllo-Inositol		46	s	3.34	3.35
Taurine	S—CH_2	47	t	3.42	3.43
β-Glucose	C3H	48	t	3.49	3.4
Choline	βCH_2	49	m	3.51	3.43
myo-Inositol	C1H, C3H	50	dd	3.52	3.54
α-Glucose	C2H	51	t	3.53	3.54
Glycine	αCH_2	52	s	3.55	3.56
myo-Inositol	C4H, C6H	53	dd	3.61	3.62
Leucine	aCH	54	t	3.68	ND
Glutamate	αCH	55	t	3.75	3.75
Glutamine	αCH	56	t	3.76	3.77
Lysine	αCH	57	t	3.77	3.74
Alanine	αCH	58	q	3.78	3.77
Aspartate	αCH	59	dd	3.90	3.89
Creatine	CH_2	60	s	3.92	3.94
Phosphocreatine	CH_2	61	s	ND	3.94

Continued

Table 2. Continued

Metabolite		Assigned number	^{1}H multiplet	MAS	PCA
Tyrosine	αCH	62	dd	3.99	3.93
Aspargine	αCH	63	dd	4.00	4.00
Phosphoethanolamine	P—O—CH_2	64	t	4.01	ND
Choline	αCH_2	65	m	4.06	3.96
myo-Inositol	C2H	66	t	4.06	4.07
Glyceryl in triglycerides	$\frac{1}{2}CH_2OCOR$	67	m	4.10	ND
Lactate	CH	68	q	4.11	4.12
Glyceryl in triglycerides	$\frac{1}{2}CH_2OCOR$	69	m	4.30	ND
β-Glucose	C1H	70	d	4.64	4.65
Water, residual	(HOD)	71	m	4.75	4.85
Glyceryl in triglycerides	—C2H—	72	m	5.23	ND
α-Glucose	C1H	73	d	5.23	5.24
Fatty acids	—CH=CH—CH_2—CH=CH—	74	m	5.34	ND
UDP-GlcNAc and GalNAc	C1H	75	d	ND	5.52
Uracil	C6H, ring	76	d	5.79	ND
Uridine diphosphate hexoses	C1H	77	d	ND	6.1
NADH	N1′H	78	d	ND	6.04
NADH	A1′H	79	d	ND	6.09
Ribose in ribonucleotides	C1H	80	d	ND	6.15
Tyrosine	C3H, 5H ring	81	d	6.88	6.90
Histidine	C4H, ring	82	s	7.13	7.07
Tyrosine	C2H, 6H ring	83	d	7.18	7.20
Phenylalanine	C2H, C6H, ring	84	m	7.32	7.33
Phenylalanine	C4H, ring	85	m	7.37	7.38
Phenylalanine	C3H, C5H, ring	86	m	7.42	7.41
Uracil	C5H, ring	87	d	7.86	ND
Histidine	C2H, ring	88	s	7.97	7.81
NADH	N5 ring	89	d	ND	8.19
Inosine	C2 ring	90	s	8.22	8.24
ADP and ATP	C2 ring	91	s	ND	8.27
Inosine	C8 ring	92	s	8.34	8.35
NADH	A8H ring	93	s	ND	8.43
Formate	$HCOO^-$	94	s	ND	8.46
ADP	C8 ring	95	s	ND	8.53
ATP	C8 ring	96	s	ND	8.54
NADH	N4 ring	97	d	ND	8.83
NADH	N6 ring	98	d	ND	9.14
NADH	N2 ring	99	s	ND	9.33

ND, not detected.

10 kHz were collected into 32K points, giving an acquisition time of 1.64 s. The T_2-filtering was performed with a delay of 1 ms repeated 48, 136 and 272 times, giving three different spectra with effective echo times of 102, 270 and 580 ms. The raw data were multiplied with a 0.7 Hz exponential line broadening before Fourier transformation into 64K points. Chemical shift referencing was performed relative to the methyl group in the alanine resonance that shifts 1.47 ppm downfield from TSP.

J-resolved spectra were obtained by a standard spin-echo sequence with 2 s water presaturation (Jrespr, Bruker). Eight transients were collected into 8K data points over a 10 kHz spectral region. The interpulse delay was incremented 64 times, resulting in 78.1 Hz spectral region in the F1 dimension. The raw data were processed using an unshifted sine window function in both dimensions, tilted and symmetrized. Homonuclear correlated spectra (COSY) were recorded by acquisition of 16 transients per increment for 512 increments collected into 2K data points. A spectral width of 8 kHz was used in both dimensions. The time domain data were zero-filled and multiplied with a sine window function in both dimensions before Fourier transformation.

RESULTS

CPMG spin-echo ^{1}H MAS MR spectra of intact tissue (top) and PCA extract from breast cancer tissue (bottom) are shown in Fig. 1. The tissue specimens are from two patients diagnosed with invasive ductal carcinoma, grade II and III respectively. Assigned metabolites are presented in Table 2. The assignments of MAS spectra were performed using published data,[30,33–35] previous studies of PCA extracts[19] and two-dimensional *J*-

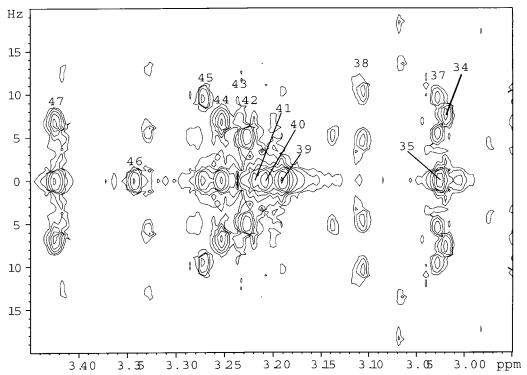

Figure 2. High-resolution *J*-resolved MAS spectrum of a breast cancer tissue sample (invasive ductal carcinoma grade III). The displayed region is 2.95–3.45 ppm. Annotations of peaks are as in Table 2

resolved and proton-proton correlated spectroscopy (COSY). More than 30 different metabolites were detected and assigned. The resonances are well resolved, as can clearly be seen in the spectral region of 0.9–1.2 ppm [Fig. 1(A)], where CH_3 signals from the amino acids valine, isoleucine and leucine can be separated. The predominant resonances in the MAS spectra arise from lipids, amino acids and choline-containing compounds. Lactate was apparent as a shoulder on the lipid peak, but is not shown due to scaling. In the PCA extract spectrum, however, lactate is clearly visible. In the low field region [Fig. 1(B)], the aromatic amino acids phenylalanine and tyrosine are intense signals in the MAS spectra. The nucleotide signals dominating the same region in the PCA extract spectra have not been detected in MAS spectra of intact breast cancer specimens.

A *J*-resolved spectrum of a tumor sample from patient no. 4 is presented in Fig. 2; the spectral region shown is from 3.1 to 3.5 ppm. Choline, phosphocho-

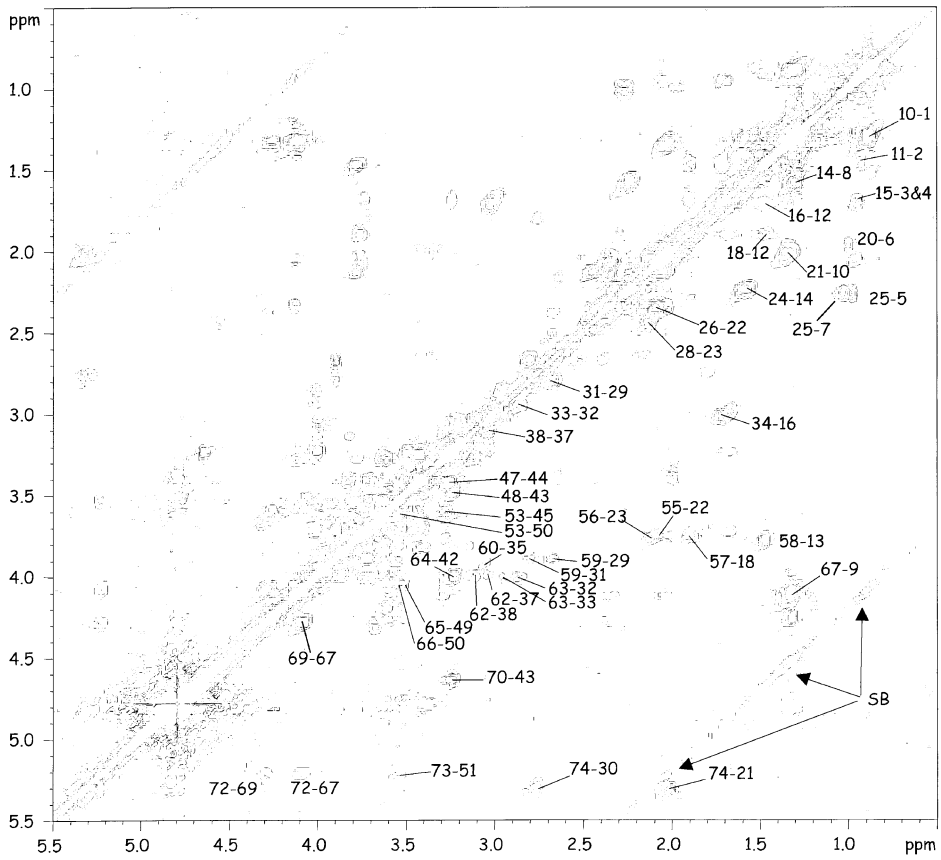

Figure 3. Proton chemical shift correlated spectrum of a breast cancer specimen (invasive ductal carcinoma grade I). The spectral region shown is 0.6–5.6 ppm. Assignments are in accordance with Table 2. Spinning sidebands can be seen parallel to the diagonal and are denoted SB

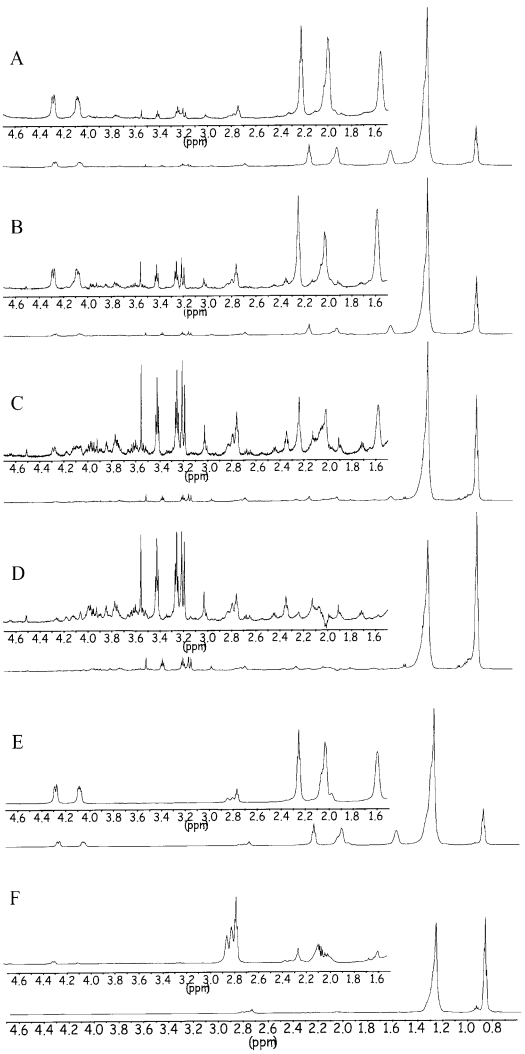

Figure 4. Spectra of tumor tissue sample acquired with water presaturation (A) and a spin echo sequence (cpmgpr; Bruker) with varied repetitions of the echo sequence, resulting in different echo times of 102 (B), 290 (C) and 580 ms (D). The water suppressed spectrum (E) and spin-echo spectrum (F) of non-involved breast tissue are shown as well. The spectrum in (F) is recorded with a 580 ms total echo time

line, glycerophosphocholine and phosphoethanolamine as well as β-glucose, *myo*-inositol and taurine have resonance peaks in the spectral region 3.19 to 3.27 ppm. The *J*-resolved spectrum enables the triplet from phosphoethanolamine (N-CH_2) to be distinguished from the singlets from the CH_3 groups in cholines. The C2H signals from β-glucose and the triplets from taurine (N-CH_3) and *myo*-inositol (C5H) are also clearly separated in the *J*-resolved spectrum. These compounds can be individually assigned in the MAS spectra of intact breast cancer specimens. The signal often called the creatine peak at 3.03 ppm consists of three resonances. From the two-dimensional spectra it can be confirmed that the signal also comprises tyrosine ($\frac{1}{2}\beta$-CH_2) and lysine (ε-CH_2).

Assignments performed by *J*-resolved spectra were compared with proton–proton correlated spectra. In Fig. 3, the spectral region 5.6–0.6 ppm of a COSY spectrum is presented (patient number 1); assignments correlate with the data in Table 2. This spectrum in particular reveals the connections of triglycerides with fatty acids and the glycerol backbone. The presence of triglycerides is confirmed by detection of characteristic resonances from the glycerol backbone at 4.10 ppm ($\frac{1}{2}CH_2$), 4.30 ppm ($\frac{1}{2}CH_2$) and 5.23 ppm (C2H) that show cross correlations to each other. In addition to the dominating resonances and cross peaks from fatty acids, this two-dimensional spectrum reveals cross-correlations within the amino acid residues, for instance leucine, isoleucine and valine (Fig. 3).

Different T_2-filtering was explored to optimize the suppression of lipid signals. Three different spectra with different echo times are displayed in Fig. 4(B–D) in addition to a spectrum recorded with water presaturation alone [Fig. 4(A)] of a tumor sample from patient number 7 (Table 1). The relative intensities of the lipid signals at 0.9 and 1.3 ppm change with increasing echo times, as well as there being an overall reduction. In general, increasing echo time leads to a loss in signal-to-noise ratio. Lipid signals and signals from macromolecules are more reduced than signals from smaller molecules, which leads to an efficient increase in signals from low molecular weight metabolites. A spectrum of non-involved breast tissue specimen recorded with water presaturation is shown in Fig. 4(E) and a spin-echo spectrum, with echo time of 512 ms, of the same sample in Fig. 4(F). The majority of peaks in the spectra arise from lipids.

Intensities of choline components vary in spectra of cancer specimens from different patients, illustrated in Fig. 5. All choline metabolites, choline, phosphocholine and glycerophosphocholine, can be detected. In the spectra of tumor samples from patient numbers 3, 6 and 9 glycerophosphocholine can only be seen as a low field shoulder on the phosphocholine peak. Scyllo-inositol is detected in all spectra except that of the specimen from patient number 6.

The difference in spectra of a sample from patient number 9, first analyzed in D_2O, thereafter flushed and analyzed in D_2O, is demonstrated in Fig. 6. For both samples subjected to this protocol it was found that flushing with D_2O led to a reduction in signal-to-noise by more than 50%.

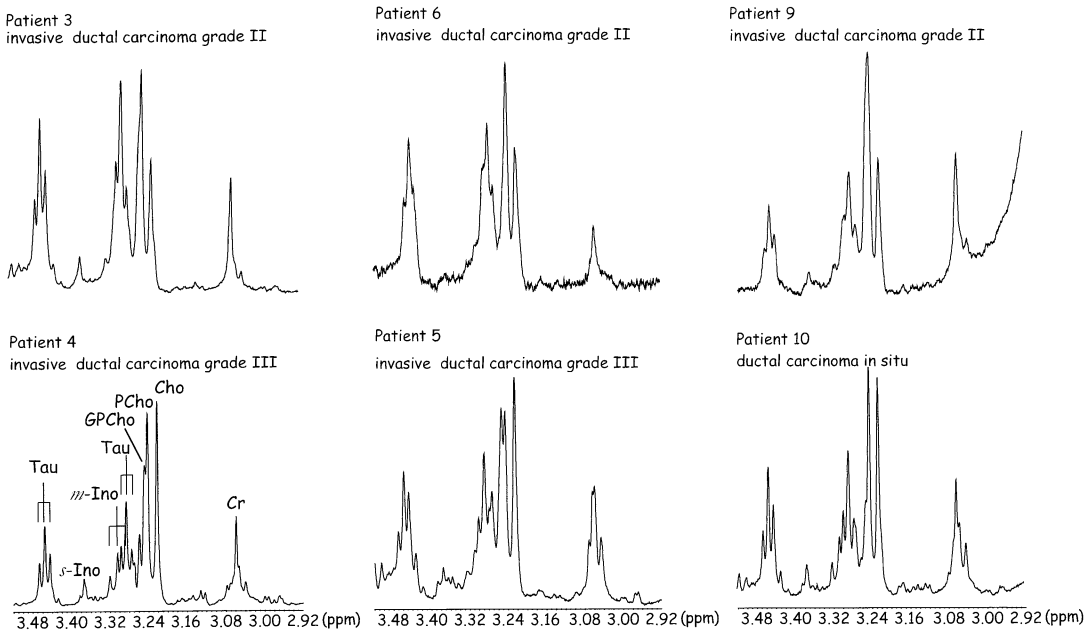

Figure 5. Spin-echo ^{1}H HR MAS spectra (total echo time of 290 ms) from six different tumor samples. The spectral region shown is 3.50–2.90 ppm. Assignments are given in the lower left spectrum (patient 4). Tau, taurine; *s*-Ino, *scyllo*-inositol; GPC, glycerophosphocholine; PC, phosphocholine; Cho, choline; Cr, creatine

DISCUSSION

The high-resolution one-dimensional MAS spectrum presented in Fig. 1 shows resolution comparable to the PCA extract spectrum. Most of the metabolites detected in PCA extracts were also detected in the MAS spectra of intact breast cancer tissue (Table 2). This includes metabolites like amino acids, lactate, choline, inositol and glucose. In addition to providing detailed information on metabolic composition close to what is obtained by high-resolution MR of extracted tissue, the information is not restricted to water- or lipid-soluble components. Even in regions with dominant lipid signals the combination of MAS and spin-echo experiments provides good resolution, as in the spectral region of 1.3–0.9 ppm (Fig. 1).

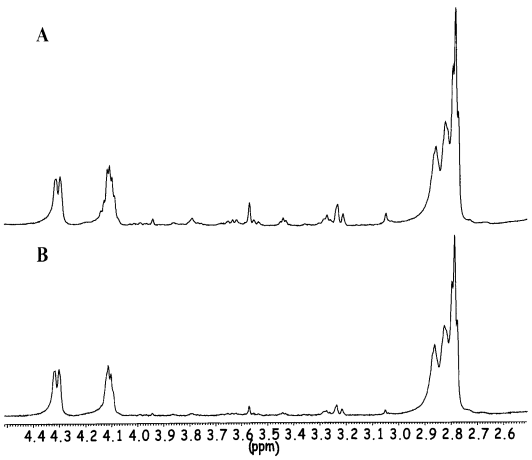

Figure 6. Spin-echo ^{1}H HR MAS spectra of breast tumor sample from patient number 9 analyzed in D_2O (A) and in D_2O after flushing in solvent (B)

Some metabolites found in spectra of PCA extracts are not detected in the MAS spectrum. This is clearly visible in the low-field region from the water resonance at 4.7 to 9.4 ppm, where the number of MR-detectable metabolites is much lower in the MAS spectrum. In particular most signals from different nucleotides are absent. Degradation will occur under the experimental conditions and might contribute to this observation. The degradation products generate resonance signals in this spectral region. However, the low content of signals in this region suggests other possible effects. The differences between PCA extract and HR MAS spectra of breast tumor tissue in this respect are not fully understood and should be further investigated.

The heterogeneity of breast tissue makes it difficult to

obtain homogeneous magnetic fields. In addition lipids and macromolecules appear as broad and overlapping resonances, hiding signals from metabolites that are more interesting for comparison with PCA extracts. This complex profile of breast tissue is simplified by the application of spin-echo experiments with the appropriate T_2 relaxation delays (Fig. 4). Spin echo techniques have the advantage of reducing signal contributions from lipids and macromolecules, enhancing the relative signal intensity of smaller molecules. It also leads to resolution enhancement since the signals that are filtered by this method are low in intensity and appear as an elevation of the baseline. Disadvantages of the spin-echo method include the general loss of signal intensity. Furthermore, for quantitative measurements of the different metabolites detected using spin-echo techniques, T_2 values should be measured.

The various signals in the choline region (Fig. 5) are believed to be related to histopathological grading as well as percentage of tumor in the investigated tissue sample. In spectra from patient numbers 3, 6 and 9 choline is about half the intensity of phosphocholine, while in the spectra of patient numbers 4, 5 and 10 choline and phosphocholine are about equal in intensity. Glycerophosphocholine is found to be lower in intensity than phosphocholine in all spectra, except for the spectrum of tumor tissue from patient number 5. *In vivo* MRS studies of breast cancer patients have shown elevated levels of choline metabolites in malignant tumors, but only rarely in benign tissues.[20,36] Findings in these studies have also demonstrated large variations in choline levels in different tumor tissues.[20,36,37] In a recent study of PCA extracts from breast cancer and non-involved tissue we found that the total amount of cholines on average is more than 10 times higher in tumor tissue than in non-involved tissue.[32] The relative intensities of the resonances of these compounds were also found to be different in cancerous and non-involved tissue. In tumor tissue phosphocholine was found in concentrations three times that of glycerophosphocholine and as the dominating contribution to total choline, while glycerophosphocholine was found in twice as large amounts as phosphocholine in non-involved tissue. Natarajan *et al.* have recently shown that phospholipid profiles of invasive breast cancer cells change during anti-inflammatory treatment towards a non-malignant profile of the choline components.[38]

Sample preparation and handling are important when analyzing intact tissue specimens. Freezing of rat renal tissue has been reported by Middleton *et al.*[39] to lead to an increase in signal intensities from water soluble amino acids. Waters *et al.*[40] also found that frozen renal cortex specimens contained increased amounts of smaller amino acids and decreased choline, glucose, glycerophosphocholine, *myo*-inositol, trimethylamine N-oxide and taurine compared to fresh tissue. HR MAS spectra of frozen rat liver samples, however, did not show significant differences compared with fresh liver. A snap freezing procedure was reported to minimize changes in metabolic profile due to sample freezing.[30] All the samples analyzed in this project were fast frozen. It is presumed that the sample handling in freezing and defrosting steps has minor influence on the MAS spectra of breast cancer tissue.

The sample temperature is assumed to increase due to the rapid spinning during MAS analysis. HR MAS spectra were recorded at room temperature, while the actual temperature in the tissue sample presented in Fig. 1 was calculated to be 29.8 °C.[41] The temperature of the sample will affect the spectral intensities and resolution due to the Boltzman distribution and increased mobility of molecules. The spinning speed can be lowered without significant loss of resolution and sample heating due to rapid spinning can be reduced.[30] Tissue degradation increases with temperature so keeping the sample temperature down (0–2 °C) during sample handling and MR analysis suppresses degradation processes. Due to the effect of temperature on excised tissue specimens the exploration of HR MAS analysis as a possible diagnostic tool in cancer should preferably be performed at low temperatures. The aims of this study were to identify metabolites in breast tumor tissue and compare with PCA extract spectra of the same tissue type. For studies with quantitative comparisons, a low sample temperature is important.

Waters *et al.*[40] also found that *in situ* superfusion of the organs with D_2O increased resolution of the MAS spectra, presumably due to removal of residual blood and reducing susceptibility effects due to erythrocytes. Analyzing tissue samples in solvent will also remove air in the sample, minimizing the paramagnetic contribution from oxygen. In Fig. 6 two spectra of the same sample (patient number 9) are presented, analyzed without and with flushing in solvent (D_2O). The lipid content of this sample was high and the relative intensities of low molecular weight metabolites low. The spectra of samples flushed with solvents showed reduction in intensities of cholines by more than 50% and lipid signals by 40% compared with the spectra without solvent flushing. Since breast tissue often contains large amounts of adipose tissue, optimizing the conditions for studying the water-soluble components is a major challenge. In addition, the heterogeneous nature of breast tissue might lead to different degrees of washout of these components. Since the metabolites of interest can be separated in spectra of tissue without prior flushing of the sample, the gain in resolution is considered less important than the danger of losing metabolites.

HR MAS analysis of intact tissue specimens is at an early stage. Before this method can become an additional tool in diagnosis, results have to be compared with the well-established histopathological evaluation. The major advantages of this new technique appears to be rapid and simple sample handling prior to HR MAS analysis and

that an HR MAS spectrum can be recorded within a few minutes. This leads to a total analysis time of about 15 min, which is highly competitive with today's traditional histopathological methods. HR MAS provides a rapid and simple way into the biochemical complexity of healthy and cancerous tissue.

CONCLUSION

High-resolution MAS spectra of intact breast tissue specimens show resolution close to conventional MR spectroscopy of PCA extracts of breast tumor tissue, giving a unique opportunity to study the biochemical composition of intact tissue specimens.

Most of the metabolites detected in PCA extracts were also detected in MAS spectra of intact breast cancer tissue. Choline-containing compounds, which have been found to correlate to histology in PCA extracts of breast tumor tissue, can be detected and separated in the HR MAS spectra. A study including a larger group of breast patients is needed to assess the value of HR MAS as method in breast cancer diagnosis.

Acknowledgements

A sincere thanks to Bruker Analytik, Germany for support in HR MAS method implementation. The Norwegian Research Council granted financial support for this project.

REFERENCES

1. Levi F, Lucchini F, La Vecchia C, Negri E. Trends in mortality from cancer in the European Union, 1955–94. *Lancet* 1999; **354**: 742–743.
2. Kvinnsland S. Kan brystkreft forebygges med medikament? *Tidsskr. Nor. Laegeforen.* 1997; **117**: 1437.
3. Zahl P-H. Brystkreft—insidens, mortalitet og stadiemigrasjon i Norge. *Tidsskr. Nor. Laegeforen.* 1997; **117**: 3765–3767.
4. Moore MP, Kinne DW. Axillary lymphadenectomy: a diagnostic and therapeutic procedure. *J. Surg. Oncol.* 1997; **66**: 2–6.
5. Sox HC. Benefit and harm associated with screening for breast cancer. *New Engl. J. Med.* 1998; **338**: 1145–1146.
6. Tabar L, Fagerberg G, Day NE, Duffy SW, Kitchin RM. Breast cancer treatment and natural history: new insights from results of screening. *Lancet* 1992; **339**: 412–414.
7. van Dijck JA, Verbeek AL, Hendriks JH, Holland R. The current detectability of breast cancer in a mammographic screening program. A review of the previous mammograms of interval and screen-detected cancers. *Cancer* 1993; **72**: 1933–1938.
8. Kopans DB. The positive predicitve value of mammography. *Am. J. Roentgenol.* 1992; **160**: 660–661.
9. Gøtzsche PC, Olsen O. Is screening for breast cancer with mammography justifiable? *Lancet* 2000; **355**: 129–134.
10. Nystrom L, Andersson I, Bjurstam N, Frisell J, Nordenskjold B, Rutqvist LE. Long-term effects of mammography screening: updated overview of the Swedish randomised trials. *Lancet* 2002; **359**: 909–919.
11. Gribbestad IS, Nilsen G, Fjøsne H, Fougner R, Haugen OA, Petersen SB, Rinck PA, Kvinnsland S. Contrast-enhanced magnetic-resonance-imaging of the breast. *Acta Oncol.* 1992; **31**: 833–842.
12. Kvistad KA, Rydland J, Vainio J, Smethurst HB, Lundgren S, Fjøsne H, Haraldseth O. Breast lesions: evaluation with dynamic contrast-enhanced T_1-weighted MR imaging and with T_2*-weighted first-pass perfusion MR imaging. *Radiology* 2000; **216**: 545–553.
13. Rieber A, Zeitler H, Rosenthal H, Gorich J, Kreienberg R, Brambs HJ, Tomczak R. MRI of breast cancer: influence of chemotherapy on sensitivity. *Br. J. Radiol.* 1997; **70**: 452–458.
14. Peeling J, Sutherland G. High-resolution ^{1}H NMR spectroscopy studies of extracts of human cerebral neoplasm. *Magn. Reson. Med.* 1992; **24**: 123–136.
15. Fowler AH, Pappas AA, Holder JC, Finkbeiner AE, Dalrymple GV, Mullins MS, Sprigg JR, Komoroski RA. Differentiation of human prostate cancer from benign hypertrophy by *in vitro* ^{1}H NMR. *Magn. Reson. Med.* 1992; **25**: 140–147.
16. Carpinelli G, Carapella CM, Palombi L, Raus L, Caroli F, Podo F. Differentiation of Glioblastoma Multiforme from Astrocytomas by *in vitro* ^{1}H MRS Analysis of Human Brain Tumors. *Anticancer Res.* 1996; **16**: 1559–1564.
17. Moreno A, Arùs C. Quantitative and qualitative characterization of ^{1}H NMR spectra of colon tumors, normal mucosa and their perchloric acid extracts: decreased levels of *myo*-inositol in tumors can be detected in intact biopsies. *NMR Biomed.* 1996; **8**: 33–45.
18. Gribbestad IS, Fjøsne H, Haugen OA, Nilsen G, Krane J, Petersen SB, Kvinnsland S. *In vitro* proton NMR spectroscopy of extracts from human breast tumours and non-involved breast tissue. *Anticancer Res.* 1993; **13**: 1973–1980.
19. Gribbestad IS, Petersen SB, Fjøsne H, Kvinnsland S, Krane J. ^{1}H NMR Spectroscopic characterization of perchloric acid extracts from breast carcinomas and non-involved breast tissue. *NMR Biomed.* 1994; **7**: 181–194.
20. Gribbestad IS, Singstad TE, Nilsen G, Fjøsne HE, Engan T, Haugen OA, Rinck PA. *In vivo* ^{1}H MRS of normal breast and breast tumors using a dedicated double breast coil. *J. Magn. Reson. Imag.* 1998; **8**: 1191–1197.
21. Mackinnon WB, Barry PA, Malycha PL, Gillett DJ, Russell P, Lean CL, Doran ST, Barraclough BH, Bilous M, Mountford CE. Fine-needle biopsy specimens of benign breast lesions distinguished from invasive cancer *ex vivo* with proton NMR spectroscopy. *Radiology* 1997; **204**: 661–666.
22. Delikatny EJ, Russell P, Hunter JC, Hancock R, Atkinson KH, van Haaften-Day C., Mountford CE. Proton MR and human cervical neoplasia: *ex vivo* spectroscopy allows distinction of invasive carcinoma of the cervix from carcinoma *in situ* and other preinvasive lesions. *Radiology* 1993; **188**: 791–796.
23. Smith ICP, Blandford DE. Nuclear magnetic resonance spectroscopy. *Anal. Chem.* 1995; **67**: 509R-518R.
24. Smith ICP, Blandford DE. Diagnosis of cancer in humans by ^{1}H NMR of tissue biopsies. *Biochem. Cell Biol.* 1998; **76**: 472–476.
25. Andrew ER, Bradbury A, Eades RG. Removal of dipolar broadening of nuclear magnetic spectra of solids by specimen rotation. *Nature* 1959; **183**: 1802–1803.
26. Andrew ER. The narrowing of NMR spectra of solids by high-speed specimen rotation and the resolution of chemical shift and spin multiplet structures for solids. *Prog. NMR Spectrosc.* 1971; **8**: 1–39.
27. Cheng LL, Ma MJ, Becerra L, Ptak T, Tracey I, Lackner A, González RG. Quantitative Neuropathology by High Resolution Magic Angle Spinning Proton Nuclear Magnetic Resonance Spectroscopy. *Proc. Natl Acad. Sci. USA* 1997; **94**: 6408–6413.
28. Millis K, Weybright P, Campbell N, Fletcher JA, Fletcher CD, Cory DG, Singer S. Classification of human liposarcoma and lipoma using ex-vivo NMR spectroscopy. *Magn. Reson. Med.* 1999; **41**: 257–267.
29. Moka D, Vorreuther R, Schicha H, Spraul M, Humpfer E, Lipinski M, Foxall PJD, Nicholson JK, Lindon JC. Biochemical classification of kidney carcinoma biopsy samples using magic-angle-spinning ^{1}H nuclear magnetic resonance spectroscopy. *J. Pharm. Biomed. Anal.* 1998; **17**: 125–132.
30. Garrod S, Humpfer E, Spraul M, Connor SC, Polley S, Connelly J, Lindon JC, Nicholson JK, Holmes E. High-resolution magic angle spinning ^{1}H NMR spectroscopic studies on intact Rat renal cortex and medulla. *Magn. Reson. Med.* 1999; **41**: 1108–1118.

31. Cheng LL, Chang I-W, Smith BL, González RG. Evaluating human breast ductal carcinomas with high-resolution magic-angle spinning proton magnetic resonance spectroscopy. *J. Magn. Reson.* 1998; **135**: 194–202.
32. Gribbestad IS, Sitter B, Lundgren S, Krane J, Axelson D. Metabolite composition in breast tumors examined by proton nuclear magnetic resonance spectroscopy. *Anticancer Res.* 1999; **19**: 1737–1746.
33. Fan TWM. Metabolite profiling by one- and two-dimensional NMR analysis of complex mixtures. *Prog. NMR Spectrosc.* 1996; **28**: 161–219.
34. Behar KL, Ogino T. Assignment of resonances in the ^{1}H spectrum of rat brain by two-dimensional shift correlated and *J*-resolved NMR spectroscopy. *Magn. Reson. Med.* 1991; **17**: 285–303.
35. Nicholson JK, Foxall PJD, Spraul M, Farrant RD, Lindon JC. 750 MHz ^{1}H and ^{1}H–^{13}C NMR spectroscopy of human blood plasma. *Anal. Chem.* 1995; **67**: 793–811.
36. Kvistad KA, Bakken IJ, Gribbestad IS, Ernholm B, Lundgren S, Fjøsne HE, Haraldseth O. Characterization of neoplastic and normal human breast tissues with *in vivo* ^{1}H MR spectroscopy. *J. Magn. Reson. Imag.* 1999; **10**: 159–164.
37. Bakken IJ, Axelson D, Kvistad KA, Brodtkorb E, Müller B, Aasly J, Gribbestad IS. Applications of neural network analysis to *in vivo* ^{1}H magnetic resonance spectroscopy of epilepsy patients. *Epilepsy Res.* 1999; **35**: 245–252.
38. Natarajan K, Mori N, Artemov D, Aboagye EO, Chacko VP, Bhujwalla ZM. Phospholipid profiles of invasive human breast cancer cells are altered towards a less invasive phospholipid profile by the anti-inflammatory agent indomethacin. *Adv. Enzyme Regul.* 2000; **40**: 271–284.
39. Middleton DA, Bradley DP, Connor SC, Mullins PG, Reid DG. The effect of sample freezing on proton magic-angle spinning NMR spectra of biological tissue. *Magn. Reson. Med.* 1998; **40**: 166–169.
40. Waters NJ, Garrod S, Farrant RD, Haselden JN, Connor SC, Connelly J, Lindon JC, Holmes E, Nicholson JK. High-resolution magic angle spinning ^{1}H NMR spectroscopy of intact liver and kidney: optimization of sample preparation procedures and biochemical stability of tissue during spectral acquisition. *Anal. Biochem.* 2000; **282**: 16–23.
41. Farrant RD, Lindon JC, Nicholson JK. Internal temperature calibration for ^{1}H NMR spectroscopy studies of blood plasma and other biofluids. *NMR Biomed.* 1994; **7**: 243–247.

Paper III

URN:NBN:no-3463

Comparison of HR MAS MR spectroscopic profiles of breast cancer tissue to clinical parameters

Beathe Sitter[1,2], Steinar Lundgren[2], Tone F. Bathen[2], Jostein Halgunset[3], Hans E. Fjosne[4], Ingrid S. Gribbestad[2]

[1]Institute of Neuroscience, NTNU, [2]Cancer Clinic, [3]Department of Histology and [4]Department of Surgery, St. Olavs Hospital Trondheim University Hospital, Norway

Running title: HR MAS of breast cancer

Corresponding author:

Beathe Sitter

St. Olavs Hospital

Cancer Clinic

7006 Trondheim

Norway

Telephone: +47 73 55 13 53

Fax: +47 73 86 77 08

E-mail: beathesi@ntnu.no

Grant Sponsor: The Norwegian Research Council. Grant number: 133673/420

Abstract

High resolution magic angle spinning (HR MAS) MR spectra were acquired of breast cancer tissue from 85 patients and adjacent non-involved tissue from 18 of these patients. Tissue specimens were investigated by microscopy after MR analysis. Tumor samples could be distinguished from non-involved samples (82% sensitivity, 100% specificity) based on relative intensities of signals from glycerophosphocholine, phosphocholine and choline in spin echo spectra. Tissue concentrations were estimated from water suppressed spectra for eight metabolites: choline, creatine, β-glucose, glycerophosphocholine, glycine, *myo*-inositol, phosphocholine and taurine. Metabolite concentrations were compared to patient diagnosis, tumor grading, tumor size, patient lymph node status and microscopic evaluation of tissue composition for each sample. The tissue concentrations of choline and glycine were found to be significantly higher in tumors larger than 2 cm compared to smaller tumors. Principal component analysis (PCA) was used to compare the MR spectra to the same parameters as metabolite concentrations. Metabolite estimates and PCA of MAS spectra indicate that the spectral patterns depend on sample tissue composition. A possible prediction of spread to axillary lymph nodes was found in PCA of samples without fat tissue from patients with invasive ductal carcinomas.

Keywords: HR MAS, MR spectroscopy, breast cancer, tissue samples

Abbreviations used: Cho; choline, GPC; glycerophosphocholine, DCIS, ductal carcinoma in situ; IDC, infiltrating ductal carcinoma, MAS; magic angle spinning; PC; phosphocholine and PCA; principal component analysis

Introduction

Breast cancer is the cancer form with the highest incidence and mortality of all malignant diseases among women globally, with more than one million new cases each year.[1] Early detection is important for successful treatment, and screening programs have been effected in most western countries.[2] Histopathologic evaluation of the tumor and lymph node status are the basis for the patient treatment plan. The strongest prognostic factor for breast cancer patients is their lymph node status. In a retrospective study of 384 breast cancer patients with negative axillary lymph nodes, the 5-year survival rate was found to be almost 86%.[3]

In Europe, 72.5% of all breast cancer patients survive more than five years.[2] The risk of recurring breast cancer is highest the first two years post surgery but is present for the rest of the patients life.[4] The most common sites of secondary tumors in breast cancer patients are bone, lung, liver and brain.[5] About 25% of node negative patients experience recurrence or metastasis.[6] Increased sensitivity in detection of tumor spread could provide better distinction between patients in need of close follow-up. Metabolic patterns in tumors have been suggested as tools in cancer characterization and as possible prognostic factors. Lactate concentration in biopsies from cervix of the uterus has been found to correlate to metastatic spread[7] and chemical profiles of fine needle aspirates from breast cancer patients have been found to predict lymph node involvement.[8]

In vitro studies of cell cultures[9], extracts of tissue[10] and intact tissue[11] using MR spectroscopy have been applied in cancer research since the late 1980's. MR

spectroscopy provide detailed information on chemical composition of the studied sample and has contributed to increased understanding of cancer biology.[12] Several studies of breast cancer using MR spectroscopy have reported that the biochemical properties can characterize the tumor.[13-15] In a study of perchloric acid extracts of breast tissue the different cholines were shown to be elevated in tumor compared to adjacent non-involved tissue.[16] Conventional MR spectroscopy of fine needle aspirates have been described to classify cancer tissue.[8,17] MacKinnon *et al.*[17] were able to distinguish malignant (n=82) from benign (n=106) breast lesions based on the total choline to creatine ratio. In a study using multivariate analysis of the MR spectra[8], malignant lesions (n=59) could be discriminated from benign lesions (n=49) (98% sensitivity, 94% specificity) and positive lymph nodes (n=29) could be predicted (96% sensitivity, 94% specificity) in samples with low fat content.

Magic angle spinning (MAS) MR spectroscopy has provided the opportunity to study intact tissue specimens since 1996. Increased spectral resolution give more detailed metabolic information than conventional MR spectroscopic analysis. The specimens can be evaluated by microscopy after spectral analysis, making direct comparisons to morphologic characteristics feasible. The HR MAS technique has been applied in studies of various human tissues and diseases, as cancer in the brain[18,19], prostate[20,21] and breast.[15,22] In a study by Cheng *et al.*[15], 19 specimens from breast cancer patients were examined using HR MAS. The results suggested a possible correlation between metabolites and tumor grading.

The purpose of this study was to investigate if HR MAS spectra of biopsies from breast cancer patients correlated to clinical parameters. Spectra were acquired of tumor samples from 85 patients and from non-involved adjacent tissue from 18 of the same patients. The resulting spectra were examined by three different approaches for comparisons to clinical parameters: [1] Relative intensities of glycerophosphocholine (GPC), phosphocholine (PC) and choline were examined, [2] Tissue concentrations of selected metabolites were estimated from the recorded spectra and [3] the spectra were used as input in principal component analysis (PCA). Tissue samples were examined by a pathologist after the MAS analysis for evaluation of tissue composition.

Materials and Methods

Subjects

The local ethics committee approved the study protocol and all patients signed an informed written consent. Specimens of breast cancer tissue and adjacent non-involved tissue were excised from patients (n=85) with palpable breast lesions undergoing scheduled surgery for breast cancer at St. Olavs Hospital in Trondheim, Norway. The average age of the patients was 61.0 years (range 30.5 - 91.6). Samples were divided in classes based on histopathological diagnosis and ranked within each group by increasing tumor size. Patient data are summarized in Table 1.

Samples

The tissue samples were put in liquid nitrogen immediately after dissection and stored from 9 to 41 months before HR MAS analysis. All tissue samples (n = 103) were cut to

fit a 4 mm o.d. rotor with inserts (total sample volume 50 µL). The sample was immersed in 40 µL phosphate buffered saline (PBS) in D_2O in the rotor, and excess fluid was removed when assembling the rotor. Two different concentrations were used of the internal standard trimethylsilyl tetradeuteropropionic acid (TSP). One group of samples (n=25) were added PBS containing 1 mM TSP, while the remaining samples (n=78) were added buffer with 5mM TSP. Samples weighed 20.5 mg in average (2.6 to 40.1 mg).

MR experiments

HR MAS experiments were performed on a Bruker AVANCE DRX600 spectrometer equipped with a $^{1}H/^{13}C$ MAS probe with gradient aligned with the magic angle axis (Bruker BioSpin GmbH, Germany). Samples were spun at 5 kHz and all experiments performed at instrumental temperature setting of 4° C. (Actual temperature was measured to 5.8°C in spectra with glucose signals (n=68), as described by Farrant *et al.*[23]). Spectra were recorded within 1 hour and 40 minutes for all samples.

Two sets of one-dimensional experiments were performed for all samples. A single pulse experiment with 2.0 seconds of water presaturation (zgpr; BRUKER) was performed using a 60° flip angle over a sweep width of 20 ppm. The FID was acquired during 1.64 seconds and Fourier transformed into 64K after 0.7 Hz line broadening. The baseline was corrected using a cubic approximation and chemical shift scale was calibrated to the TSP signal at 0 ppm.

Spin-echo experiments (cpmgpr; BRUKER) were performed using 2 seconds of water suppression prior to a 90 degrees excitation pulse. 128 transients over a spectral region of 10 kHz were collected into 32K points, giving an acquisition time of 1.64 seconds. The T_2-filtering was obtained using a delay of 1 ms repeated 136 times resulting in 285 ms effective echo time. Spectra were Fourier transformed after 0.7 Hz linebroadening and baseline was adjusted using a linear function. Chemical shifts were calibrated to the TSP singlet at 0 ppm. Spectral assignments were performed based on a previous study on HR MAS of breast cancer lesions[22] and renal and hepatic tissue.[24]

Histopathologic examination of MAS analyzed tissue samples

After HR MAS analysis, the tissue specimens were fixed in 10% formalin and embedded in paraffin. One 5 μm section was cut from each block, stained with haematoxylin, erythrosin and saffron, and examined microscopically. The relative areas of normal and neoplastic epithelial elements, necrotic tissue, fat and fibrous connective tissue were scored visually. Three tumor samples and seven non-involved samples were severely traumatized and could not be evaluated microscopically.

Estimating metabolite concentrations

Tissue metabolic concentrations were estimated from the water suppressed spectra for β-glucose, glycine, *myo*-inositol, taurine, GPC, PC, choline and creatine. The spectral regions 4.6 to 4.7 ppm (β-glucose) and 3.0 to 3.6 ppm (metabolite regions) and ÷0.1 to 0.1 ppm (TSP) were individually baseline corrected using a 5^{th} order function. Peak areas were calculated using combined Lorentzian and Gaussian line functions (Voigt area) in a curve fitting program (PeakFit from Jandel Scientific, USA). A HR MAS

spectrum and the corresponding calculated spectrum is shown in Figure 1. The correlation coefficient, r^2 was 0.98 or larger for all area calculations.

Metabolite peak areas were related to the internal standard TSP and sample wet weight. It was assumed that only buffer (with TSP) was lost in rotor assembling (sample preparation for MAS analysis) for sample weight and TSP concentration calculation. The MAS rotor was reassembled for nine tumor samples before spectral analysis, involving loss and refilling of buffer with TSP. Spectra from these samples were excluded in metabolite estimations. Spectra from the samples that were too damaged for microscopy (three tumor and seven non-involved samples) and from two non-involved samples that proved to contain cancer cells were left out from peak fitting. Totally 73 spectra from tumor and nine spectra from non-involved samples were analyzed for metabolite concentrations. Estimates of β-glucose was excluded from samples where glucose was undetectable in water suppressed spectra (glucose concentration set to 0 μmol per gram tissue) but apparent in spin echo spectra (three tumor and one non-involved sample). β-Glucose was estimated from spectra from 70 tumor and eight non-involved samples. Signal intensities in the metabolite region (3.0 - 3.6 ppm) were low (creatine S/N < 10) in spectra from one tumor sample and eight non-involved samples. The selected signals could be identified in spin-echo spectra but not peak fitted from water suppressed spectra. As a result, tissue metabolic concentrations were estimated from 72 spectra from tumor and one non-involved specimens. Statistical significance testing of calculated values was performed using ANOVA and Student t-test (SPSS).

Principal component analysis

PCA were performed using both water suppressed spectra and spin-echo spectra. The spectral region 0.5 - 4.7 ppm from the water suppressed spectra and 2.9 - 4.7 ppm from spin-echo spectra of all samples (n=103) were used as the two basic matrices. Various spectral regions and sample groups were selected for PCA. Spectra from patients treated with chemotherapy prior to surgery, from tumor samples without tumor cells and non-involved samples containing tumor cells were excluded systematically.

Spectral regions were normalized (by mean normalization) before PCA with full cross validation (The Unscrambler, from Camo, Norway). Score values and principal components were visually compared to patient diagnosis, tumor grading, tumor size, patient age, lymph node status, microscopic evaluation of sample tissue composition and sample storage period.

Results

Histopathologic evaluation of MAS analyzed tissue samples

The tumor and non-involved samples showed different tissue composition. Eleven of the 18 non-involved samples could be examined by microscopy after HR MAS analysis. Cancer cells were identified in two of them (5% or less of section area) and nine samples were described as fat and connective fibrous tissue. The remaining samples were damaged by the MR procedure and could not be examined in detail.

Cancer cells were confirmed in 76 of the 82 tumor samples investigated by microscopy (three samples could not be examined due to tissue damage), while no cancer cells could be identified in the six remaining samples. Tumor samples were mainly dominated by connective tissue and cancer cells. The investigated tissue slices showed typical cancer cell contents of 10 to 50% (48 samples). Eighteen of the tumor samples contained cancer cells in less than 10% of the sample area, while 10 samples contained more than 50% cancer cells. 25 of the 76 verified cancerous samples contained additional fat tissue, 12 samples contained a significant proportion of glandular cells and five samples were partly necrotic (up to 35% of the sample).

MAS spectra

Representative spectra from tumor and adjacent non-involved tissue from a patient with invasive ductal carcinoma (IDC) grade II are shown in Figure 2. The cancerous sample (A) was described as 95% connective tissue and 5% tumor samples, whereas the non-involved specimens (B) consisted of 85% connective tissue and 15% fat. Both water suppressed spectra (a1 and b1) showed a high content of lipid signals, which was typical for all spectra. The water soluble metabolites in the spectral region from 3.0 to 4.8 ppm (a2 and b2) are better resolved and more intense in the spectrum from the cancerous sample. Better signal-to-noise ratio for all observed peaks can be seen in the tumor spectrum compared to the spectrum from the non-involved sample (a3 and b3). GPC show the most intense signal from cholines in the selected region of the spin-echo spectrum from the non-involved sample, whereas PC is the dominant choline in the spectrum from the tumor. Glycine, taurine and lactate represent the most intense metabolite signals in the spectrum from the tumor, whereas none of these peaks

dominate the spectrum from the non-involved specimen. Glucose can be found in both spectra.

The relative intensities of GPC, PC and choline were examined in spectra from the microscopy confirmed cancerous (n=76) and non-involved samples (n=9). GPC showed the most intense signal of the cholines in spin-echo spectra from non-involved samples, whereas PC was the dominant choline peak in the majority of spectra from tumor samples. By describing intensities of PC or choline being larger than GPC in spin-echo MAS spectra from tumor samples (PC>GPC or Cho>GPC), tumor samples could be discriminated from non-involved with a sensitivity and specificity of 82 and 100%, respectively.

Spin-echo ^{1}H HR MAS spectra of invasive ductal carcinoma specimens from four breast cancer patients are presented in Figure 3, the spectral region 2.9 to 4.8 ppm is shown. The spectrum shown in Figure 3A is from a large tumor (5.3 cm) from a patient diagnosed with invasive ductal carcinoma, grade III and is dominated by betaine, choline containing compounds, taurine and lactate. GPC give the most intense signal of the choline resonances. Glucose could not be detected. The sample was described to contain 30% tumor cells, 65% connective tissue and 5% fatty tissue. Spectra in Figure 3B and 3C are acquired from tumor samples from patients diagnosed with invasive ductal carcinoma, grade II. Tumor size was 1.6 and 1.5 cm respectively, and both specimens were described as 15% tumor cells and 85% fibrous connective tissue. The two spectra show many similar features, but have clearly different levels of glucose and glycine. Figure 3D shows a spectrum from tumor sample from patient with ductal

carcinoma in situ (DCIS). The biopsy was described as 80% tumor and 20% connective tissue. The glycine peak is dominant, and choline gives the most intense resonance signal of the choline metabolites.

Twenty of the 85 HR MAS spectra obtained from tumor samples showed one singlet at 3.28 ppm and one at 3.92 ppm (Figure 3A), tentatively assigned to the N-$(CH_3)_3$ and CH_2 group in betaine respectively.[24] These resonances were detected in spectra of samples from patients diagnosed with different histopathologic breast cancer types. The tentative betaine signals could not be verified in spectra from non-involved samples.

Tissue metabolite concentrations

Tissue metabolite calculations were estimated from 72 tumor samples and one non-involved sample. β-glucose concentrations were calculated from 70 spectra from tumors and eight spectra from non-involved samples. Samples from chemotherapy treated patients and tumor samples without verified cancer cells were removed from the original grouping in Table 1 and separated in two new groups. Metabolite concentrations from sample from metastasis from lung (patient number 83) was kept out. Tissue concentrations for all selected metabolites are presented in Table 2. ANOVA of mean tissue concentrations showed that differences between the groups were not significant, except for choline and creatine. Pairwise multiple comparisons (Bonferoni, SPSS) showed that samples from tumors without cancer cells was significantly different from IDC III in concentration of choline and from chemotherapy treated patients in levels of creatine. Some trends of different metabolite levels between groups could be observed for other metabolites. Content of choline and GPC increased with grading of

IDC (Table 2). Samples from patients treated with chemotherapy before surgery had variable contents of GPC and PC.

Four of the samples analyzed for metabolite contents contained necrotic tissue, three from patients with IDC and one from patient with metastasis from lung. The tissue sample from the lung metastasis was found to have high concentration of *myo*-inositol (23.0, µmol / gram tissue), while the three samples from patients with invasive ductal carcinoma did not show remarkable values of any of the investigated metabolites.

Tissue metabolite concentrations were also compared to patient lymph node status and tumor size. Metabolite concentrations in tissue samples from patients who received chemotherapy before surgery were left out. In addition, tumor size and lymph node status were inaccessible from three patients, resulting in comparisons of 60 samples. The results are presented in Figure 4. Tumors larger than 2.0 cm were found to have significant higher levels of glycine ($p=0.03$) and choline ($p=0.04$) compared to tumors smaller than or equal to 2.0 cm. When comparing tissue levels of metabolites to patients lymph node status no significant differences could be found in samples from node positive and negative patients. There was however a trend of increased *myo*-inositol in samples from node positive patients ($p=0.08$). A comparison of glycine to taurine concentration ratio of these samples (34 from negative and 26 from positive lymph node patients) showed no difference between negative (0.49 ± 0.38) and positive (0.51 ± 0.48) lymph node samples.

Principal component analysis

Inspection of the different score plots against clinical parameters revealed few apparent relationships. The most noticeable connection was found between PCA score values of the HR MAS spectra and fraction of tumor cells in samples. This tendency was found in both water suppressed and spin echo spectra. A PCA of spin-echo spectra (spectral region 4.8 to 2.9 ppm) of all samples (n=103) led to a grouping of twenty samples (results not shown). These twenty samples were verified non-involved samples (n=8), unconfirmed non-involved samples (n=6) and six tumor samples containing 0% (n=5) and less than 5% (n=1) tumor cells. Score values of the remaining samples had a weak tendency of increased distance to the non-involved samples score values with tumor cell content. The clearest association between spectral profile and sample content of tumor cells was found by PCA of samples from patients diagnosed with invasive ductal carcinoma, grade II. A PCA score plot and loading profile based on the spin echo spectra (spectral region 2.9 to 4.7 ppm) of samples from these patients are shown in Figure 5. Samples of higher fraction tumor tissue showed higher scores for PC1, which was dominated by glycine and PC. Tumor cells of this histopathologic cancer class tend to contain relatively higher levels of glycine and PC than fat and fibrous connective tissue.

Samples from breast cancer patients with spread to lymph nodes could generally not be classified based on principal component analysis. A trend towards grouping of samples from node negative and positive samples were found for samples from IDC patients (Figure 6A). Samples from patients with unknown lymph node status were left out (n=4). Samples from lymph node positive patients have higher scores for PC2,

representing high glycine and PC and low taurine and GPC. β-glucose, lactate, creatine, betaine and choline also contributed to this principal component (Figure 6B). Nearly separation of lymph node positive and negative samples was found for IDC patients when spectra from samples containing fat tissue were excluded (Figure 6C). Lymph node positive samples showed higher score for PC4 and slightly lower for PC3 compared to lymph node negative samples. PC4 was dominated by a positive glycine peak and negative contribution from taurine (Figure 6D). β-glucose, lactate, GPC, PC, choline and betaine also contributed to this principal component. A comparison of the score values for PC4 showed a highly significant difference ($p=0.001$ by Student t-test, equal means) between tumor samples from node positive and node negative patients. This finding indicate increased content of glycine and reduced taurine in samples from node positive relative to node negative IDC patients.

Discussion

MR spectra from breast cancer specimens of different histopathologic type and grading, different tumor size and fraction of tumor tissue have many similar characteristics, as demonstrated in Figure 3. Analyses of HR MAS spectra of breast cancer samples indicated that the diversities in the metabolic profiles from specimens of different clinical classifications may be small.

Tissue metabolite concentrations estimated from the HR MAS spectra were not accurate. The concentrations of the internal standard in the different samples are approximate due to the excess fluid removal in MAS rotor assembling. Peak areas calculated by curve fitting may also vary due to heavily overlapping peaks, especially in

the choline region. In several of the spectra from samples in PBS buffer with 5mM TSP, the intensity difference between TSP and metabolites of interest was large and buffer with 1mM TSP was preferred. A Student t-test between tissue metabolite concentrations estimated from the differently prepared samples showed no significant differences for any of the measured metabolites.

The samples had been stored for several months before MR analyses were performed. The metabolite degradation at -196 °C is considered negligible, whereas tissue rupture and the risk of metabolic leakage due to the storage condition can be extensive.[25,26] Breast tissue specimens were frozen without storage buffer, avoiding metabolite leakage to buffer. Reports suggest that the procedure of freezing and thawing are more important than storage period.[26] Storage period for each sample was compared to score values in PCA and estimated tissue metabolite content (ANOVA). No significant correlation could be found. Except for buffer TSP concentration, the sample treatment was similar concerning storage procedures, MAS experiments and metabolite analysis. This first attempt on quantification of metabolites in intact breast cancer tissue from MAS spectra allowed a comparison of metabolite levels between various samples.

Tissue concentration of lactate from the water suppressed spectra could not be calculated due to overlapping lipid signals with both lactate resonances. Also, low molecular weight molecules in non-involved tissue were undetectable from water suppressed spectra. Spin echo spectra show effective suppression of signals from lipids and macromolecules with short T_2 values and increase the S/N ratio for water soluble metabolites (Figure 2). However, in order to determine metabolite concentrations from

spin echo spectra, the signal dependency on transversal relaxation times must be taken into account.[18] In further studies, quantification will be attempted based on spin-echo spectra. Alternative standards as formate could be used as internal standard since TSP can bind to proteins.[27]

In a study of Beckonert *et al.,* 49 tumor and 39 healthy samples from breast were analyzed after dual extraction, and the resulting spectra examined using neural networks (k-nn) and self-organizing maps.[13] They reported increased PC and taurine according to grading, and elevated levels of β-glucose and *myo*-inositol in non-involved tissue compared to malignant. Our findings of higher levels of taurine and PC in tissue specimens from tumors of type IDC grade II and III compared to grade I (Table 2) are in accordance with these findings. Previous estimated β-glucose concentrations in perchloric acid extracs from breast tissue also showed higher levels (p=0.16) in non-involved breast tissue (0.53 μmol/g) compared to malignant (0.28 μmol/g) (not detected levels in eight of 16 spectra is set to 0 μmol/g).[16] Reduced glucose content in malignant tissue is assumed to be due to increased glycolytic activity in solid tumors.[28,29] However, tissue content of β-glucose estimated from MAS spectra was found to be lower in non-involved tissue compared to tumor tissue (Table 2). High content of fat tissue in non-involved specimens is a likely cause for low levels of water soluble metabolites, but can not explain the different results from extracts of breast cancer tissue.[13,16] Further studies will be performed in attempt to explain these results.

Several studies of breast cancer using MR spectroscopy, *in vivo* and *ex vitro*, have shown that malignant lesions from breast have increased levels of choline containing

components.[12,30] Studies on extracts of breast cancer tissue have reported elevated levels of PC in cancerous tissue compared to non-involved tissue[13,14,16] and benign breast lesions.[17] MacKinnon *et al.*[17] managed to classify malignant from benign breast lesions based on the choline to creatine ratio. The different choline to creatine ratios found in our study did not correlate to clinical parameters. However, since metabolites in non-involved samples were difficult to quantify, only comparisons between different stages of cancer was obtainable. No tendency of correlation between tumor grading, size or lymph node status could be found to any of the cholines to creatine ratios. Cheng *et al.* presented the first study on HR MAS MR spectroscopy of breast cancer tissue, correlating tissue metabolite ratios to histopathologic grade.[15] In that study, the reported PC/Cho ratio was 1.90 for IDC II (n=9) and 4.90 for IDCIII (n=6).[15] In our study, average PC/Cho ratios for IDC II (n=26) and IDC III (n=19) were 2.76 and 1.88 respectively. The relative decrease from IDC II to IDC III in our study reflects the larger increase in choline than PC. Clinically, invasive ductal carcinoma grade II and III have many similar characteristics, and small differences in the chemical properties are plausible.

The pathways of intracellular choline metabolism in breast is synthesis of phosphatidylcholine (a membrane phospholipid) or oxidation to the methyl donor betaine.[9] Betaine has previously been reported in mammary cancer cell lines (MCF-7) [9,31] and in renal tissue.[24] The possible finding of betaine in a fraction of the analyzed samples is interesting with regard to characterization of breast tumor tissue. Estimation of tissue concentrations could not be performed in the selected spectral region because of overlap with signals from taurine, glycine and β-glucose. The observation of betaine

in breast cancer tissue should be verified by two-dimensional MR spectroscopic methods.

Elevated levels of glycine was found in large tumors (Figure 4), and was also associated with samples with high content of cancer cells (Figure 5) and tumors from samples with positive lymph nodes (Figure 6). Glycine levels have been found to contribute to characterization of brain tumors in previous reports.[32,33] Altered glycolysis (aerob) in tumors has been suggested as a source of elevated glycine.[32] Glycine and taurine was found to be central in the possible discrimination of samples from lymph node positive and negative patients (Figure 6B and D), but the mechanisms behind these findings are not apparent. Taurine has been found in elevated levels in prostate[21], breast[13] and colon cancer.[34] The roles of taurine are not fully understood, and it appears to have different functions in different tissues.[35]

The tissue concentrations of glycine and choline were significantly lower in samples not containing tumor cells (Table 2). Related findings were observed by PCA of the MAS spectra (Figure 5). Smith *et al.*[36] suggested that the heterogeneity of breast cancer tissue led to dilution of signals by other tissues than cancerous tissue. A strong influence on metabolite findings from tissue heterogeneity have been suggested in several studies.[21,36,37] The trend seen in our results indicate differentiation of samples due to the fraction of tumor cells.

A study on fine needle aspirates from breast cancer samples by Mountford *et al.*[8] provided classification of samples from patients with positive lymph nodes with an 94%

accuracy using a statistical classification strategy involving linear discrimination analysis. This method was not successful on core biopsies due to their high content of fat.[8] PCA of our HR MAS spectra obtained from samples without fat tissue from ductal carcinomas led to a separation of samples from lymph node positive and negative samples ($p=0.001$). Also spectra from samples containing fat showed a trend towards grouping of samples from node positive and negative IDC patients. To investigate if this method has a clinical impact, MAS spectra from a larger number of samples should be examined. A comparison of the spectral profiles to patient outcome after 5 or 10 years would be important to assess the clinical value of the results.

Cancerous and non-involved breast tissue can be distinguished based on their chemical profiles from HR MAS analysis of intact tissue specimens. This can be seen by comparisons of relative choline peak intensities and by principal component analysis. Small differences between tissue metabolite concentrations was associated with grading, tumor size and lymph node status. The heterogeneity of breast cancer biopsies influence the metabolic profile. Correlation between tumor size and glycine and choline concentration was still found. Estimation of tissue concentrations of metabolites could benefit from a method based on spin-echo spectra. PCA described a possible correlation between spectral profiles and patient lymph node status. Our results suggest a potential method of discriminating samples from patients with lymph node involvement.

References

1. Parkin DM, Bray F, Ferlay J, Pisani P. Estimating the world cancer burden: Globocan 2000. *Int J Cancer.* 2001; **94**: 153-156.

2. Kleihues P, Stewart BW, World Health OrganizationWorld cancer report. WHO, IARC Press: Lyon, 2003.

3. Kuru B, Camlibel M, Ali GM, Alagol H. Prognostic factors affecting survival and disease-free survival in lymph node-negative breast carcinomas. *J Surg Oncol.* 2003; **83**: 167-172.

4. Saphner T, Tormey DC, Gray R. Annual hazard rates of recurrence for breast cancer after primary therapy. *J Clin Oncol.* 1996; **14**: 2738-2746.

5. Campos SM, Hayes DF. Breast cancer. In *Atlas of diagnostic oncology*, Shaffer, Kitt, Wieczorek, Tad, and Skarin, Arthur T. (eds). Mosby: Edinburgh, 2003; 243-281.

6. Noguchi M. Therapeutic relevance of breast cancer micrometastases in sentinel lymph nodes. *Brit J Surg.* 2002; **89**: 1505-1515.

7. Walenta S, Wetterling M, Lehrke M, Schwickert G, Sundfor K, Rofstad EK, Mueller-Klieser W. High lactate levels predict likelihood of metastases, tumor

recurrence, and restricted patient survival in human cervical cancers. *Cancer Res.* 2000; **60**: 916-921.

8. Mountford CE, Somorjai RL, Malycha PL, Gluch L, Lean CL, Russell P, Barraclough BH, Gillett DJ, Himmelreich U, Dolenko B, Nikulin AK, Smith ICP. Diagnosis and prognosis of breast cancer by magnetic resonance spectroscopy of fine-needle aspirates analysed using a statistical classification strategy. *Brit J Surg.* 2001; **88**: 1234-1240.

9. Katz-Brull R, Seger D, Rivenzon-Segal D, Rushkin E, Degani H. Metabolic markers of breast cancer: enhanced choline metabolism and reduced choline-ether-phospholipid synthesis. *Cancer Res.* 2002; **62**: 1966-1970.

10. Tosi MR, Fini G, Tinti A, Reggiani A, Tugnoli V. Molecular characterization of human healthy and neoplastic cerebral and renal tissues by in vitro (1)H NMR spectroscopy (review). *Int J Mol Med.* 2002; **9**: 299-310.

11. Mountford CE, Delikatny EJ, Dyne M, Holmes KT, Mackinnon WB, Ford R, Hunter JC, Truskett ID, Russell P. Uterine cervical punch biopsy specimens can be analyzed by 1H MRS. *Magn Reson Med.* 1990; **13**: 324-331.

12. Podo F. Tumour phospholipid metabolism. *NMR Biomed.* 1999; **12**: 413-439.

13. Beckonert O, Monnerjahn J, Bonk U, Leibfritz D. Visualizing metabolic changes in breast-cancer tissue using 1H-NMR spectroscopy and self-organizing maps. *NMR Biomed.* 2003; **16**: 1-11.

14. Gribbestad IS, Fjosne HE, Haugen OA, Nilsen G, Krane J, Petersen SB, Kvinnsland S. *In Vitro* Proton NMR Spectroscopy of Extracts from Human Breast Tumours and Non-Involved Breast Tissue. *Anticancer Res.* 1993; **13**: 1973-1980.

15. Cheng LL, Chang I-W, Smith BL, González RG. Evaluating human breast ductal carcinomas with high-resolution magic-angle spinning proton magnetic resonance spectroscopy. *J Magn Reson.* 1998; **135**: 194-202.

16. Gribbestad IS, Sitter B, Lundgren S, Krane J, Axelson D. Metabolite Composition in Breast Tumors Examined by Proton Nuclear Magnetic Resonance Spectroscopy. *Anticancer Res.* 1999; **19**: 1737-1746.

17. Mackinnon WB, Barry PA, Malycha PL, Gillett DJ, Russell P, Lean CL, Doran ST, Barraclough BH, Bilous M, Mountford CE. Fine-Needle Biopsy Specimens of Benign Breast Lesions Distinguished from Invasive Cancer *ex Vivo* with Proton NMR Spectroscopy. *Radiol.* 1997; **204**: 661-666.

18. Cheng LL, Chang I-W, Louis DN, González RG. Correlation of High-Resolution Magic Angle Spinning Proton Magnetic Resonance Spectroscopy with Histopathology of Intact Human Brain Tumor Specimens. *Cancer Res.* 1998; **58**: 1825-1832.

19. Barton SJ, Howe FA, Tomlins AM, Cudlip SA, Nicholson JK, Bell BA, Griffiths JR. Comparison of in vivo 1H MRS of human brain tumours with 1H HR-MAS spectroscopy of intact biopsy samples in vitro. *MAGMA.* 1999; **8**: 121-128.

20. Taylor JL, Wu CL, Cory D, Gonzalez RG, Bielecki A, Cheng LL. High-resolution magic angle spinning proton NMR analysis of human prostate tissue with slow spinning rates. *Magn Reson Med.* 2003; **50**: 627-632.

21. Swanson MG, Vigneron DB, Tabatabai ZL, Males RG, Schmitt L, Carroll PR, James JK, Hurd RE, Kurhanewicz J. Proton HR-MAS spectroscopy and quantitative pathologic analysis of MRI/3D-MRSI-targeted postsurgical prostate tissues. *Magn Reson Med.* 2003; **50**: 944-954.

22. Sitter B, Sonnewald U, Spraul M, Fjosne HE, Gribbestad IS. High-resolution magic angle spinning MRS of breast cancer tissue. *NMR Biomed.* 2002; **15**: 327-337.

23. Farrant RD, Lindon JC, Nicholson JK. Internal Temperature Calibration for ^{1}H NMR Spectroscopy Studies of Blood Plasma and other Biofluids. *NMR Biomed.* 1994; **7**: 243-247.

24. Garrod S, Humpfer E, Connor SC, Connelly JC, Spraul M, Nicholson JK, Holmes E. High-resolution ^{1}H NMR and magic angle spinning NMR spectroscopic investigation of the biochemical effects of 2-bromoethanoamine in intact renal and hepatic tissue. *Magn Reson Med.* 2001; **45**: 781-790.

25. Middleton DA, Bradley DP, Connor SC, Mullins PG, Reid DG. The effect of Sample Freezing on Proton Magic-Angle Spinning NMR Spectra of Biological Tissue. *Magn Reson Med.* 1998; **40**: 166-169.

26. Waters NJ, Garrod S, Farrant RD, Haselden JN, Connor SC, Connelly J, Lindon JC, Holmes E, Nicholson JK. High-resolution magic angle spinning ^{1}H NMR spectroscopy of intact liver and kidney: optimization of sample preparation procedures and biochemical stability of tissue during spectral acquisition. *Anal Biochem.* 2000; **282**: 16-23.

27. Kriat M, Confort-Gouny S, Vion-Dury J, Sciaky M, Viout P, Cozzone PJ. Quantitation of Metabolites in Human Blood Serum by Proton Magnetic Resonance Spectroscopy. A Comparative Study of the Use of Formate and TSP as Concentration Standards. *NMR Biomed.* 1992; **5**: 179-184.

28. Warburg O. On the origin of cancer cells. *Science.* 1956; **123**: 309-314.

29. Dang CV, Semenza GL. Oncogenic alterations of metabolism. *Trends Biochem Sci.* 1999; **24**: 68-72.

30. Negendank W. Studies of human tumors by MRS: a review. *NMR Biomed.* 1992; **5**: 303-324.

31. Katz-Brull R, Margalit R, Degani H. Differential routing of choline in implanted breast cancer and normal organs. *Magn Reson Med.* 2001; **46**: 31-38.

32. Peeling J, Sutherland G. High-resolution ^{1}H NMR spectroscopy studies of extracts of human cerebral neoplasm. *Magn Reson Med.* 1992; **24**: 123-136.

33. Lehnhardt FG, Rohn G, Ernestus RI, Grune M, Hoehn M. ^{1}H- and ^{31}P-MR spectroscopy of primary and recurrent human brain tumors in vitro: malignancy-characteristic profiles of water soluble and lipophilic spectral components. *NMR Biomed.* 2001; **14**: 307-317.

34. Moreno A, Arùs C, Fabra A. ^{1}H MRS markers of tumor growth in intrasplenic tumours and liver metastasis induced by injection of HT-29 cells in nude mice spleen. *NMR Biomed.* 1998; **11**: 93-106.

35. Stapleton PP, O'Flaherty L, Redmond HP, Bouchier-Hayes DJ. Host defense--a role for the amino acid taurine? *J Parenter Enteral Nutr.* 1998; **22**: 42-48.

36. Smith TA, Glaholm J, Leach MO, Machin L, McCready VR. The effect of intra-tumour heterogeneity on the distribution of phosphorus-containing metabolites within human breast tumours: an in vitro study using 31P NMR spectroscopy. *NMR Biomed.* 1991; **4**: 262-267.

37. Cheng LL, Anthony DC, Comite AR, Black PM, Tzika AA, González RG. Quantification of microheterogeneity in glioblastoma multiforme with ex vivo high-resolution magic-angle spinning (HRMAS) proton magnetic resonance spectroscopy. *Neuro-Oncology.* 2000; **2**: 87-95.

Figure Legends

Figure 1 **a**: Water suppressed HR MAS spectrum of breast cancer sample from patient diagnosed with invasive ductal carcinoma grade II (patient number 16). Spectral region 4.8 to ÷0.2 ppm **b**: Three regions from the spectrum in A were used for peak area calculations to estimate tissue concentrations of selected metabolites: 4.7 to 4.6 ppm: β-Glc; β-glucose, 3.6 to 2.9 ppm: Gly; glycine, *m*-Ino; *myo*-inositol, Tau; taurine, *s*-Ino; *scyllo*-inositol, GPC; glycerophosphocholine, PC; phosphocholine, Cho; choline and Cr; creatine, and 0.10 to ÷0.10 ppm: TSP. **c**: Peakfitted presentation of the selected spectral regions. Spectral assignments are as in B. In addition: UA; unassigned and PE; phosphoetanolamine. The hatched peaks were not included in metabolite calculations.

Figure 2 Spectra of tumor (**a**) and adjacent non-involved tissue (**b**) from the same breast cancer patient diagnosed with invasive ductal carcinoma, grade II. The spectral region from 5.5 to ÷0.5 ppm of water suppressed spectra are presented in a1 and b1. The spectral region 4.8 to 2.9 ppm from the same spectra are presented in a2 and b2 whereas the same spectral regions (4.8 to 2.9 ppm) from the corresponding spin-echo spectra are shown in a3 and b3. W annotates residual water, while L is noted above signals from lipids.

Figure 3 Spin echo HR MAS spectra of breast cancer specimens from four breast cancer patients. Patient diagnoses are presented in the figure: IDC; invasive ductal carcinoma and DCIS; ductal carcinoma in situ. Only the spectral regions 4.8 to 2.9 ppm are shown. Spectral assignments are given in **d**. Abbreviations: β-Glc; β-glucose, Lac;

lactate, *m*-Ino; *myo*-inositol, Cr; creatine Gly; glycine, Tau; taurine, *s*-Ino; *scyllo*-inositol, GPC; glycerophosphocholine, PC; phosphocholine and Cho; choline.

Figure 4 Tissue metabolite concentrations (μmol per gram tissue) and metabolite concentration ratios calculated from HR MAS spectra (n=60). Samples from chemotherapy treated patients were left out. Lymph node status and tumor size were unavailable for three patients. **a**: Metabolite concentrations in tumors smaller and larger than 2.0 cm. * : p=0.039, §: p=0.027. **b**: Metabolite concentrations in tumors from node positive and negative patients.

Figure 5 **a**: Score plot of PC1 and PC2 from PCA of spin-echo spectra of samples from patients diagnosed with invasive ductal carcinoma, grade II. Spectra from samples from chemotherapy treated patients were excluded (n=6). The principal components PC1 and PC2 describe 44% and 15% of the variation in the spectra respectively. The symbols representing the different samples were in accordance to the microscopic evaluation of fraction of tumor cells: m: microscopic examination was not performed, x: less than 10%, Δ: 10-25%, •: 26-49% and ∗: more than 50% tumor. **b**: Loading profile of PC1, representing the dominant features of the analyzed spectral region. The loading profile corresponds to the spectral region 4.7 to 2.9 ppm excluding the residual glycerol backbone signals from 4.4 to 4.2 ppm. Abbreviations: β-Glc; β-glucose, Lac; lactate, Cr; creatine Gly; glycine, PC; phosphocholine.

Figure 6 **a**: Score plot of PC1 and PC2 from PCA of spin-echo spectra of samples from patients with invasive ductal carcinoma (n=73). The principal components PC1 and PC2 describe 33% and 13% of the variation in the spectra respectively. + denotes samples from patients with lymphatic spread and o from lymph node negative patients. **b**: Loading profile of PC2 in which most samples from patients with lymphatic spread showed high score. The loading profile corresponds to the spectral region 4.7 to 2.9 ppm excluding the residual glycerol backbone signals from 4.4 to 4.2 ppm. Abbreviations: β-Glc; β-glucose, Lac; lactate, Cr; creatine Gly; glycine, Tau; taurine, GPC; glycerophosphocholine, PC; phosphocholine and Cho; choline. **c**: Score plot of PC3 and PC4 from PCA of spin-echo spectra of samples from patients with invasive ductal carcinoma (n=41). Samples containing fat tissue (n=26) or not examined by microscopy (n=3) were excluded. The principal components PC3 and PC4 describe 11% and 10% of the variation in the spectra respectively. + denotes samples from patients with lymphatic spread and o from lymph node negative patients. **d**: Loading profile of PC4 in which most samples from patients with lymphatic spread showed high score. The loading profile corresponds to the same spectral region as in b. Abbreviations are the same as in b.

Table 1 Patient data. Patient diagnoses are abbreviated: IDC, Invasive ductal carcinoma, the roman numbers represent tumor grading; ILC, invasive lobular carcinoma; SA and IDP, sclerosing adenosis and intraductal papilloma; DCIS, Ductal carcinoma in situ. In cases of more than one type of tumor morphology, only the most severe type was used in the table.

Sample number	Patient diagnosis	Number of patients	Patient age (years)	Tumor size [§] (cm)	Lymphatic spread		Steroid hormone receptor status ER / PgR	
					positive	negative	positive	negative
1-6	IDC I	6	64 (± 13)	2.3 (± 1.6)	1	5	6	0
7-43	IDC II	37	64 (± 15)	2.5 (± 1.5)	20	14	33	4
44-71	IDC III	28	60 (± 16)	3.3 (± 1.6)[*]	14	14	20	8
72-73	IDC, grading not known	2	67 (± 16)	5.0[*]	1	0	1	0
74-78	ILC	5	62 (± 13)	3.4 (± 2.6)	4	1	5	0
79-81	Colloid carcinoma	3	60 (± 14)	2.1 (± 0.5)	0	3	3	0
82	Secondary tumor from lung	1	59	ND	NA		NA	
83	SA and IDP (benign)	1	31	1.9	ND		ND	
84-85	DCIS	2	63 (± 22)	2.5[*]	0	2	1	0
1-85	All tumors	85	62 (± 15)	2.8 (± 1.6)	40	39	69	12
86-103	Adjacent non-malignant tissue	18	56 (± 13)	NA	NA	NA	NA	NA

NA: Not applicable
ND: Not done
ER / PgR: Estrogene and progesterone receptor. Positive: one or both positive, Negative: both negative.
[*]: Tumor size could not be determined for patients number 43, 73 and 85.
[§]: Determined by histopathology, except patient number 39 and 64 (clinical palpation). Patients number 6, 41, 67 and 84 were diagnosed with two foci of the tumor and the sum of the two foci was used.
The following subtypes of ductal carcinomas are included: Patient number 53: comedo subtype, patient number 68: medullary carcinoma and patient number 73: neuroendocrine differentiation.
The biopsies from patients number 20 and 36 were excised during surgery for bilateral breast cancer.
Thirteen of the patients in this study received neoadjuvant therapy (adriamycin; epirubicin; 5-fluorouracil, epirubicin and cyclophosphamid in combination; tamoxifen; taxotere or taxol) prior to surgery. These were patients number 8, 18, 32, 38, 39, 41, 55, 64, 65, 68, 69, 70 and 78.

Table 2 Mean tissue metabolic concentrations (µmol per gram tissue) and standard deviation (SD) of metabolites estimated from water suppressed HR MAS spectra of intact breast cancer specimens. Numbers of samples analyzed for glucose content are given in brackets.

Number of samples	IDC 1 5 (5)		IDC 2 26 (26)		IDC 3 19 (18)		Colloid 3 (3)		ILC 3 (3)		DCIS 1 (1)	Non-involved 1 (8)		Chemo 9 (9)		Non-cancer 5 (4)	
	Mean	SD	Mean	SD	Mean	SD	Mean	SD	Mean	SD		Mean	SD	Mean	SD	Mean	SD
choline	0.60	0.20	0.77	0.32	0.92	0.37	0.67	0.24	0.56	0.42	0.60	0.29		0.83	0.36	0.30	0.10
creatine	1.18	0.95	1.62	0.88	1.71	1.01	0.92	0.36	1.28	0.97	0.55	0.24		2.78	2.33	0.53	0.17
GPC	0.74	0.15	1.13	0.67	1.35	0.69	0.42	0.10	1.06	0.83	0.37	0.40		1.78	2.04	0.28	0.06
β-glucose	2.67	2.76	1.21	1.17	1.44	1.99	2.04	1.78	0.70	0.98	1.57	0.65	0.5434	0.76	1.04	2.89	2.33
glycine	1.43	0.92	3.54	3.66	3.15	1.81	2.20	0.46	1.60	1.21	1.40	0.60		4.44	3.41	0.73	0.36
myo-inositol	2.67	1.90	3.13	1.92	2.80	1.21	2.42	1.06	4.15	3.13	1.87	1.77		3.05	1.15	1.96	0.49
PC	1.05	0.56	2.13	2.74	1.73	0.87	0.87	0.28	0.97	0.74	0.49	0.29		2.47	2.56	0.32	0.10
taurine	4.23	1.54	7.04	3.95	6.78	3.30	3.26	1.65	8.00	6.07	2.62	1.89		5.97	3.53	2.77	1.11
sum cholines	3.38	1.10	4.97	3.58	5.20	1.85	2.62	0.48	3.67	2.80	2.08	1.75		6.51	4.72	1.19	0.15

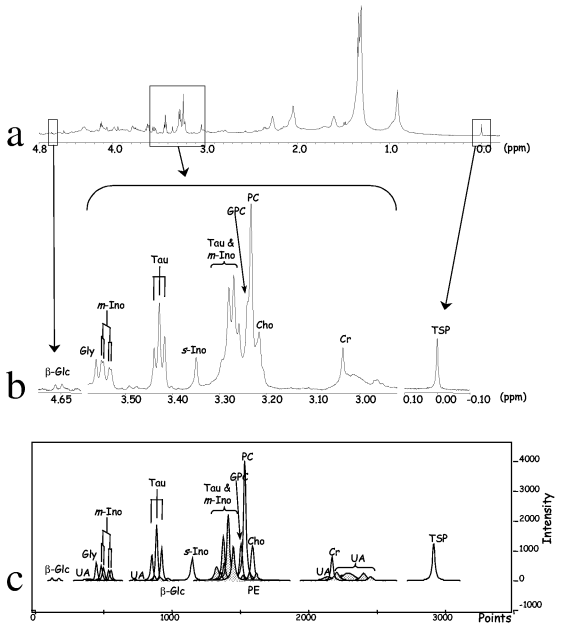

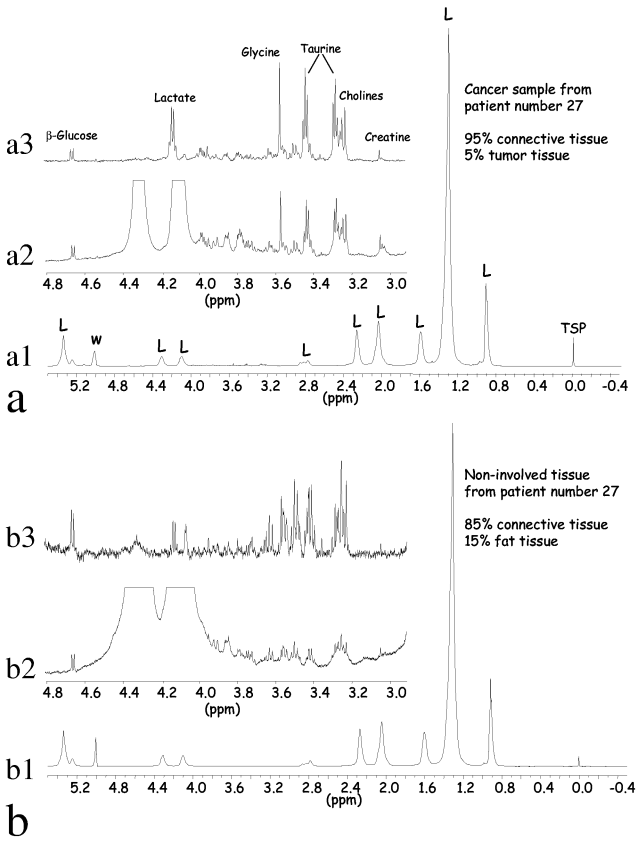

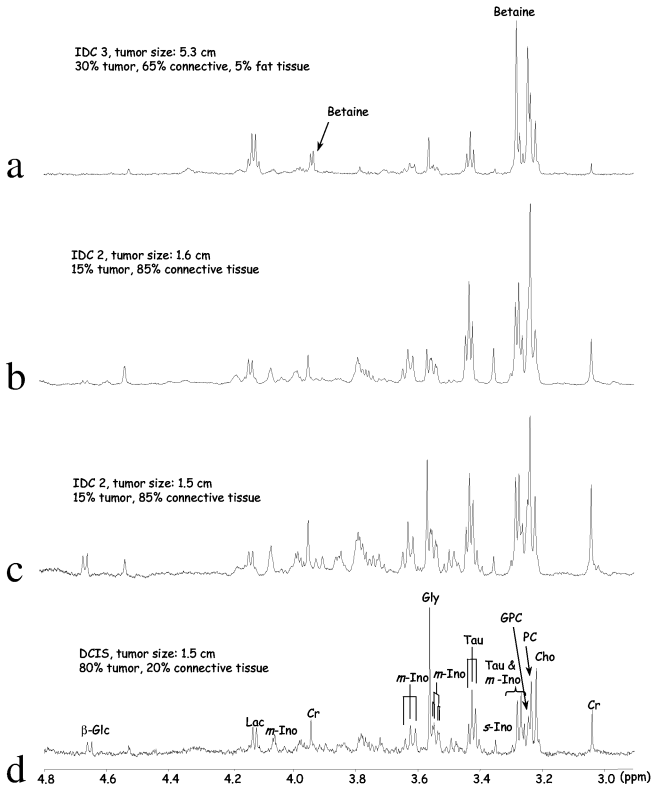

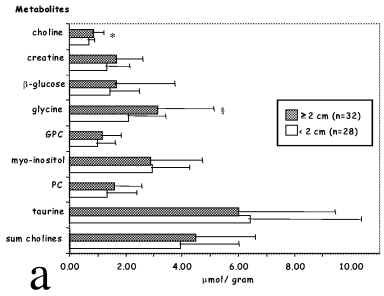

a

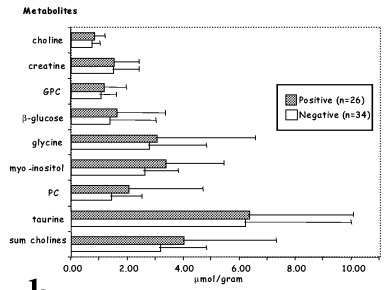

b

a

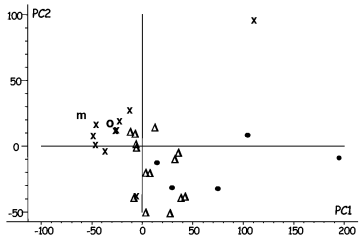

b

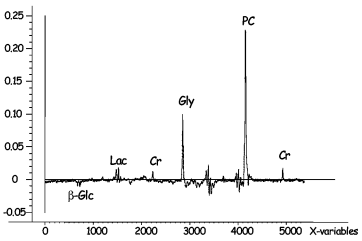

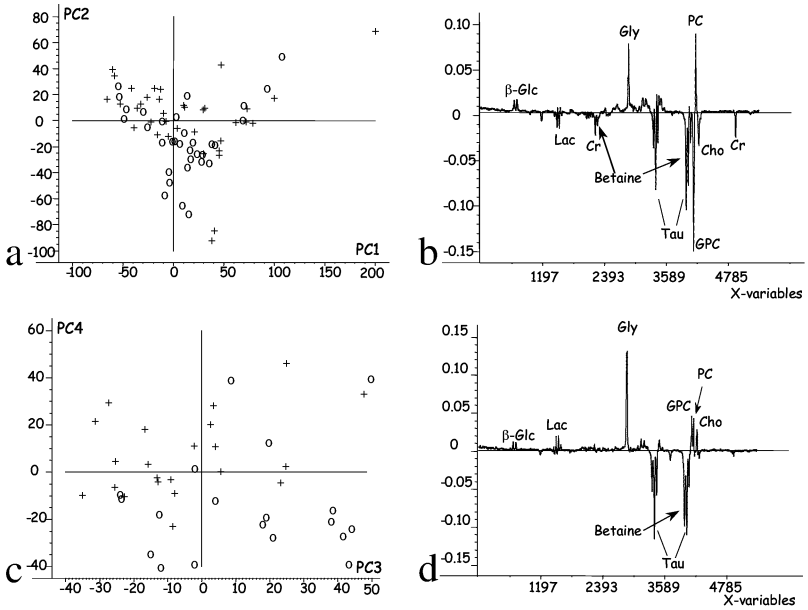

Paper IV

URN:NBN:no-3463

MAGMA (2004) 16: 174–181
DOI 10.1007/s10334-003-0025-5

RESEARCH ARTICLE

Beathe Sitter
Tone Bathen
Bjørn Hagen
Cecilie Arentz
Finn Egil Skjeldestad
Ingrid S. Gribbestad

Cervical cancer tissue characterized by high-resolution magic angle spinning MR spectroscopy

Received: 27 June 2003
Accepted: 3 November 2003
Published online: 27 February 2004

B. Sitter (✉) · T. Bathen
I. S. Gribbestad
SINTEF Unimed,
7465 Trondheim, Norway
E-mail: beathe.sitter@medisin.ntnu.no

B. Sitter
Department of Neuroscience,
Faculty of Medicine,
Norwegian University of Science
and Technology (NTNU)

B. Hagen · F. E. Skjeldestad
Institute of Laboratory Medicine,
Children and Woman's Diseases,
Norwegian University of Science
and Technology (NTNU)

C. Arentz
Department of Physics,
Norwegian University of Science
and Technology (NTNU)

F. E. Skjeldestad
Section of epidemiological research,
Unimed, SINTEF

I. S. Gribbestad
Clinical Cancer Research Unit,
Cancer Clinic, St. Olav University Hospital,
7465 Trondheim, Norway

Abstract *Objective*: In recent years, high-resolution magic angle spinning (HR MAS) has provided the opportunity to explore detailed biochemical composition of intact tissue. Previous studies of intact cervical biopsies with high-resolution magnetic resonance spectroscopy (MRS) have correlated well with histopathology. Lactate level in cervical cancer tissue has been found to correlate to metastatic spread. The purpose of this study was to explore the potential of the HR MAS technique as a tool for chemical characterization of cervical cancer tissue. *Materials and methods*: Tissue samples from the cervix were collected after hysterectomy from patients with cervical cancer ($n = 8$) and patients with nonmalignant disease ($n = 8$). The tissue specimens were analyzed using HR MAS MR spectroscopy combined with principal component analysis (PCA). *Results*: The resulting spectra showed resolution comparable with high-resolution MR spectra of extracts. Multivariate analysis confirmed that MAS spectra classified according to patient diagnosis. *Conclusion*: Malignant tissue of the cervix differed from nonmalignant tissue with regard to higher levels of cholines and amino acid residues and lower levels of glucose.

Keywords Cervical cancer · MR spectroscopy · Choline · Principal component analysis

Abbreviations *Cho* choline · *GPC* glycerophosphocholine · *MAS* magic angle spinning · *PC* phosphocholine · *PCA* principal component analysis

Introduction

Cervical cancer represents nearly 10% of all cancers in women from the western world [1]. Screening programs in developed countries have contributed to a decline in incidence and mortality over the last 50 years; in less developed countries, however, screening has often not been established and cervical cancer is the most frequent cancer form in women in many third world countries [2].

Tissue from cervical cancer patients have been examined by magnetic resonance (MR) spectroscopy (MRS) in vivo [3, 4], and Lee et al. [3] found that spectra of adenocarcinomas differed slightly from those from squamous cell carcinomas. Furthermore, Mountford et al. have shown that standard proton MRS of tissue

samples can distinguish inflammation from malignant lesions in the cervix [5]. In a later work [6], the same research group was able to separate invasive and preinvasive lesions applying proton MRS. The results from these studies, which are based on broad and overlapping resonances, indicate that higher resolved spectra can provide more detailed information in cervical cancer tissue.

Progress has been made in in vitro MR analysis of tissue samples due to the implementation of high-resolution magic angle spinning (HR MAS) spectroscopy. In tissue, restriction of molecular motion and magnetic susceptibility results in spectral broadening as compared with liquids. Rapidly spinning the sample around its own axis in a 54.7° angle to the static magnetic field, the so-called magic angle, eliminates some of the factors contributing to line broadening. The result is spectra of intact tissue samples with resolution comparable with high-resolution spectra of extracts [7]. MAS spectroscopy has been applied in various studies of human tissues and diseases, such as cancers of the brain [8], prostate [9], and breast [10].

Because MRS allows identification of a large number of metabolites simultaneously, the vast amount of information makes visual inspection and analysis difficult. Spectra of tumors are often found to differ from spectra of nonmalignant tissue in intensities of almost all peaks [11, 12], and multivariate analysis of the full MR spectra has proven useful in interpreting the MR findings [13, 14].

The purpose of this study was to evaluate HR MAS analysis of tissue from the uterine cervix as a tool in cancer metabolic studies. MR spectra were obtained from biopsy material from the cervix from patients with cervical cancer and compared with spectra from cervical biopsies from patients without cancer. Multivariate analysis of the HR MAS spectra was used to evaluate whether classification of the different tissue types was in accordance with patient diagnosis. The MR spectra were explored in detail in an attempt to reveal the biochemical composition of the tissues and identify characteristics of tumor tissue.

Methods

Subjects

Eight women with a mean age of 50 years (range 39–67), who underwent hysterectomy due to cervical cancer, were included in the study. None of the patients received any anticancer treatment prior to hysterectomy. Histopathological examination of the surgical specimens revealed six squamous cell carcinomas (stages IB and IIA) and two adenocarcinomas (stage IIB). Two of the patients with squamous cell carcinomas had lymphatic spread. In addition, eight women, mean age 50 years (range 29–69), who underwent hysterectomy for various benign reasons, served as controls.

Samples

After excision, the uterus was kept in saline compresses until tissue specimens were taken from the cervix uteri as soon as possible after surgery. The sample for MAS was taken from a tumor-representative site in the fresh surgical specimen. A total of 16 samples was obtained. The samples were stored in liquid nitrogen until HR MAS MR spectroscopic analysis. Samples were cut to fit a 4-mm (o.d.) rotor and added D_2O before MR analysis.

MR experiments

High-resolution proton MAS spectra were recorded using a BRUKER AVANCE DRX600 spectrometer equipped with a $^{1}H/^{13}C$ MAS probe with possibilities for a gradient along the magic angle axis (BRUKER Analytic, Germany). Samples were spun at 6 kHz and acquisitions obtained using two different one-dimensional sequences for each sample. Water-suppressed spectra were acquired using a single pulse sequence with 2 seconds preirradiation of the water resonance (zgpr, BRUKER) before a 60-degree pulse angle was applied. The second type of spectra was acquired using a spin-echo sequence with water suppression (2 seconds) included (cpmgpr, BRUKER). The acquisitions were performed with a delay of 1 ms repeated 136 times, giving spectra with a total echo time of 285 ms. For both experiments, 128 transients over a spectral region of 10 kHz were collected into 32K points, giving an acquisition time of 1.64 seconds. All experiments were performed at room temperature. The raw data were multiplied with 0.7 Hz exponential line broadening before Fourier transformation into 64K points. Chemical shift referencing was done relative to the methyl group in the lactate resonance, which shifts 1.32 ppm downfield from TSP.

J-resolved spectra were obtained by a standard spin-echo sequence with 2 s water presaturation (Jrespr, BRUKER). Eight transients were collected into 8K data points of 10 kHz spectral region. The interpulse delay was incremented 64 times with 6.4 ms, resulting in 78.1 Hz spectral region in the F1 dimension. The raw data were processed using a sine window function in both dimensions, tilted and symmetrized. Homonuclear correlated spectra (COSY; cosygspr, BRUKER) were recorded by acquisition of 16 transients per increment for 512 increments collected into 2K data points. A spectral width of 8 kHz was used in both dimensions. The time domain data were zero filled and multiplied with a sine window function in both dimensions before Fourier transform.

Multivariate analysis

Water-suppressed and spin-echo spectra were used as inputs in two separate PC analyses.

Water suppressed spectra were Fourier transformed after applying 0.7 Hz exponential line broadening. Baseline offset was adjusted and chemical shifts were referenced to the lactate doublet (1.32 ppm). The spectral regions 0.0–4.5 ppm were saved and collected into one matrix of 16 samples × 2,945 variables.

The FIDs from spin-echo acquisitions were Fourier transformed without window function. Baseline offset was adjusted and chemical shifts were referenced to the lactate doublet (1.32 ppm). The regions from 1.4 to 4.3 ppm were saved as ASCII files and collected into a matrix of 16 samples × 2,700 variables.

For both matrices, the spectra were normalized to the area below the curve (mean normalization). Principal component analysis (PCA) was carried out in an unsupervised manner and was performed with full cross-validation and mean centering [15]. The score plots were examined for correlation with patient diagnosis and age, and the time period samples were subject to room temperature before spectral recordings.

Results

HR MAS ^{1}H spin-echo spectra of biopsies from cervix gave good signal resolution, allowing almost complete separation of the different compounds in the one-dimensional spectra. Additional information from two-dimensional spectra and literature values [7, 16, 17] enabled almost total spectral assignment, providing detailed information on the biological composition of the different tissue samples. In Fig. 1, a ^{1}H spin-echo HR MAS spectrum of cervical tissue specimens from a patient with cervical cancer is shown. The assignments in the figure correspond with the data in Table 1.

Representative spin-echo MAS spectra of cervix uteri tissue specimens from one cervix cancer patient and one control patient are presented in Fig. 2. All spectra showed high resolution. The vast majority of peaks were of similar intensity in all spectra and visual inspection between the two groups revealed very few differences. Spin-echo recorded MAS spectra of the malignant cervical samples deviated from spectra of nonmalignant tissues in levels of glucose and uracil. Glucose was detected in all but one of the eight nonmalignant tissue specimens, but in only three of the eight cervix cancer tissue specimens. Uracil was found in all cervical cancer samples, but could not be detected in any of the nonmalignant tissue specimens. Furthermore, an unas-

Fig. 1 High-resolution spin-echo proton MAS spectra of cervix cancer biopsy from patient diagnosed with squamous cell carcinoma of the cervix uterus. Assignments are given in Table 1. Scaling of the three different parts of the spectrum is done individually and led to cutting the lactate doublet at 1.33 ppm. The spectral region from 5.5 to 4.7 ppm has been excluded. For detailed acquisition parameters, see "Methods"

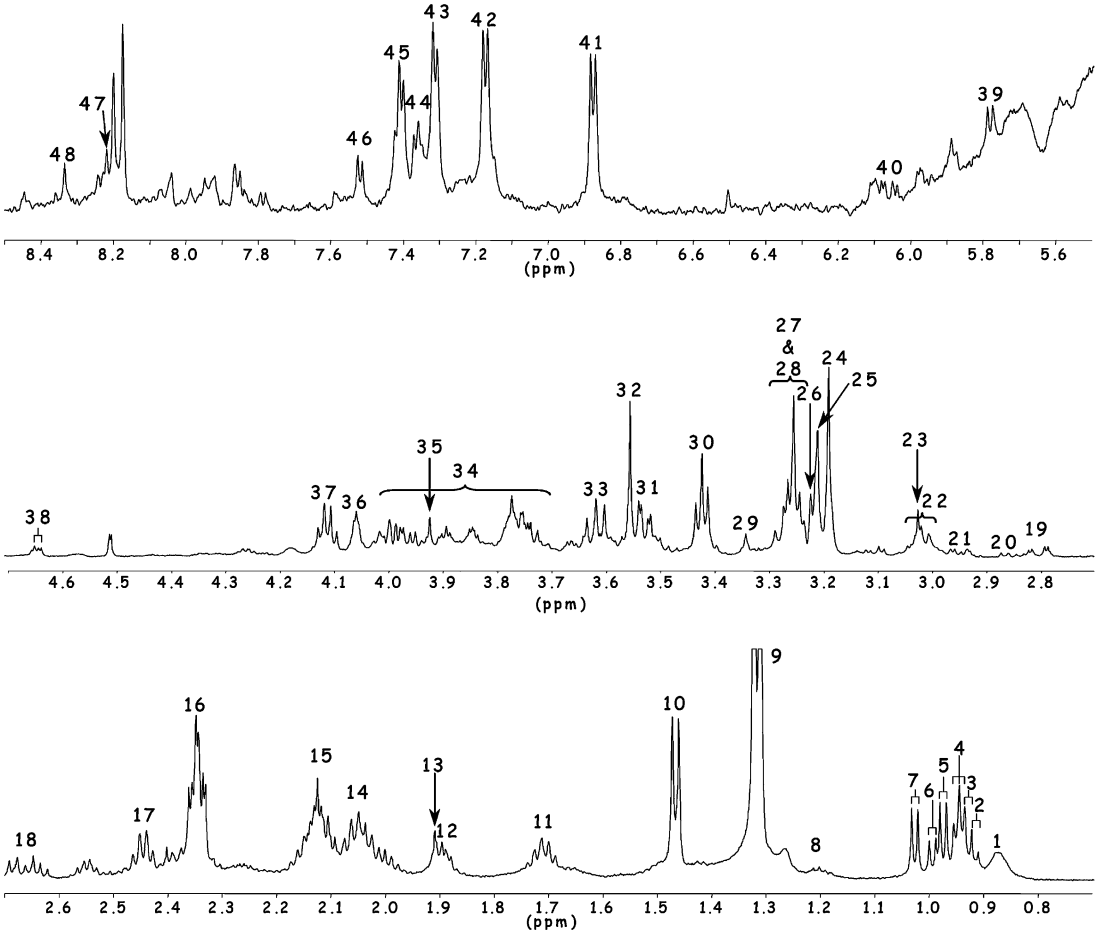

signed peak was detected at 2.02 ppm in the spectrum from one of the two adenocarcinomas, shown in Fig. 2A.

The water-suppressed spectra were used to calculate fatty acid CH_2/CH_3 ratio based on the intensity of the broad resonances at 1.3 and 0.9 ppm respectively (spectra not shown). Cervical cancer samples showed a slightly higher ratio (1.57 ± 0.20) than nonmalignant cervical samples (1.50 ± 0.20), but the difference was not significant.

Table 1 Tentative ^{1}H chemical shift assignment on HR MAS spectra of cervical and uterine tissue samples. Assigned numbers correspond to numbering in Fig. 1

Metabolite		Assigned number	^{1}H Multipl.	chem. shift (ppm)
Fatty acids	$-CH_3$	1	t	0.87
Isoleucine	δCH_3	2	t	0.93
Leucine	$\delta' CH_3$	3	d	0.94
Leucine	δCH_3	4	d	0.96
Valine	γCH_3	5	d	0.98
Isoleucine	γCH_3	6	d	1.00
Valine	$\gamma' CH_3$	7	d	1.03
β-hydroxybutyrate	CH_3	8	d	1.19
Lactate	CH_3	9	d	1.32
Alanine	CH_3	10	d	1.47
Lysine	δCH_2	11	m	1.72
Lysine	βCH_2	12	m	1.90
Acetate	(CH_3)	13	s	1.91
Glutamate	βCH_2	14	c	2.05
Glutamine	βCH_2	15	c	2.13
Glutamate	γCH_2	16	dt	2.34
Glutamine	γCH_2	17	c	2.45
Aspartate	βCH	18	dd	2.67
Aspartate	$\beta' CH$	19	dd	2.80
Aspargine	βCH	20	dd	2.87
Aspargine	$\beta' CH$	21	dd	2.95
Lysine	εCH_2	22	t	3.02
Creatine	CH_3	23	s	3.03
Choline	$N(CH_3)_3$	24	s	3.19
Glycerophospho-choline	$N(CH_3)_3$	25	s	3.21
Phosphocholine	$N(CH_3)_3$	26	s	3.21
Taurine	$N\text{-}CH_2$	27	t	3.25
myo-Inositol	C5H	28	t	3.27
scyllo-Inositol		29	s	3.34
Taurine	$S\text{-}CH_2$	30	t	3.42
myo-Inositol	C1H, C3H	31	dd	3.53
Glycine	αCH_2	32	s	3.55
myo-Inositol	C4H, C6H	33	dd	3.61
Amino acid residues	αCH	34		3.75–4.00
Creatine	CH_2	35	s	3.92
myo-Inositol	C2H	36	t	4.05
Lactate	CH	37	q	4.11
β-Glucose	C1H	38	d	4.64
Uracil	C6H, ring	39	d	5.79
Inosine	C1H ribose	40	d	5.88
Tyrosine	C3H, 5H ring	41	d	5.88
Tyrosine	C2H, 6H ring	42	d	7.18
Phenylalanine	C2H, C6H, ring	43	m	7.32
Phenylalanine	C4H, ring	44	m	7.36
Phenylalanine	C3H, C5H, ring	45	m	7.41
Uracil	C5H, ring	46	d	7.86
Inosine	C2, ring	47	s	8.22
Inosine	C8, ring	48	s	8.34

The results from the multivariate analysis of the MR spectra are presented in Figs 3 and 4. Both principal component analyses showed that the MAS spectra describe biochemical properties that discriminate between malignant and nonmalignant cervical tissue. Sample score values did not correlate with patient age or the time period samples were subject to room temperature.

In Fig. 3A, the score plot of principal components 1 and 2 from PCA of Water-suppressed spectra from cervical tissue are presented. The malignant samples (X) can be separated from the nonmalignant samples (O) by a linear decision boundary. Tissue from cervical cancer patients mainly differed from tissue from controls in high score for the first principal component (PC1). The four cancer samples showing the highest scores for PC1 are the two adenocarcinomas (X_A) and the biopsies from the two patients with lymphatic spread (X_L). This principal component (Fig. 3B), describing 63% of the variation in the spectra, is dominated by lactate, the methyl and methylene groups of lipids, and to some extent, choline-containing compounds. The higher scores for PC1 of cervical cancer samples imply that they have higher contents of these compounds than the nonmalignant cervical samples.

Figure 4A gives the score plot of the first two principal components from PCA of the spin-echo recorded spectra and describes 57% of the total variation in the original 16 spectra. Spectra of cervical cancer biopsies (X) and noninvolved cervical tissue (O) are situated in two distinct groups that can be separated based on their different scores for PC1. Examination of the loading profile of PC1 (Fig. 4B) shows that the samples from patients with cervical cancer may be associated with higher concentrations of cholines (Cho, PC, GPC) and amino acid residues (creatine, taurine, and alanine). In addition, the cancer samples seem to have reduced levels of glucose.

Discussion

Previous reports on MR spectroscopy of cervical cancer biopsies have largely been concerned with lipids and lipid ratios [6, 18]. The CH_2/CH_3 ratio we found for the malignant lesions (1.57) was lower than the ratio (1.89) reported by Delikatny et al. [6], whereas our finding for the noninvolved specimens was higher (1.50/1.28).

Principal component analysis was found to be a better approach for analyzing the HR MAS spectra of cervical specimens. Analysis of the water-suppressed

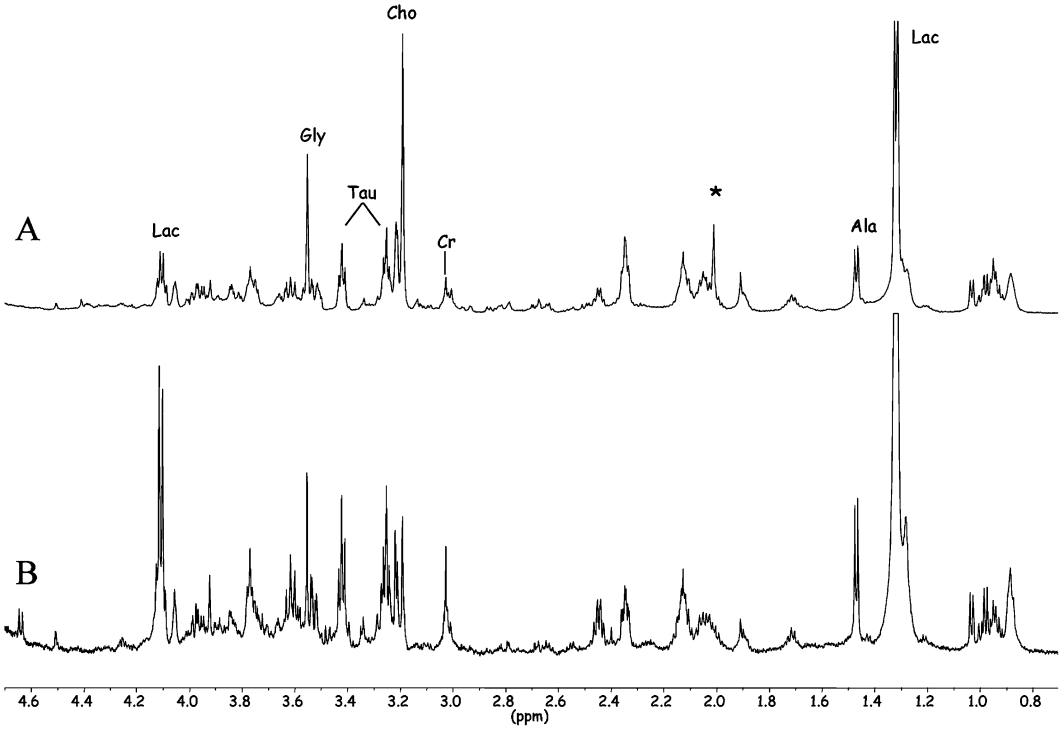

Fig. 2 Spin-echo proton MAS spectra of biopsy samples from (**A**) cervix uterus from cervical cancer patient diagnosed with adenocarcinoma and (**B**) cervix uterus from control. Scaling of the spectra led to cutting of the lactate doublet at 1.33 ppm. For full spectral assignments, see Fig. 1. Abbreviations used in annotations: Lac, lactate; Gly, glycine; Tau, taurine; Cho, choline; Cr, creatine; and Ala, alanine. The peak labeled * is unassigned. For detailed acquisition parameters, see "Methods"

spectra, dominated by lipid signals, led to discrimination of adenocarcinomas and squamous cell carcinomas with lymphatic spread. The spin-echo spectra, where contributions from lipids and other broad resonances are suppressed, separated malignant cervical tissue from noninvolved. The region on the low-field side of the water peak was omitted from the spectra in both multivariate analyses because peaks in this area have intensity variations due to water saturation. Furthermore, the lactate peak at 1.32 ppm was excluded for PCA of spin-echo spectra because the remaining lipid signals influence the intensity of the lactate peak.

The HR MAS spectra of cervix cancer tissue and nonmalignant cervix tissue are dominated by the same metabolites. Classification of the tissue types is made on relative amounts of the same metabolites. As can be seen in the loading profile of PC1 in Fig. 4B, the metabolites that contribute most to classification of the spectra are present in high amounts in all samples.

The loading profile in Fig. 4B shows that lowered glucose levels contribute to the characterization of cervical cancer tissue. This correlates with undetectable levels of glucose in five out of eight MAS spectra of malignant samples. Decreased glucose levels in tumor tissue is due to elevated energy requirement in the proliferation process, and numerous studies have been performed on the increased glucose metabolism in tumors [19, 20] since the Warburg effect was first presented in 1930 [21].

Furthermore, PCA of spin-echo MAS spectra shows that there is extensive variation in creatine concentration among the samples. This indicates the inaccuracy that may occur when utilizing creatine as an internal concentration standard.

The relative concentrations of all cholines were found to be higher in the cervical cancer biopsies. GPC, PC and Cho are important metabolites in the phospholipid metabolism and are thus believed to play roles as tumor markers, describing an increased cell turnover. In vivo MRS has been shown to differentiate between malignant and benign breast lesions based on the choline compounds [22]. The relative concentration of taurine was

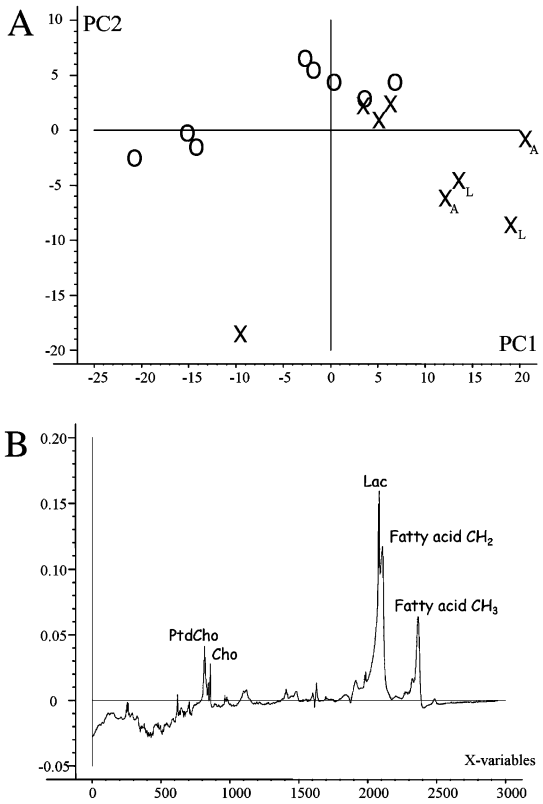

Fig. 3 Score plot of PC1 and PC2 from principal component analysis of the spectral region 0–4.5 ppm of the water-suppressed MAS spectra of biopsies from the cervix from 16 patients. PC1 and PC2 account for 80% of the variation in the spectra. O denotes cervix tissue from noncancer patients while X denotes cervical cancer tissue. The adenocarcinomas and cervical cancer samples from patients with lymphatic spread were denoted X_A and X_L respectively. **B** Loading profile of PC1, representing 63% of the spectral variations. Abbreviations used in assignments: PtdCho, phosphatidylcholine; Cho, choline; and Lac, lactate

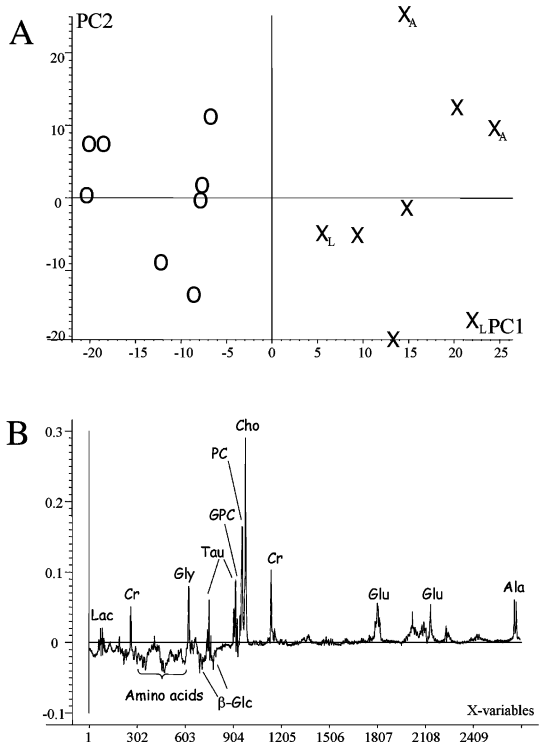

Fig. 4 **A** Score plot of PC1 and PC2 from principal component analysis of the spectral region 4.1–1.4 ppm from spin-echo MAS spectra of biopsies from cervix from 16 patients. PC1 and PC2 account for 55% of the variation in the spectra. X denotes cervical cancer tissue, while O denotes cervix tissue from non-cancer patients. The adenocarcinomas and cervical cancer samples from patients with lymphatic spread were denoted X_A and X_L respectively. **B** Loading profile of PC1. Abbreviations used in assignments: Cr, creatine; Gly, glycine; Tau, taurine; β-Glc, β-glucose; GPC, glycerophosphocholine; PC, phosphocholine; Cho, choline; Glu, glutamate; and Ala, alanine

found to be higher in cervical cancer tissue than in the cervical control tissue. Taurine has been shown to be present in high levels in breast cancerous tissue [23, 24]. It is possible that this rise in taurine levels may be an endogenous defense mechanism against tumor proliferation. Relative levels of glycine were also found to be higher in cervical cancer biopsies. In a study concerning in vitro MRS on specimens of human brain tumors, gliomas were characterized by an increase of the ratios of alanine, choline and glycine over creatine [25].

The peak detected at 2.02 ppm in the spectrum from one of the two adenocarcinomas is probably the same peak as previously reported in six out of seven adenocarcinomas studied by in vivo MRS by Lee et al. [3]. Further two-dimensional spectroscopic analysis of tissue samples should be performed to assign this peak in HR MAS MR spectra.

Walenta et al. [26] found that lactate levels correlated with metastatic spread. Lactate was found to contribute in discriminating adenocarcinomas and samples from patients with lymphatic spread (Fig. 3). The methyl and methylene peaks from lipids contribute to this discrimination, which imply a relatively higher content of lipids. Altered lipid profiles in malignant tissue has been reported in several studies [18, 27, 28].

The tissue biopsies were analyzed at room temperature. Sample temperatures were calculated to 26.17 °C

(range 25.1–27.5 °C) from the 10 spin-echo spectra where glucose was detectable [29]. Samples have been exposed to room temperature for 1.6 hours on average prior to the MR acquisition. Biochemical degradation is assumed to be distinctive. Because lactate is a product of anaerobic degradation of glucose, classification influenced by these metabolites can be unreliable.

The MR spectra enabled classification, even though degradation of metabolites had occurred. Because no clear correlation was found between sample score (Figs 3A and 4A) and time period, metabolic degradation was assumed to be similar at room temperature for the two tissue types. This implies that some of the observed spectral features have to be tissue dependent. Spin-echo spectra, containing signals from small, water-soluble molecules, separate malignant from non-malignant cervical tissue. This result implies that the spectra from malignant samples contain metabolic information specific for cancerous tissue. Spectra including lipids and macromolecules might contain metabolic information that can distinguish types of cervical cancers and maybe predict metastasis. The experimental conditions, however, require caution in interpreting metabolic differences. Further investigations should be performed at low temperature (4 °C) to reduce metabolic degradation and on samples of cytological size.

Combined with multivariate analysis, MR spectra of intact tissue biopsies from cervix uteri discriminate between cancerous and normal cervical tissue. In addition, the high resolution of the HR MAS spectra of tissue specimens from the cervix provides detailed information on the biochemical composition of the tissues. Studies of samples from a larger number of patients are needed in order to evaluate the clinical value of this method in the pathology of cervix uteri.

References

1. Franco EL, Duarte-Franco E, Ferenczy A (2001) Cervical cancer: epidemiology, prevention and the role of human papillomavirus infection. Can Med Assoc J 164:1017–1025
2. Kleihues P, Stewart BW, World Health Organization. (2003) World cancer report. WHO, IARC Press, Lyon
3. Lee JH, Cho KS, Kim Y-M et al (1998) Localized in vivo ^{1}H nuclear MR spectroscopy for evaluation of human uterine cervical carcinoma. Am J Roentgenol 170:1279–1282
4. Allen JR, Prost RW, Griffith OW et al (2001) In vivo proton (H1) magnetic resonance spectroscopy for cervical carcinoma. Am J Clin Oncol 24:522–529
5. Mountford CE, Delikatny EJ, Dyne M et al (1990) Uterine cervical punch biopsy specimens can be analyzed by ^{1}H MRS. Magn Reson Med 13:324–331
6. Delikatny EJ, Russell P, Hunter JC et al (1993) Proton MR and human cervical neoplasia: ex vivo spectroscopy allows distinction of invasive carcinoma of the cervix from carcinoma in situ and other preinvasive lesions. Radiology 188:791–796
7. Sitter B, Sonnewald U, Spraul M et al (2002) High-resolution magic angle spinning MRS of breast cancer tissue. NMR Biomed 15:327–337
8. Cheng LL, Chang I-W, Louis DN et al (1998) Correlation of high-resolution magic angle spinning proton magnetic resonance spectroscopy with histopathology of intact human brain tumor specimens. Cancer Res 58:1825–1832
9. Kurhanewicz J, Swanson MG, Nelson SJ et al (2002) Combined magnetic resonance imaging and spectroscopic imaging approach to molecular imaging of prostate cancer. J Magn Reson Imaging 16:451–463
10. Cheng LL, Chang I-W, Smith BL et al (1998) Evaluating human breast ductal carcinomas with high-resolution magic-angle spinning proton magnetic resonance spectroscopy. J Magn Reson 135:194–202
11. Peeling J, Sutherland G (1992) High-resolution ^{1}H NMR spectroscopy studies of extracts of human cerebral neoplasm. Magn Reson Med 24:123–136
12. Beckonert O, Monnerjahn J, Bonk U et al (2003) Visualizing metabolic changes in breast-cancer tissue using 1H-NMR spectroscopy and self-organizing maps. NMR Biomed 16:1–11
13. Hagberg G (1998) From magnetic resonance spectroscopy to classification of tumors. A review of pattern recognition methods. NMR Biomed 11:148–156
14. Lindon JC, Holmes E, Nicholson JK (2001) Pattern recognition methods and applications in biomedical magnetic resonance. Prog Nucl Magn Reson Spectrosc 39:1–40
15. Martens H, Næs T (1991) Multivariate calibration. Wiley, New York
16. Fan TWM (1996) Metabolite profiling by one- and two-dimensional NMR analysis of complex mixtures. Prog Nucl Magn Reson Spectrosc 28:161–219
17. Garrod S, Humpfer E, Spraul M et al (1999) High-resolution magic angle spinning ^{1}H NMR spectroscopic studies on intact rat renal cortex and medulla. Magn Reson Med 41:1108–1118
18. Künnecke B, Delikatny EJ, Russell P et al (1994) Proton magnetic resonance and human cervical neoplasia. II. Ex vivo chemical-shift microimaging. J Magn Reson B 104:135–142
19. Semenza GL, Artemov D, Bedi A et al (2001) The metabolism of tumors: 70 years later. Novartis Foundation Symposium 240:251–264
20. Dang CV, Semenza GL (1999) Oncogenic alterations of metabolism. Trends Biochem Sci 24:68–72
21. Warburg O. (1930) The metabolism of tumors. Constable, London
22. Gribbestad IS, Singstad TE, Nilsen G et al (1998) In vivo ^{1}H MRS of normal breast and breast tumors using a dedicated double breast coil. J Magn Reson Imaging 8:1191–1197
23. Gribbestad IS, Petersen SB, Fjøsne H et al (1994) ^{1}H NMR Spectroscopic characterization of perchloric acid extracts from breast carcinomas and non-involved breast tissue. NMR Biomed 7:181–194

24. Gribbestad IS, Sitter B, Lundgren S et al (1999) Metabolite composition in breast tumors examined by proton nuclear magnetic resonance spectroscopy. Anticancer Res 19:1737–1746
25. Lehnhardt FG, Rohn G, Ernestus RI et al (2001) ^{1}H- and ^{31}P-MR spectroscopy of primary and recurrent human brain tumors in vitro: malignancy-characteristic profiles of water soluble and lipophilic spectral components. NMR Biomed 14:307–317
26. Walenta S, Wetterling M, Lehrke M et al (2000) High lactate levels predict likelihood of metastases, tumor recurrence, and restricted patient survival in human cervical cancers. Cancer Res 60:916–921
27. Louw L, Engelbrecht AM, Cloete F (1998) Comparison of the fatty acid compositions in intraepithelial and infiltrating lesions of the cervix: part I, total fatty acid profiles. Prostaglandins Leukot Essent Fatty Acids 59:247–251
28. Engelbrecht AM, Louw L, Cloete F (1998) Comparison of the fatty acid compositions in intraepithelial and infiltrating lesions of the cervix: part II, free fatty acid profiles. Prostaglandins Leukot Essent Fatty Acids 59:253–257
29. Farrant RD, Lindon JC, Nicholson JK (1994) Internal temperature calibration for ^{1}H NMR spectroscopy studies of blood plasma and other biofluid. NMR Biomed 7:243–247

Paper V

URN:NBN:no-3463

HR MAS ^{1}H MR spectroscopy reveal significantly altered neuronal metabolite profiles in CLN1 but not in CLN3

Beathe Sitter[1,2], Taina Autti[3], Jaana Tyynelä[4,6], Ursula Sonnewald[2], Tone F. Bathen[1], Johanna Puranen[3], Pirkko Santavuori[5], Matti J. Haltia[6], Anders Paetau[6], Tuomo Polvikoski[6], Ingrid S. Gribbestad[1], Anna-Maija Häkkinen[3, 7]

[1] SINTEF Unimed, Trondheim, Norway

[2] Dept. of Neuroscience, NTNU, Trondheim, Norway

[3] Dept. of Radiology, Helsinki University Central Hospital, Finland

[4] Institute of Biomedicine/Biochemistry, University of Helsinki, Finland

[5] Dept. of Child Neurology, Helsinki University Central Hospital, Finland

[6] Dept. of Pathology, Haartman Institute and Helsinki University Central Hospital, Finland

[7] Dept. of Oncology, Helsinki University Central Hospital, Finland

Running title: MR Spectroscopy of NCLs

Corresponding author:

Anna-Maija Häkkinen,

Dept. of Oncology, POB 180

00029 Helsinki University Central Hospital

University of Helsinki, Finland

Phone No: +358 9 471 73248

Fax No: +358 9 471 74201

email:anna-maija.hakkinen@hus.fi

Abstract

The neuronal ceroid lipofuscinoses (NCLs) are among the most severe inherited progressive neurodegenerative disorders of children. The purpose of this study was to compare the *in vivo* 1.5 T ^{1}H MR and *ex vivo* 14.3 T HR MAS ^{1}H MR brain spectra of patients with infantile (CLN1) and juvenile (CLN3) types of NCL, to obtain detailed information about the alterations in the neuronal metabolite profiles in these diseases, and to test the suitability of the *ex vivo* HR MAS technique in analysis of autopsy brain tissue.

Ex vivo spectra from CLN1 autopsy brain tissue (n=10) significantly differed from those of the control (n=9) and CLN3 (n=5) groups, while no differences were found between the CLN3 and control groups. Principal component analysis of *ex vivo* data showed that decreased levels of *N*-acetylaspartate (NAA), gamma-aminobutyric acid (GABA), glutamine and glutamate as well as increased levels of inositols characterized the CLN1 spectra. Also, the intensity ratio of lipid methylene/methyl protons was decreased in CLN1 brain tissue compared to CLN3 and control brain tissue. In concordance with the *ex vivo* data, the *in vivo* spectra of late stage patients with CLN1 (n=3) revealed dramatic decrease of NAA and proportional increase of *myo*-inositol and lipids compared to control subjects. Again, the spectra of patients with CLN3 (n =13) did not differ from those of controls (n =15).

In conclusion, the *ex vivo* and *in vivo* spectroscopic findings were in good agreement within all analyzed groups, and revealed significant alterations in metabolite profiles in CLN1 brain tissue but not in CLN3 compared to controls. Furthermore, HR MAS spectra facilitated refined detection of neuronal metabolites, including GABA and composition of lipids, in the autopsy brain tissue of NCL patients.

Keywords: neuronal ceroid lipofuscinosis, magic angle spinning, principal component analysis

Introduction

Neuronal ceroid lipofuscinoses (NCLs) are recessively inherited storage diseases, and they comprise the most common reason for progressive childhood encephalopathies leading to death (Mole, 1999; Hofmann and Peltonen, 2001, Haltia, 2003). All forms of NCLs are characterized by lysosomal storage of autofluorescent lipopigments in several types of tissues, and particularly in neurons of the central nervous system (Haltia, 2003). Another typical feature of NCLs is the progressive neurodegeneration. At present, altogether eight different forms of NCL have been postulated (Mole, 1999; Hofmann and Peltonen, 2001). Six genes and the respective proteins underlying the NCLs have been identified (Gao *et al*., 2002; Ranta *et al*., 1999; Savukoski *et al*., 1998; Sleat *et al*., 1997; The International Batten Disease Consortium, 1995; Vesa *et al*., 1995; Wheeler *et al*., 2002). Among these are the palmitoyl protein thioesterase 1 (PPT1) and CLN3 protein, the defects of which cause infantile NCL (CLN1 or INCL) and juvenile NCL (CLN3 or JNCL), respectively (The International Batten Disease Consortium, 1995; Vesa *et al*., 1995). Infantile CLN1 is a rapidly progressing form, with extreme brain atrophy and life expectancy of 8-14 years, while juvenile CLN3 is associated with moderate brain atrophy and life expectancy of 16-35 years. The frequencies of CLN1 and CLN3 vary between different populations: CLN1 is enriched in Finland with the incidence of 1:18 000, while the incidence of CLN3 is 1:21 000 in Finland and 1:25 000 in the Northern European countries (Santavuori, 1988; Hofmann and Peltonen, 2001).

In vivo magnetic resonance imaging (MRI) and spectroscopy (MRS) have been used in differential diagnosis between NCLs and other neurodegenerative diseases (Autti *et al*., 1997; Brockmann *et al*., 1996; Confort-Gouny *et al.*, 1993; Lauronen *et al*., 1999). High-resolution MR spectra can provide detailed and complex information of the biochemical composition of the tissue under investigation. The magic angle spinning (MAS) technique facilitates a high-resolution MRS (HR MRS) of tissue samples *ex vivo,* eliminating the need for metabolite extraction (Sitter *et al*., 2002). HR MAS spectra

have resolution comparable to spectra of solutions and provide information about a larger number of metabolites than *in vivo* MR spectra. In biomedical research, e*x vivo* HR MAS ^{1}H MRS has been successfully applied in studies on various human tissues and diseases including breast cancer (Cheng *et al*., 1998; Sitter *et al*., 2002), prostate carcinomas (Cheng *et al*., 2001; Taylor *et al*., 2003), and brain tumors (Barton *et al*., 1999; Cheng *et al*., 2000; Tzika *et al*., 2002). *Ex vivo* ^{1}H MR MAS has also been used for characterization of neuronal loss in a macaque model of AIDS (Gonzales *et al*., 2000), Pick disease (Cheng *et al*., 1997) and Alzheimer's disease (Cheng *et al*., 2002).

The vast amount of metabolites detected in MAS MR spectra makes visual inspection and analysis difficult. In addition to handling large data sets, multivariate analysis, such as principal component analysis (PCA), has the potential to detect small variations between spectra.

The aims of the present study were to compare the *in vivo* 1.5 T ^{1}H MR and *ex vivo* 14.3 T HR MAS ^{1}H MR brain spectra of patients with CLN1 and CLN3, to obtain detailed information about the alterations in the neuronal metabolite profiles in these diseases, and to test the suitability of the *ex vivo* HR MAS technique in analysis of autopsy brain tissue.

Subjects

Informed consents were obtained from the parents of the patients, and the controls or their families. The local ethical committee approved the study protocol.

Three late stage patients with CLN1 (4, 6 and 7 years), thirteen patients with CLN3 (mean age 14.8 years, range from 7 to 30 years, 5 patients < 12 years and 8 > 12 years), and fifteen healthy volunteers (mean age 22.5 years, range from 7 to 35 years), were examined by *in vivo* ^{1}H MRS. All patients with CLN1 (two girls and one boy) were markedly affected and unable to move since the age of 2.5 years. They all had epilepsy and myoclonic jerks. Patients with CLN3 (eight boys and five girls) under 12 years had only visual failure and slight cognitive decline, whereas older patients (except for one) had epilepsy, motor and speech problems, and marked cognitive decline. The controls (one girl, nine men and five women) were healthy and had no neurological deficits.

Autopsy samples for *ex vivo* MR spectroscopy were excised from the frontal cortices of patients with CLN1 and CLN3, and controls without neurological deficits. Samples were frozen and stored at –80 ^{o}C until analyzed. The group of patients with CLN1 (n=9) consisted of two boys and seven girls with a mean age of 12.3 years at the time of death (range 10.6-15 years). All had had myoclonic epilepsy and had been severely affected and bedridden since the age of 2.5 years. Dystonia had also been common. The patients with CLN3 (n=5) were two man and three women who died at a mean age of 27.4 years (range from 20 to36 years). During the second decade of their life, three of them had shown a more rapid clinical course than the others (Järvelä et al., 1997). The control group (n=9) consisted of six women and three men who had no neurological deficits and their mean age was 80.2 years at death (range from 36 to 106 years). Mini-Mental State Examination or Short Portable Mental Status Questionnaire were used to assess the cognitive status of the old controls (>85 years of age) and they were not cognitively impaired, neither did they show

any gross pathology in the forebrain as confirmed by neuropathological examination (*Polvikoski et al.* 2001).

Methods

In vivo ^{1}H MRS

Localized single voxel ^{1}H MR spectra were recorded on a 1.5 T (63 MHz) Magnetom Vision MR imager (Siemens, Erlangen, Germany) by using a standard circularly polarized head coil. The thalamic nuclei were examined using *in vivo* ^{1}H MRS. The size of the selected volume of interest ranged from 4-8 cm^3. A stimulated echo (STEAM) mode acquisition with selective water suppression was used for MRS. The echo time (TE) were 270 ms and 20 ms, repetition time (TR) 3000 ms, and mixing time (TM) 30 ms. Unsuppressed tissue water signal was also collected with TR of 5000 ms in the corresponding voxel. The metabolite spectrum were acquired using 256 (TE = 270 ms) and 128 (TE = 20 ms) acquisitions, and eight acquisitions for tissue water, over a spectral region of 1000 Hz collected into 1024 data points. The chemical shifts were referenced to water at 4.75 ppm. The cerebral metabolite signal intensities were determined using frequency domain fitting with Siemens software, and for CLN1 also with SPW-software (Järvi *et al.*, 1997). For comparison of the spectra of the different individuals the signal intensities were corrected for coil loading and VOI size.

Ex vivo ^{1}H HR MAS MRS

^{1}H HR MAS MR spectra of autopsy brain samples were recorded using a BRUKER AVANCE DRX600 (14.3T) spectrometer equipped with a ^{1}H/^{13}C MAS probe with gradient directed along the magic angle axis (BRUKER Analytik GmbH, Germany). Samples were spun at 3.5 kHz. All spectra were recorded at room temperature.

Two different one-dimensional spectra were recorded for each sample. A spin-echo experiment with water suppression included (cpmgpr, BRUKER) was performed with a delay of 1 ms repeated 136 times, giving spectra with a total echo time of 285 ms. The second type of spectra were acquired using a single pulse sequence with water suppression (zgpr, BRUKER). The water resonance was irradiated for 2 seconds before a 60-degree pulse angle was applied. For both experiments, 128 transients over a spectral region of 10 kHz were collected into 32K points, giving an acquisition time of 1.64 seconds. All experiments were performed at room temperature. Chemical shifts were referenced to creatine (3.03 ppm).

Before multivariate analysis, all spectra were Fourier transformed and baseline offset was adjusted. From the spin-echo spectra the spectral region from 0.6 to 4.6 ppm was selected for multivariate analysis. From the single pulse water-suppressed spectra the spectral region between 0.8 and 3.5 ppm was selected. The region describing the lactate peak at 1.32 ppm (40 points) was removed from all spectra due to the much higher signal intensity compared to the rest of the spectrum. The final matrix of spin-echo spectra consisted of 25 samples × 3810 variables, while the final matrix of single pulse spectra consisted of 25 samples × 2610 variables. Mean normalization was performed on the selected spectral regions. Principal Component Analysis (PCA) was carried out in an unsupervised manner, with full cross-validation and mean centering using the program The Unscrambler from Camo.

The program PeakFit from Jandel Scientific was used to calculate areas of the methyl (CH_3, 0.9 ppm) and methylene (CH_2, 1.3 ppm) signals from fatty acids in the single pulse (water suppressed) spectra. The spectral region 1.8 – 0.5 ppm was used, and all peaks in this region were fitted to a combined Lorenzian-Gaussian lineshape ($r^2 > 0.99$). ANOVA was used to test the resulting methylene/methyl-ratios of lipids for statistical significance.

Results

In vivo ^{1}H MRS

In the patients with CLN1 (4, 6 and 7 years) the metabolites measured from thalami (Figure 1) showed markedly altered intensities: *N*-acetylaspartate (NAA) was only 40, 15 and 30 %, creatine + phosphocreatine (Cr) 80, 50 and 70 %, and choline containing compounds (Cho) 110, 120 and 90 %, respectively, of the control (TE =270 ms). The proportional intensities of inositols, mainly composed of *myo*-inositol (*m*-Ino), as well as those of lipids (TE= 20 ms) were markedly higher in CLN1 than in the control. In addition, the lactate signal was detectable in CLN1 (TE =270 ms). In contrast, the spectra of the CLN3 patients did not differ from those of the controls. The mean values ±SD for NAA in CLN3 patients and controls were 29±6 and 29±5 institutional units (i.u.); for Cr 11±3 and 10±2 i.u; and for Cho 12±4 and 9±2 i.u., respectively (TE=270 ms).

Ex vivo ^{1}H HR MAS MRS

Typical spin-echo ^{1}H HR MAS spectra (spectral region 4.6 – 0.6 ppm) of autopsy tissue of the frontal cortex from patients with CLN1 and CLN3 and control subjects are presented in Figure 2. Long total echo times lead to a reduction in signals from macromolecules and lipids, and thereby higher signal intensities of numerous water-soluble metabolites. In the spectra of CLN1 tissues compared to spectra of control subjects and CLN3 autopsy tissues; gamma-aminobutyric acid (GABA) could not be detected in any of the spectra of CLN1 tissue, while NAA was undetectable in seven of the nine spectra and acetate could not be detected in six of the spectra. Glutamate could not be detected in two of the spectra, and was considerably reduced in the other spectra (Figure 2A). Intensities of the glutamine signals did, however, vary between samples within each group. The spectra of CLN3 frontal cortices (Figure 2b) showed no differences compared to those of controls (Figure 2c).

PCA of spin echo HR MAS spectra showed that autopsy samples from patients with CLN1 had a different metabolic profile than the autopsy samples from controls and patients with CLN3. Statistical representation of the data was obtained by the score plot of the first (PC1) and second principal components (PC2) from PCA of spin echo HR MAS spectra, explaining 66% of the total variation in the 25 original spectra, as given in Figure 3. In the score plot, the CLN1 samples were linearly separated from the CLN3 and control samples, while CLN3 and control samples were not separable. The loading profile of the first principal component (PC1) showed the important features characterizing most CLN1 autopsy samples (Figure 4). The intense signals from *m*-Ino, *scyllo*-inositol (*s*-Ino) and glycerophosphocholine (GPC) indicated that these compounds dominate the spectra from CLN1 patients. Furthermore, glutamine, glutamate, GABA, NAA and acetate appeared as negative peaks in the loading profile, describing the low levels of these compounds in autopsy samples from CLN1 patients compared to autopsy samples of controls and CLN3 patients.

PCA of the single pulse water suppressed spectra also led to differentiation of the CLN1 samples from the other samples. The score plot of PC1 versus PC2, resulting from PCA of single pulse water suppressed spectra, is given in Figure 5. PC1 and PC2 account for 63 % of the total variation in these spectra where lipids and macromolecules were detected in addition to the smaller molecules. The grouping of samples from CLN1 patients in the upper right quadrant of the score plot was evident. Further, the control samples tended to score lower in PC1 and PC2 than CLN3 samples, but, as in PCA of spin-echo spectra, CLN3 samples and control samples were not separable. The loading profile of PC1 (Figure 6) showed that CLN1 samples, which had a high score for PC1, were characterized by increased relative levels of Cr, *m*-Ino, *s*-Ino and cholines, as well as decreased levels of NAA and acetate compared controls and CLN3 samples. In addition, the loading profile of

PC1 showed that the ratio of methylene/methyl protons of lipids was lower in CLN1 samples than in the other samples.

Single pulse water suppressed HR MAS spectra were used to further analyze the lipid signals in the CLN1, CLN3 and control brain tissue (the region 1.8-0.5 ppm). The ratio of methylene/methyl protons of lipids was found to be significantly ($p < 0.01$) decreased in CLN1 tissue (CH_2/CH_3 ratio 1.32) compared to CLN3 (CH_2/CH_3 ratio 2.33) and control tissues (CH_2/CH_3 ratio 2.52).

Discussion

In vivo ^{1}H MRS

Our *in vivo* ^{1}H MRS study showed a dramatic loss of NAA, reduction of Cr as well as proportional elevation of *m*-Ino and lipids in the patients with CLN1. These observations are in good accordance with a previous study on one patient with CLN1, except that we did not observe an increase in taurine (Confort-Gouny et al., 1993). NAA is used as a neuronal marker, Cr is involved in energy metabolism, and Cho reflects membrane phospholipid turnoverQUOTE, while *m*-Ino is a glial marker and a potential osmoregulator (Baslow, 2002; Brand et al., 1993; Kuhmonen et al., 1994; Monge et al., 1993; Yuan et al., 1992). Thus, the present findings reflect the almost complete neuronal loss and extreme gliosis typical for CLN1 (Santavuori *et al*., 2000). The spectra of the 13 patients with CLN3 were very similar to those of controls. This observation is in concordance with the findings of Brockman *et al.* (1996), who examined three patients with CLN3 using *in vivo* MRS.

Ex vivo ^{1}H HR MAS MRS

In good agreement with the *in vivo* data, principal component analysis of the ^{1}H HR MAS spectra showed altered concentrations of NAA, Cr, Cho, *m*-Ino and *s*-Ino in the CLN1 samples. In addition,

ex vivo HR MAS MRS allowed refined detection of two neurotransmitters, glutamate and GABA. The observed decrease in the levels of GABA and glutamate in CLN1 correspond well with the decrease in NAA, reflecting the extreme neuronal loss. Previously, markedly low cerebrospinal fluid GABA concentrations in patients with CLN1 have been reported (Riikonen *et al*., 2000). It seems that the concentration of GABA is decreased more significantly than that of glutamate. Imbalance between the inhibition (GABA) and excitation (glutamate) could explain the severe myoclonic epilepsy, which is a common symptom in CLN1. Further, the patients with CLN1 respond clinically well to GABAergic drugs like sodium valproate, bentzodiazipines and baclophen.

Furthermore, the loading profile of PC1 from PCA and peak area calculations (peak fitting) of single pulse spectra (water suppressed) showed that the ratio of methylene/methyl protons of lipids was lower in CLN1 samples than in the control or CLN3 samples. These results may indicate shorter chain lengths or a higher content of double bonds in the fatty acids. The recent results using liquid chromatography-electrospray ionization mass spectrometry have shown that, indeed, the proportion of saturated short-chain fatty acids in phospholipids was increased in CLN1 autopsy brains but not in CLN3 brains (Käkelä *et al*., 2003), thus being in agreement with the present results. In the PCA score plots, the CLN3 autopsy samples tend to appear closer to CLN1 samples than controls (Figure 3 and 5). However, in agreement with the *in vivo* data, the HR-MAS spectra of CLN3 autopsy samples did not show significant differences compared to controls. This is somewhat surprising since the terminal stage of CLN3 is characterized by moderate neuronal loss and gliosis, also observed by MRI (Autti *et al.*, 1996).

Methodological considerations

The autopsy material from normal children or young adults is rarely available. Therefore, the mean age of the *ex vivo* control group was considerably higher than that of either patient group. However,

as NCL-diseases are considered as models of ageing (Armstrong *et al*., 1981), the old controls were relevant in this study.

In the present study, the *ex vivo* HR MAS spectra were recorded from the grey matter of the frontal cortex while the *in vivo* spectra were recorded from the deep grey matter of thalami. The CLN1 brains are extremely atrophic, the brain weight being only 300-350g at the time of death (Haltia *et al.*, 1973). In these shrunken brains, the thalami are best preserved, while the cerebral cortex is extremely thin (Figure 1D). Therefore, the *in vivo* spectra were recorded from the thalamus, which was unfortunately not available for the *ex vivo* analysis. Minor metabolite differences between the deep grey matter and cortical grey matter can not be excluded. Despite this, the *ex vivo* findings were in good agreement with *in vivo* findings.

The HR MAS ^{1}H MRS of the brain autopsy samples was performed at room temperature and tissue samples were subject to room temperature for 25 minutes in average before MR spectra were recorded. Under these conditions, anaerobic respiration and degradation of tissue metabolites is likely to occur. Indeed, the signal intensities of lactate, which reflects the anaerobic respiration (Wolfson *et al.*, 2000), were high in HR MAS spectra compared to the *in vivo* spectra, and thus lactate was not included in the data analysis. Also acetate was observable. Cheng *et al*. (1997) showed evidence indicating that in autopsy brains, acetate is mostly produced by degradation of NAA. There was an inverse correlation between the post-mortem delay time and NAA concentration, and thus they suggested that the initial NAA concentration in the tissue can best be estimated by summarizing the NAA and acetate signals. In the CLN1 tissues, both NAA and acetate were decreased, while they were similar to controls in CLN3 tissues.

NAA in neurodegeneration

The decreased level of NAA has been associated with neuronal damage or loss (Burtscher and Holtås, 2001; Vermathen *et al*., 2003, Baslow, 2003), and an inverse correlation of the tissue NAA concentration and neuronal loss has been demonstrated in Pick and Alzheimer's disease (Cheng *et al*., 1997, 2002). In the central nervous system, NAA is synthesized and stored in neurons, but catabolized in oligodendrocytes. Increasing recent evidence indicate that one important role of the NAA intercompartmental cycle is osmoregulatory, by removing intracellular water from myelinated neurons (Baslow and Guilfoyle, 2002; Baslow, 2003; Baslow *et al*., 2003). In CLN1, the neuronal loss is extreme, and thus the dramatic decrease of neuronal metabolites, including NAA, were expected. However, it is somewhat surprising that despite the well-documented, moderate cerebrocortical neurodegeneration (Haltia, 2003), the samples from patients with CLN3 failed to show significant alterations in the concentration of NAA. This might be partially explained by the fact, that in the CLN3 brains, the remaining neurons are filled with storage material (Haltia, 2003) and osmotic imbalance may exist, potentially leading to compensation of the NAA concentration via upregulation. Would this be the case, then the NAA concentration may not directly reflect the degree of neurodegeneration in lysosomal storage diseases with potential osmotic imbalance. Indeed, we are aware of one further example fitting this theory: *in vivo* MRS studies of patients with aspartylglucosaminuria, showing mild to moderate cortical atrophy, indicated NAA concentrations within the normal range (Autti and Häkkinen, unpublished results).

Conclusions

In the present study, we show that the results obtained from *in vivo* ^{1}H MR spectra and *ex vivo* HR MAS ^{1}H MR spectra of patients with CLN1 and CLN3 and controls were in good agreement. The PC1 loading profile of CLN1 samples was characterized by the intense positive peaks from m-Ino,

s-Ino and GPC, and by the negative peaks of glutamine, glutamate, GABA, NAA and acetate. Also the ratio of lipid methylene/methyl protons was lower in CLN1 samples than in the other samples. Thus, despite the necessary post mortem delay, ^{1}H HR MAS MRS provided a reliable technical possibility to analyze the metabolic profiles in autopsy brain tissue, and allowed refined detection of metabolites such as GABA and glutamate, as well as knowledge of lipid composition in CLN1 and CLN3 brains. HR MAS spectra allowed clear differentiation of the CLN1 samples from the CLN3 and control samples, while the CLN3 and control samples were not separable.

Acknowledgement

This study was financially supported by the Academy of Finland (JT 207016) and the University of Helsinki Research Funds (JT 2103029). The authors wish to thank Dr Riitta Salonen for support during the study.

References

Autti T, Raininko R, Vanhanen SL, Santavuori P. 1996. MRI of neuronal ceroid lipofuscinosis. I. Cranial MRI of 30 patients with juvenile neuronal ceroid lipofuscinosis. Neuroradiology 38:476-482.

Autti T, Raininko R, Vanhanen SL, Santavuori P. 1997. Magnetic resonance techniques in neuronal ceroid lipofuscinoses and some other lysosomal diseases affecting the brain. Curr Opin Neurol 10:519-524.

Armstrong D, Koppang N. 1981. Ceroid-lipofucinosis, a model for aging. In: Sohal RS, editor. Age pigments. Amsterdam: Elsevier, p 355-382.

Barton SJ, Howe FA, Tomlins AM, Cudlip SA, Nicholson JK, Bell BA, Griffiths JR. 1999. Comparison of in vivo 1H MRS of human brain tumours with 1H HR-MAS spectroscopy of intact biopsy samples in vitro. MAGMA 8:121-128.

Baslow MH. 2003. N-acetylaspartate in the vertebrate brain: metabolism and function. Neurochem Res. 28:941-53.

Baslow MH and Guilfoyle DN. 2002. Effect of *N*-acetylaspartic acid on the diffusion coefficient of water: a proton magnetic resonance phantom method for measurement of osmolyte-obligated water. Anal Biochem 311:133-138.

Baslow MH, Suckow RF, Gaynor K, Bhakoo KK, Marks N, Saito M, Saito M, Duff K, Matsuoka Y, Berg MJ. 2003. Brain damage results in down-regulation of *N*-acetylaspartate as a neuronal osmolyte. Neuromolecular Med. 3:95-104.

Burtscher IM, Holtås S. 2001. Proton MR spectroscopy in clinical routine. J Magn Reson Imag 13:560-567.

Brand A, Richter-Landsberg C, Leibfritz D. 1993. Multinuclear NMR studies on the energy metabolism of glial and neuronal cells. Dev Neurosci 15:289-298.

Brockmann K, Pouwels PJ, Christen HJ, Frahm J, Hanefeld F. 1996. Localized proton magnetic resonance spectroscopy of cerebral metabolic disturbances in children with neuronal ceroid lipofuscinosis. Neuropediatrics 27:242-248.

Cheng LL, Ma MJ, Becerra L, Ptak T, Tracey I, Lackner A, González RG. 1997. Quantitative neuropathology by high resolution magic angle spinning proton nuclear magnetic resonance spectroscopy. Proc Natl Acad Sci USA 94:6408-6413.

Cheng LL, Chang IW, Smith BL, Gonzalez RG. 1998. Evaluating human breast ductal carcinomas with high-resolution magic-angle spinning proton magnetic resonance spectroscopy. J Magn Res 135:194-202.

Cheng LL, Anthony DC, Comite AR, Black PM, Tzika AA, González RG. 2000. Quantification of microheterogeneity in glioblastoma multiforme with ex vivo high-resolution magic-angle spinning (HRMAS) proton magnetic resonance spectroscopy. Neuro-Oncology 2:87-95.

Cheng LL, Wu C, Smith MR, Gonzalez RG. 2001. Non-destructive quantitation of spermine in human prostate tissue samples using HRMAS ^{1}H NMR spectroscopy at 9.4 T. FEBS Lett. 494:112-116.

Cheng LL, Newell K, Mallory AE, Hyman BT, Gonzalez RG. 2002. Quantification of neurons in Alzheimer and control brains with ex vivo high resolution magic angle spinning proton magnetic resonance spectroscopy and stereology. Magn Reson Imaging 20:527-533.

Confort-Gouny S, Chabrol B, Vion-Dury J, Mancini J, Cozzone PJ. 1993. MRI and localized proton MRS in early infantile form of neuronal ceroid- lipofuscinosis. Pediatr Neurol 9:57-60.

Gao H, Boustany RM, Espinola JA, Cotman SL, Srinidhi L, Antonellis KA, Gillis T, Qin X, Liu S, Donahue LR, Bronson RT, Faust JR, Stout D, Haines JL, Lerner TJ, MacDonald ME. 2002. Mutations in a novel CLN6-encoded transmembrane protein cause variant neuronal ceroid lipofuscinosis in man and mouse. Am J Hum Genet 70:324-335.

Gonzalez RG, Cheng LL, Westmoreland SV, Sakaie KE, Becerra LR, Lee PL, Masliah E, Lackner AA. 2000. Early brain injury in the SIV-macaque model of AIDS. AIDS 14:2841-2849.

Haltia M, Rapola J, Santavuori P. 1973. Infantile type of so-called neuronal ceroid-lipofuscinosis. Histological and electron microscopic studies. Acta Neuropathol (Berl) 26:157-70.

Haltia M. 2003. The neuronal ceroid-lipofuscinoses. J Neuropathol Exp Neurol 62:1-13.

Hofmann SL and Peltonen L. 2001. The neuronal ceroid lipofuscinoses. In: Scriver CR, Beaudet AL, Sly WS, Valle D, editors. The Metabolic & Molecular Bases of Inherited Disease (8th Edition), Vol III. Columbus: McGraw-Hill Companies Inc. p 3877-3894.

The International Batten Disease Consortium. 1995. Isolation of a novel gene underlying Batten disease, CLN3. Cell 82:949-957.

Järvelä I, Autti T, Lamminranta S, Aberg L, Raininko R, Santavuori P. 1997. Clinical and magnetic resonance imaging findings in Batten disease: analysis of the major mutation (1.02-kb deletion). Ann Neurol 42:799-802.

Järvi J, Nyman S, Komu M, Forsström JJ. 1997. A PC program for automatic analysis of NMR spectrum series. Computer Methods and Programs. Biomedicine 52:213-222.

Kuhmonen J, Sivenius J, Riekkinen PJ, Sr., Kauppinen RA. 1994. Decrease in brain choline-containing compounds following a short period of global ischemia in gerbils as detected by 1H NMR spectroscopy in vivo. NMR Biomed 7:231-236.

Käkelä R, Somerharju P, Tyynelä J. 2003. Analysis of phospholipid molecular species in brains from patients with infantile and juvenile lipofuscinosis using liquid chromatography-electrospray ionization mass spectrometry. J Neurochem 84:1051-1065.

Lauronen L, Munroe PB, Järvelä I, Autti T, Mitchison HM, O'Rawe AM, Gardiner RM, Mole SE, Puranen J, Häkkinen AM, Kirveskari E, Santavuori P. 1999. Delayed classic and protracted phenotypes of compound heterozygous juvenile neuronal ceroid lipofuscinosis. Neurology 52:360-365.

Mole SE. 1999. Batten's disease: eight genes and still counting? Lancet 354:443-445.

Monge M, Yuan J, Cabon F, Zalc B, Kanfer JN. 1993. Glycerophosphorylcholine phosphocholine phosphodiesterase activity during the differentiation of glial progenitor cells. J Neurosci Res 36:441-445.

Polvikoski T, Sulkava R, Myllykangas L, Notkola IL, Niinisto L, Verkkoniemi A, Kainulainen K, Kontula K, Perez-Tur J, Hardy J, Haltia M. 2001. Prevalence of Alzheimer's disease in very elderly people: a prospective neuropathological study. Neurology. 56:1690-6.

Ranta S, Zhang Y, Ross B, Lonka L, Takkunen E, Messer A, Sharp J, Wheeler R, Kusumi K, Mole S, Liu W, Soares MB, Bonaldo MF, Hirvasniemi A, de la CA, Gilliam TC, Lehesjoki AE. 1999. The neuronal ceroid lipofuscinoses in human EPMR and mnd mutant mice are associated with mutations in CLN8. Nat Genet 23:233-236.

Riikonen R, Vanhanen SL, Tyynela J, Santavuori P, Turpeinen U. 2000. CSF insulin-like growth factor-1 in infantile neuronal ceroid lipofuscinosis. Neurology 54:1828-1832.

Santavuori P. 1988. Neuronal ceroid lipofuscinoses in childhood. Brain Dev 10:80-83.

Santavuori P, Lauronen L, Kirveskari E, Åberg L, Sainio K, Autti T. 2000. Neuronal ceroid lipofuscinoses in childhood. Neurol Sci 21:S35-S41.

Savukoski M, Klockars T, Holmberg V, Santavuori P, Lander ES, Peltonen L. 1998. CLN5, a novel gene encoding a putative transmembrane protein mutated in Finnish variant late infantile neuronal ceroid lipofuscinosis. Nat Genet 19:286-288.

Sitter B, Sonnewald U, Spraul M, Fjosne HE, Gribbestad IS. 2002. High-resolution magic angle spinning MRS of breast cancer tissue. NMR Biomed 15:327-337.

Sleat DE, Donnelly RJ, Lackland H, Liu CG, Sohar I, Pullarkat RK, Lobel P. 1997. Association of mutations in a lysosomal protein with classical late- infantile neuronal ceroid lipofuscinosis. Science 277:1802-1805.

Taylor JL, Wu CL, Cory D, Gonzalez RG, Bielecki A, Cheng LL. 2003. High-resolution magic angle spinning proton NMR analysis of human prostate tissue with slow spinning rates. Magn Res Med 20:627-632.

Tzika AA, Cheng LL, Goumnerova L, Madsen JR, Zurakowski D, Astrakas LG, Zarifi MK, Scott RM, Anthony DC, Gonzalez RG, Black PM. 2002. Biochemical characterization of pediatric brain tumors by using in vivo and ex vivo magnetic resonance spectroscopy. J Neurosurg 96:1023-1031.

Vesa J, Hellsten E, Verkruyse LA, Camp LA, Rapola J, Santavuori P, Hofmann SL, Peltonen L. 1995. Mutations in the palmitoyl protein thioesterase gene causing infantile neuronal ceroid lipofuscinosis. Nature 376:584-587.

Wheeler RB, Sharp JD, Schultz RA, Joslin JM, Williams RE, Mole SE. 2002. The gene mutated in variant late-infantile neuronal ceroid lipofuscinosis (CLN6) and in nclf mutant mice encodes a novel predicted transmembrane protein. Am J Hum Genet 70:537-542.

Wolfson M, Bersudsky Y, Hertz E, Berkin V, Zinger E, Hertz L. 2000. A model of inositol compartmentation in astrocytes based upon efflux kinetics and slow inositol depletion after uptake inhibition. Neurochem Res 25:977-982.

Yuan J, McCartney DG, Monge M, Espinosa de Los MA, Zalc B, de Vellis J, Kanfer JN. 1992. Glycerophosphorylcholine phosphocholine phosphodiesterase activity in cultured oligodendrocytes, astrocytes, and central nervous tissue of dysmyelinating rodent mutants. J Neurosci Res 31:68-74.

Vermathen P, Laxer KD, Schuff N, Matson GB, Weiner MW. 2003. Evidence of neuronal injury outside the medial temporal lobe in temporal lobe epilepsy: *N*-acetylaspartate concentration reductions detected with multisection proton MR spectroscopic imaging--initial experience. Radiology. 226:195-202

Figure legends

Figure 1

In vivo ^{1}H spectra at 1.5T (63 MHz) of a 6-year-old (A) and a 4-year-old (B) patient with CLN1 show decrease of NAA and proportional increase of m-Ino and Cho compared to the spectra of a 7.5- year-old healthy control (C). The abbreviated assignments given in the figure are *m*-Ino, *myo*-inositol; Cho, choline; Cr, creatine; NAA, *N*-acetyl-aspartate; Lac, lactate and Lip, lipids. The MRI (T1-weighted image) of the 6-year-old patient (D) show extremely severe brain artophy. The thalami are best preserved, while the cerebral cortex is very thin. MRS localisation is marked by rectangle.

Figure 2

^{1}H HR MAS spectra at 14.7 T (600 MHz) of autopsy samples from a typical CLN1 (A) and CLN3 patients (B) and from a control subject (C). The CLN1 spectrum is extremely abnormal. The spectrum of CLN3 patient did not differ from that of the control spectrum. Assignments are given in the figure, abbreviations used are: Lac, lactate; *m*-Ino, *myo*-inositol; Cr, creatine; Tau, taurine; *s*-Ino, *scyllo*-inositol; GPC, glycerophosphocholine; PC, phosphocholine; Cho, choline; NAA, *N*-acetyl-aspartate; Gln, glutamine; Glu, glutamate; GABA, γ-aminobutyrate; Ala, alanine; and Val, valine.

Figure 3

Score plot from principal component analysis of spin echo ^{1}H HR MAS spectra with total echo time of 285 ms. Samples from controls are labeled ∇, samples from CLN3s × and samples from CLN1s O. A line is drawn to illustrate the classification of the CLN1 samples.

Figure 4

Loading profile of spin echo ^{1}H HR MAS spectra corresponding to the spectral region 4.6 to 0.6 ppm of first principal component (PC1) presented in Figure 3. The abbreviations of assignments correspond to the abbreviations used in Figure 2. The lactate peak at 1.3 ppm is excluded.

Figure 5

Score plot of PC1 and PC2 achieved from principal component analysis of the spectral region 3.5 to 0.8 ppm from single pulse water suppressed spectra. Samples from controls are labeled ∇, samples from CLN3s ✕ and samples from CLN1s ○.

Figure 6

Loading profile of first principal component (PC1), corresponding to the spectral region 3.5 to 0.8 ppm from single pulse water suppressed spectra. The lactate peak at 1.32 ppm was excluded from the analysis. The abbreviations of assignments correspond to the abbreviations used in Figure 2 in addition to lipid methyl and methylene labeled -CH_3 and -CH_2 respectively.

Figure 1

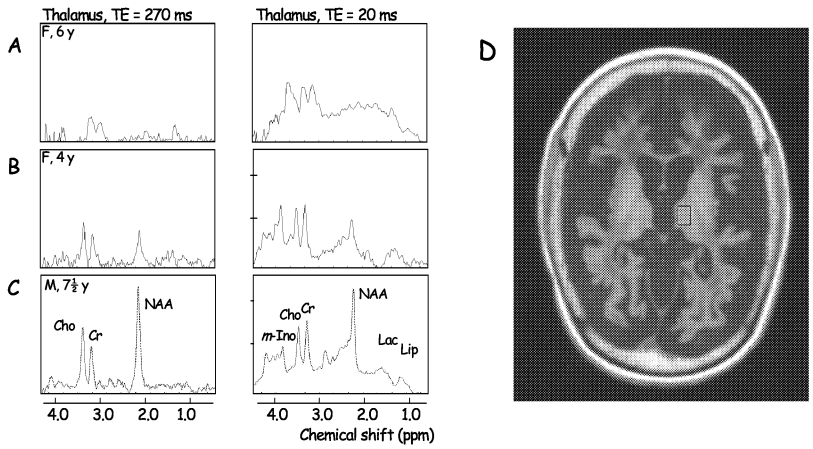

Figure 2

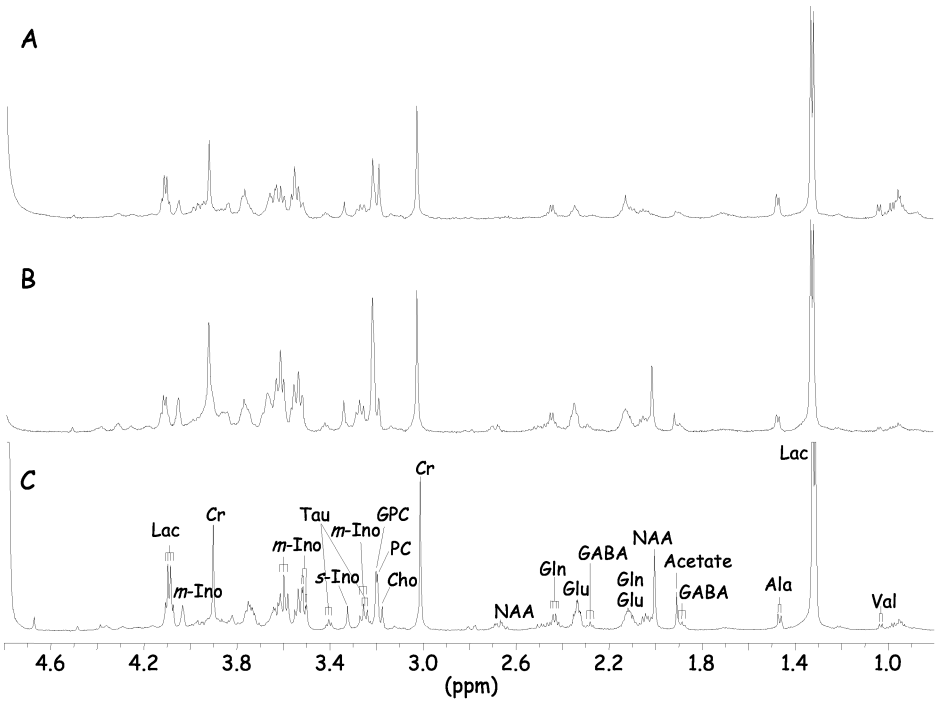

Figure 3

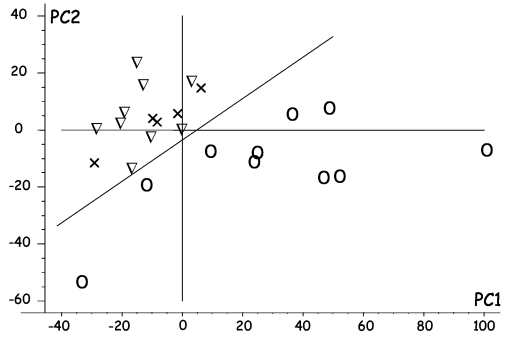

Figure 4

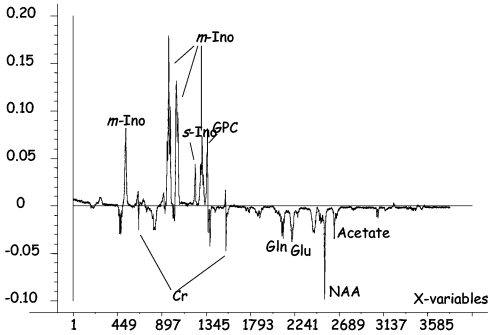

Figure 5

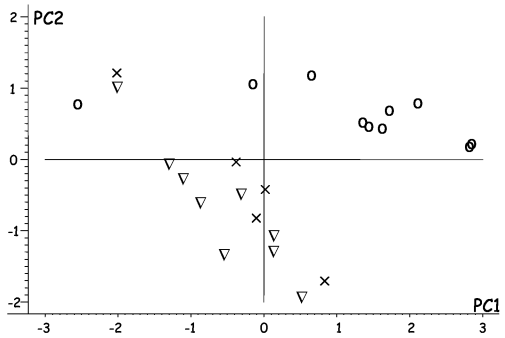

Figure 6

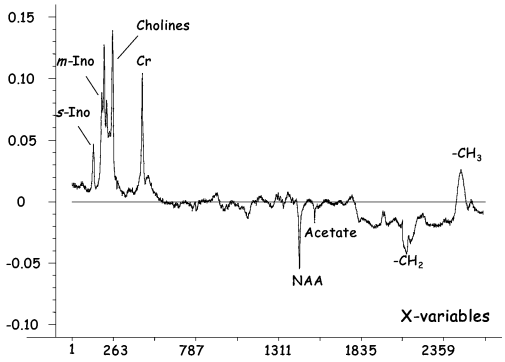

URN:NBN:no-3463

Dissertations at the Faculty of Medicine, NTNU

1977
1. Knut Joachim Berg: EFFECT OF ACETYLSALICYLIC ACID ON RENAL FUNCTION
2. Karl Erik Viken and Arne Ødegaard: STUDIES ON HUMAN MONOCYTES CULTURED *IN VITRO*

1978
3. Karel Bjørn Cyvin: CONGENITAL DISLOCATION OF THE HIP JOINT.
4. Alf O. Brubakk: METHODS FOR STUDYING FLOW DYNAMICS IN THE LEFT VENTRICLE AND THE AORTA IN MAN.

1979
5. Geirmund Unsgaard: CYTOSTATIC AND IMMUNOREGULATORY ABILITIES OF HUMAN BLOOD MONOCYTES CULTURED IN VITRO

1980
6. Størker Jørstad: URAEMIC TOXINS
7. Arne Olav Jenssen: SOME RHEOLOGICAL, CHEMICAL AND STRUCTURAL PROPERTIES OF MUCOID SPUTUM FROM PATIENTS WITH CHRONIC OBSTRUCTIVE BRONCHITIS

1981
8. Jens Hammerstrøm: CYTOSTATIC AND CYTOLYTIC ACTIVITY OF HUMAN MONOCYTES AND EFFUSION MACROPHAGES AGAINST TUMOR CELLS *IN VITRO*

1983
9. Tore Syversen: EFFECTS OF METHYLMERCURY ON RAT BRAIN PROTEIN.
10. Torbjørn Iversen: SQUAMOUS CELL CARCINOMA OF THE VULVA.

1984
11. Tor-Erik Widerøe: ASPECTS OF CONTINUOUS AMBULATORY PERITONEAL DIALYSIS.
12. Anton Hole: ALTERATIONS OF MONOCYTE AND LYMPHOCYTE FUNCTIONS IN REALTION TO SURGERY UNDER EPIDURAL OR GENERAL ANAESTHESIA.
13. Terje Terjesen: FRACTURE HEALING AN STRESS-PROTECTION AFTER METAL PLATE FIXATION AND EXTERNAL FIXATION.
14. Carsten Saunte: CLUSTER HEADACHE SYNDROME.
15. Inggard Lereim: TRAFFIC ACCIDENTS AND THEIR CONSEQUENCES.
16. Bjørn Magne Eggen: STUDIES IN CYTOTOXICITY IN HUMAN ADHERENT MONONUCLEAR BLOOD CELLS.
17. Trond Haug: FACTORS REGULATING BEHAVIORAL EFFECTS OG DRUGS.

1985
18. Sven Erik Gisvold: RESUSCITATION AFTER COMPLETE GLOBAL BRAIN ISCHEMIA.
19. Terje Espevik: THE CYTOSKELETON OF HUMAN MONOCYTES.
20. Lars Bevanger: STUDIES OF THE Ibc (c) PROTEIN ANTIGENS OF GROUP B STREPTOCOCCI.
21. Ole-Jan Iversen: RETROVIRUS-LIKE PARTICLES IN THE PATHOGENESIS OF PSORIASIS.
22. Lasse Eriksen: EVALUATION AND TREATMENT OF ALCOHOL DEPENDENT BEHAVIOUR.
23. Per I. Lundmo: ANDROGEN METABOLISM IN THE PROSTATE.

1986
24. Dagfinn Berntzen: ANALYSIS AND MANAGEMENT OF EXPERIMENTAL AND CLINICAL PAIN.
25. Odd Arnold Kildahl-Andersen: PRODUCTION AND CHARACTERIZATION OF MONOCYTE-DERIVED CYTOTOXIN AND ITS ROLE IN MONOCYTE-MEDIATED CYTOTOXICITY.
26. Ola Dale: VOLATILE ANAESTHETICS.

1987
27. Per Martin Kleveland: STUDIES ON GASTRIN.
28. Audun N. Øksendal: THE CALCIUM PARADOX AND THE HEART.
29. Vilhjalmur R. Finsen: HIP FRACTURES

1988
30. Rigmor Austgulen: TUMOR NECROSIS FACTOR: A MONOCYTE-DERIVED REGULATOR OF CELLULAR GROWTH.
31. Tom-Harald Edna: HEAD INJURIES ADMITTED TO HOSPITAL.
32. Joseph D. Borsi: NEW ASPECTS OF THE CLINICAL PHARMACOKINETICS OF METHOTREXATE.

URN:NBN:no-3463

33. Olav F. M. Sellevold: GLUCOCORTICOIDS IN MYOCARDIAL PROTECTION.
34. Terje Skjærpe: NONINVASIVE QUANTITATION OF GLOBAL PARAMETERS ON LEFT VENTRICULAR FUNCTION: THE SYSTOLIC PULMONARY ARTERY PRESSURE AND CARDIAC OUTPUT.
35. Eyvind Rødahl: STUDIES OF IMMUNE COMPLEXES AND RETROVIRUS-LIKE ANTIGENS IN PATIENTS WITH ANKYLOSING SPONDYLITIS.
36. Ketil Thorstensen: STUDIES ON THE MECHANISMS OF CELLULAR UPTAKE OF IRON FROM TRANSFERRIN.
37. Anna Midelfart: STUDIES OF THE MECHANISMS OF ION AND FLUID TRANSPORT IN THE BOVINE CORNEA.
38. Eirik Helseth: GROWTH AND PLASMINOGEN ACTIVATOR ACTIVITY OF HUMAN GLIOMAS AND BRAIN METASTASES - WITH SPECIAL REFERENCE TO TRANSFORMING GROWTH FACTOR BETA AND THE EPIDERMAL GROWTH FACTOR RECEPTOR.
39. Petter C. Borchgrevink: MAGNESIUM AND THE ISCHEMIC HEART.
40. Kjell-Arne Rein: THE EFFECT OF EXTRACORPOREAL CIRCULATION ON SUBCUTANEOUS TRANSCAPILLARY FLUID BALANCE.
41. Arne Kristian Sandvik: RAT GASTRIC HISTAMINE.
42. Carl Bredo Dahl: ANIMAL MODELS IN PSYCHIATRY.

1989

43. Torbjørn A. Fredriksen: CERVICOGENIC HEADACHE.
44. Rolf A. Walstad: CEFTAZIDIME.
45. Rolf Salvesen: THE PUPIL IN CLUSTER HEADACHE.
46. Nils Petter Jørgensen: DRUG EXPOSURE IN EARLY PREGNANCY.
47. Johan C. Ræder: PREMEDICATION AND GENERAL ANAESTHESIA IN OUTPATIENT GYNECOLOGICAL SURGERY.
48. M. R. Shalaby: IMMUNOREGULATORY PROPERTIES OF TNF-α AND THE RELATED CYTOKINES.
49. Anders Waage: THE COMPLEX PATTERN OF CYTOKINES IN SEPTIC SHOCK.
50. Bjarne Christian Eriksen: ELECTROSTIMULATION OF THE PELVIC FLOOR IN FEMALE URINARY INCONTINENCE.
51. Tore B. Halvorsen: PROGNOSTIC FACTORS IN COLORECTAL CANCER.

1990

52. Asbjørn Nordby: CELLULAR TOXICITY OF ROENTGEN CONTRAST MEDIA.
53. Kåre E. Tvedt: X-RAY MICROANALYSIS OF BIOLOGICAL MATERIAL.
54. Tore C. Stiles: COGNITIVE VULNERABILITY FACTORS IN THE DEVELOPMENT AND MAINTENANCE OF DEPRESSION.
55. Eva Hofsli: TUMOR NECROSIS FACTOR AND MULTIDRUG RESISTANCE.
56. Helge S. Haarstad: TROPHIC EFFECTS OF CHOLECYSTOKININ AND SECRETIN ON THE RAT PANCREAS.
57. Lars Engebretsen: TREATMENT OF ACUTE ANTERIOR CRUCIATE LIGAMENT INJURIES.
58. Tarjei Rygnestad: DELIBERATE SELF-POISONING IN TRONDHEIM.
59. Arne Z. Henriksen: STUDIES ON CONSERVED ANTIGENIC DOMAINS ON MAJOR OUTER MEMBRANE PROTEINS FROM ENTEROBACTERIA.
60. Steinar Westin: UNEMPLOYMENT AND HEALTH: Medical and social consequences of a factory closure in a ten-year controlled follow-up study.
61. Ylva Sahlin: INJURY REGISTRATION, a tool for accident preventive work.
62. Helge Bjørnstad Pettersen: BIOSYNTHESIS OF COMPLEMENT BY HUMAN ALVEOLAR MACROPHAGES WITH SPECIAL REFERENCE TO SARCOIDOSIS.
63. Berit Schei: TRAPPED IN PAINFUL LOVE.
64. Lars J. Vatten: PROSPECTIVE STUDIES OF THE RISK OF BREAST CANCER IN A COHORT OF NORWEGIAN WOMAN.

1991

65. Kåre Bergh: APPLICATIONS OF ANTI-C5a SPECIFIC MONOCLONAL ANTIBODIES FOR THE ASSESSMENT OF COMPLEMENT ACTIVATION.
66. Svein Svenningsen: THE CLINICAL SIGNIFICANCE OF INCREASED FEMORAL ANTEVERSION.
67. Olbjørn Klepp: NONSEMINOMATOUS GERM CELL TESTIS CANCER: THERAPEUTIC OUTCOME AND PROGNOSTIC FACTORS.

68. Trond Sand: THE EFFECTS OF CLICK POLARITY ON BRAINSTEM AUDITORY EVOKED POTENTIALS AMPLITUDE, DISPERSION, AND LATENCY VARIABLES.
69. Kjetil B. Åsbakk: STUDIES OF A PROTEIN FROM PSORIATIC SCALE, PSO P27, WITH RESPECT TO ITS POTENTIAL ROLE IN IMMUNE REACTIONS IN PSORIASIS.
70. Arnulf Hestnes: STUDIES ON DOWN´S SYNDROME.
71. Randi Nygaard: LONG-TERM SURVIVAL IN CHILDHOOD LEUKEMIA.
72. Bjørn Hagen: THIO-TEPA.
73. Svein Anda: EVALUATION OF THE HIP JOINT BY COMPUTED TOMOGRAMPHY AND ULTRASONOGRAPHY.

1992

74. Martin Svartberg: AN INVESTIGATION OF PROCESS AND OUTCOME OF SHORT-TERM PSYCHODYNAMIC PSYCHOTHERAPY.
75. Stig Arild Slørdahl: AORTIC REGURGITATION.
76. Harold C Sexton: STUDIES RELATING TO THE TREATMENT OF SYMPTOMATIC NON-PSYCHOTIC PATIENTS.
77. Maurice B. Vincent: VASOACTIVE PEPTIDES IN THE OCULAR/FOREHEAD AREA.
78. Terje Johannessen: CONTROLLED TRIALS IN SINGLE SUBJECTS.
79. Turid Nilsen: PYROPHOSPHATE IN HEPATOCYTE IRON METABOLISM.
80. Olav Haraldseth: NMR SPECTROSCOPY OF CEREBRAL ISCHEMIA AND REPERFUSION IN RAT.
81. Eiliv Brenna: REGULATION OF FUNCTION AND GROWTH OF THE OXYNTIC MUCOSA.

1993

82. Gunnar Bovim: CERVICOGENIC HEADACHE.
83. Jarl Arne Kahn: ASSISTED PROCREATION.
84. Bjørn Naume: IMMUNOREGULATORY EFFECTS OF CYTOKINES ON NK CELLS.
85. Rune Wiseth: AORTIC VALVE REPLACEMENT.
86. Jie Ming Shen: BLOOD FLOW VELOCITY AND RESPIRATORY STUDIES.
87. Piotr Kruszewski: SUNCT SYNDROME WITH SPECIAL REFERENCE TO THE AUTONOMIC NERVOUS SYSTEM.
88. Mette Haase Moen: ENDOMETRIOSIS.
89. Anne Vik: VASCULAR GAS EMBOLISM DURING AIR INFUSION AND AFTER DECOMPRESSION IN PIGS.
90. Lars Jacob Stovner: THE CHIARI TYPE I MALFORMATION.
91. Kjell Å. Salvesen: ROUTINE ULTRASONOGRAPHY IN UTERO AND DEVELOPMENT IN CHILDHOOD.

1994

92. Nina-Beate Liabakk: DEVELOPMENT OF IMMUNOASSAYS FOR TNF AND ITS SOLUBLE RECEPTORS.
93. Sverre Helge Torp: *erb*B ONCOGENES IN HUMAN GLIOMAS AND MENINGIOMAS.
94. Olav M. Linaker: MENTAL RETARDATION AND PSYCHIATRY. Past and present.
95. Per Oscar Feet: INCREASED ANTIDEPRESSANT AND ANTIPANIC EFFECT IN COMBINED TREATMENT WITH DIXYRAZINE AND TRICYCLIC ANTIDEPRESSANTS.
96. Stein Olav Samstad: CROSS SECTIONAL FLOW VELOCITY PROFILES FROM TWO-DIMENSIONAL DOPPLER ULTRASOUND: Studies on early mitral blood flow.
97. Bjørn Backe: STUDIES IN ANTENATAL CARE.
98. Gerd Inger Ringdal: QUALITY OF LIFE IN CANCER PATIENTS.
99. Torvid Kiserud: THE DUCTUS VENOSUS IN THE HUMAN FETUS.
100. Hans E. Fjøsne: HORMONAL REGULATION OF PROSTATIC METABOLISM.
101. Eylert Brodtkorb: CLINICAL ASPECTS OF EPILEPSY IN THE MENTALLY RETARDED.
102. Roar Juul: PEPTIDERGIC MECHANISMS IN HUMAN SUBARACHNOID HEMORRHAGE.
103. Unni Syversen: CHROMOGRANIN A. Phsysiological and Clinical Role.

1995

104. Odd Gunnar Brakstad: THERMOSTABLE NUCLEASE AND THE *nuc* GENE IN THE DIAGNOSIS OF *Staphylococcus aureus* INFECTIONS.
105. Terje Engan: NUCLEAR MAGNETIC RESONANCE (NMR) SPECTROSCOPY OF PLASMA IN MALIGNANT DISEASE.
106. Kirsten Rasmussen: VIOLENCE IN THE MENTALLY DISORDERED.
107. Finn Egil Skjeldestad: INDUCED ABORTION: Timetrends and Determinants.
108. Roar Stenseth: THORACIC EPIDURAL ANALGESIA IN AORTOCORONARY BYPASS SURGERY.

109. Arild Faxvaag: STUDIES OF IMMUNE CELL FUNCTION *in mice infected with* MURINE RETROVIRUS.

1996

110. Svend Aakhus: NONINVASIVE COMPUTERIZED ASSESSMENT OF LEFT VENTRICULAR FUNCTION AND SYSTEMIC ARTERIAL PROPERTIES. Methodology and some clinical applications.
111. Klaus-Dieter Bolz: INTRAVASCULAR ULTRASONOGRAPHY.
112. Petter Aadahl: CARDIOVASCULAR EFFECTS OF THORACIC AORTIC CROSS-CLAMPING.
113. Sigurd Steinshamn: CYTOKINE MEDIATORS DURING GRANULOCYTOPENIC INFECTIONS.
114. Hans Stifoss-Hanssen: SEEKING MEANING OR HAPPINESS?
115. Anne Kvikstad: LIFE CHANGE EVENTS AND MARITAL STATUS IN RELATION TO RISK AND PROGNOSIS OF CANSER.
116. Torbjørn Grøntvedt: TREATMENT OF ACUTE AND CHRONIC ANTERIOR CRUCIATE LIGAMENT INJURIES. A clinical and biomechanical study.
117. Sigrid Hørven Wigers: CLINICAL STUDIES OF FIBROMYALGIA WITH FOCUS ON ETIOLOGY, TREATMENT AND OUTCOME.
118. Jan Schjøtt: MYOCARDIAL PROTECTION: Functional and Metabolic Characteristics of Two Endogenous Protective Principles.
119. Marit Martinussen: STUDIES OF INTESTINAL BLOOD FLOW AND ITS RELATION TO TRANSITIONAL CIRCULATORY ADAPATION IN NEWBORN INFANTS.
120. Tomm B. Müller: MAGNETIC RESONANCE IMAGING IN FOCAL CEREBRAL ISCHEMIA.
121. Rune Haaverstad: OEDEMA FORMATION OF THE LOWER EXTREMITIES.
122. Magne Børset: THE ROLE OF CYTOKINES IN MULTIPLE MYELOMA, WITH SPECIAL REFERENCE TO HEPATOCYTE GROWTH FACTOR.
123. Geir Smedslund: A THEORETICAL AND EMPIRICAL INVESTIGATION OF SMOKING, STRESS AND DISEASE: RESULTS FROM A POPULATION SURVEY.

1997

124. Torstein Vik: GROWTH, MORBIDITY, AND PSYCHOMOTOR DEVELOPMENT IN INFANTS WHO WERE GROWTH RETARDED *IN UTERO*.
125. Siri Forsmo: ASPECTS AND CONSEQUENCES OF OPPORTUNISTIC SCREENING FOR CERVICAL CANCER. Results based on data from three Norwegian counties.
126. Jon S. Skranes: CEREBRAL MRI AND NEURODEVELOPMENTAL OUTCOME IN VERY LOW BIRTH WEIGHT (VLBW) CHILDREN. A follow-up study of a geographically based year cohort of VLBW children at ages one and six years.
127. Knut Bjørnstad: COMPUTERIZED ECHOCARDIOGRAPHY FOR EVALUTION OF CORONARY ARTERY DISEASE.
128. Grethe Elisabeth Borchgrevink: DIAGNOSIS AND TREATMENT OF WHIPLASH/NECK SPRAIN INJURIES CAUSED BY CAR ACCIDENTS.
129. Tor Elsås: NEUROPEPTIDES AND NITRIC OXIDE SYNTHASE IN OCULAR AUTONOMIC AND SENSORY NERVES.
130. Rolf W. Gråwe: EPIDEMIOLOGICAL AND NEUROPSYCHOLOGICAL PERSPECTIVES ON SCHIZOPHRENIA.
131. Tonje Strømholm: CEREBRAL HAEMODYNAMICS DURING THORACIC AORTIC CROSSCLAMPING. An experimental study in pigs.

1998

132. Martinus Bråten: STUDIES ON SOME PROBLEMS REALTED TO INTRAMEDULLARY NAILING OF FEMORAL FRACTURES.
133. Ståle Nordgård: PROLIFERATIVE ACTIVITY AND DNA CONTENT AS PROGNOSTIC INDICATORS IN ADENOID CYSTIC CARCINOMA OF THE HEAD AND NECK.
134. Egil Lien: SOLUBLE RECEPTORS FOR **TNF** AND **LPS**: RELEASE PATTERN AND POSSIBLE SIGNIFICANCE IN DISEASE.
135. Marit Bjørgaas: HYPOGLYCAEMIA IN CHILDREN WITH DIABETES MELLITUS
136. Frank Skorpen: GENETIC AND FUNCTIONAL ANALYSES OF DNA REPAIR IN HUMAN CELLS.
137. Juan A. Pareja: SUNCT SYNDROME. ON THE CLINICAL PICTURE. ITS DISTINCTION FROM OTHER, SIMILAR HEADACHES.
138. Anders Angelsen: NEUROENDOCRINE CELLS IN HUMAN PROSTATIC CARCINOMAS AND THE PROSTATIC COMPLEX OF RAT, GUINEA PIG, CAT AND DOG.

139. Fabio Antonaci: CHRONIC PAROXYSMAL HEMICRANIA AND HEMICRANIA CONTINUA: TWO DIFFERENT ENTITIES?
140. Sven M. Carlsen: ENDOCRINE AND METABOLIC EFFECTS OF METFORMIN WITH SPECIAL EMPHASIS ON CARDIOVASCULAR RISK FACTORES.

1999

141. Terje A. Murberg: DEPRESSIVE SYMPTOMS AND COPING AMONG PATIENTS WITH CONGESTIVE HEART FAILURE.
142. Harm-Gerd Karl Blaas: THE EMBRYONIC EXAMINATION. Ultrasound studies on the development of the human embryo.
143. Noèmi Becser Andersen:THE CEPHALIC SENSORY NERVES IN UNILATERAL HEADACHES. Anatomical background and neurophysiological evaluation.
144. Eli-Janne Fiskerstrand: LASER TREATMENT OF PORT WINE STAINS. A study of the efficacy and limitations of the pulsed dye laser. Clinical and morfological analyses aimed at improving the therapeutic outcome.
145. Bård Kulseng: A STUDY OF ALGINATE CAPSULE PROPERTIES AND CYTOKINES IN RELATION TO INSULIN DEPENDENT DIABETES MELLITUS.
146. Terje Haug: STRUCTURE AND REGULATION OF THE HUMAN UNG GENE ENCODING URACIL-DNA GLYCOSYLASE.
147. Heidi Brurok: MANGANESE AND THE HEART. A Magic Metal with Diagnostic and Therapeutic Possibilites.
148. Agnes Kathrine Lie: DIAGNOSIS AND PREVALENCE OF HUMAN PAPILLOMAVIRUS INFECTION IN CERVICAL INTRAEPITELIAL NEOPLASIA. Relationship to Cell Cycle Regulatory Proteins and HLA DQBI Genes.
149. Ronald Mårvik: PHARMACOLOGICAL, PHYSIOLOGICAL AND PATHOPHYSIOLOGICAL STUDIES ON ISOLATED STOMACS.
150. Ketil Jarl Holen: THE ROLE OF ULTRASONOGRAPHY IN THE DIAGNOSIS AND TREATMENT OF HIP DYSPLASIA IN NEWBORNS.
151. Irene Hetlevik: THE ROLE OF CLINICAL GUIDELINES IN CARDIOVASCULAR RISK INTERVENTION IN GENERAL PRACTICE.
152. Katarina Tunòn: ULTRASOUND AND PREDICTION OF GESTATIONAL AGE.
153. Johannes Soma: INTERACTION BETWEEN THE LEFT VENTRICLE AND THE SYSTEMIC ARTERIES.
154. Arild Aamodt: DEVELOPMENT AND PRE-CLINICAL EVALUATION OF A CUSTOM-MADE FEMORAL STEM.
155. Agnar Tegnander: DIAGNOSIS AND FOLLOW-UP OF CHILDREN WITH SUSPECTED OR KNOWN HIP DYSPLASIA.
156. Bent Indredavik: STROKE UNIT TREATMENT: SHORT AND LONG-TERM EFFECTS
157. Jolanta Vanagaite Vingen: PHOTOPHOBIA AND PHONOPHOBIA IN PRIMARY HEADACHES

2000

158. Ola Dalsegg Sæther: PATHOPHYSIOLOGY DURING PROXIMAL AORTIC CROSS-CLAMPING
159. CLINICAL AND EXPERIMENTAL STUDIES
160. Christina Vogt Isaksen: PRENATAL ULTRASOUND AND POSTMORTEM FINDINGS – A TEN YEAR CORRELATIVE STUDY OF FETUSES AND INFANTS WITH DEVELOPMENTAL ANOMALIES.
161. Holger Seidel: HIGH-DOSE METHOTREXATE THERAPY IN CHILDREN WITH ACUTE LYMPHOCYTIC LEUKEMIA: DOSE, CONCENTRATION, AND EFFECT CONSIDERATIONS.
162. Stein Hallan: IMPLEMENTATION OF MODERN MEDICAL DECISION ANALYSIS INTO CLINICAL DIAGNOSIS AND TREATMENT.
163. Malcolm Sue-Chu: INVASIVE AND NON-INVASIVE STUDIES IN CROSS-COUNTRY SKIERS WITH ASTHMA-LIKE SYMPTOMS.
164. Ole-Lars Brekke: EFFECTS OF ANTIOXIDANTS AND FATTY ACIDS ON TUMOR NECROSIS FACTOR-INDUCED CYTOTOXICITY.
165. Jan Lundbom: AORTOCORONARY BYPASS SURGERY: CLINICAL ASPECTS, COST CONSIDERATIONS AND WORKING ABILITY.
166. John-Anker Zwart: LUMBAR NERVE ROOT COMPRESSION, BIOCHEMICAL AND NEUROPHYSIOLOGICAL ASPECTS.
167. Geir Falck: HYPEROSMOLALITY AND THE HEART.

URN:NBN:no-3463

168. Eirik Skogvoll: CARDIAC ARREST Incidence, Intervention and Outcome.
169. Dalius Bansevicius: SHOULDER-NECK REGION IN CERTAIN HEADACHES AND CHRONIC PAIN SYNDROMES.
170. Bettina Kinge: REFRACTIVE ERRORS AND BIOMETRIC CHANGES AMONG UNIVERSITY STUDENTS IN NORWAY.
171. Gunnar Qvigstad: CONSEQUENCES OF HYPERGASTRINEMIA IN MAN
172. Hanne Ellekjær: EPIDEMIOLOGICAL STUDIES OF STROKE IN A NORWEGIAN POPULATION. INCIDENCE, RISK FACTORS AND PROGNOSIS
173. Hilde Grimstad: VIOLENCE AGAINST WOMEN AND PREGNANCY OUTCOME.
174. Astrid Hjelde: SURFACE TENSION AND COMPLEMENT ACTIVATION: Factors influencing bubble formation and bubble effects after decompression.
175. Kjell A. Kvistad: MR IN BREAST CANCER – A CLINICAL STUDY.
176. Ivar Rossvoll: ELECTIVE ORTHOPAEDIC SURGERY IN A DEFINED POPULATION. Studies on demand, waiting time for treatment and incapacity for work.
177. Carina Seidel: PROGNOSTIC VALUE AND BIOLOGICAL EFFECTS OF HEPATOCYTE GROWTH FACTOR AND SYNDECAN-1 IN MULTIPLE MYELOMA.

2001

178. Alexander Wahba: THE INFLUENCE OF CARDIOPULMONARY BYPASS ON PLATELET FUNCTION AND BLOOD COAGULATION – DETERMINANTS AND CLINICAL CONSEQUENSES
179. Marcus Schmitt-Egenolf: THE RELEVANCE OF THE MAJOR hISTOCOMPATIBILITY COMPLEX FOR THE GENETICS OF PSORIASIS
180. Odrun Arna Gederaas: BIOLOGICAL MECHANISMS INVOLVED IN 5-AMINOLEVULINIC ACID BASED PHOTODYNAMIC THERAPY
181. Pål Richard Romundstad: CANCER INCIDENCE AMONG NORWEGIAN ALUMINIUM WORKERS
182. Henrik Hjorth-Hansen: NOVEL CYTOKINES IN GROWTH CONTROL AND BONE DISEASE OF MULTIPLE MYELOMA
183. Gunnar Morken: SEASONAL VARIATION OF HUMAN MOOD AND BEHAVIOUR
184. Bjørn Olav Haugen: MEASUREMENT OF CARDIAC OUTPUT AND STUDIES OF VELOCITY PROFILES IN AORTIC AND MITRAL FLOW USING TWO- AND THREE-DIMENSIONAL COLOUR FLOW IMAGING
185. Geir Bråthen: THE CLASSIFICATION AND CLINICAL DIAGNOSIS OF ALCOHOL-RELATED SEIZURES
186. Knut Ivar Aasarød: RENAL INVOLVEMENT IN INFLAMMATORY RHEUMATIC DISEASE. A Study of Renal Disease in Wegener's Granulomatosis and in Primary Sjögren's Syndrome
187. Trude Helen Flo: RESEPTORS INVOLVED IN CELL ACTIVATION BY DEFINED URONIC ACID POLYMERS AND BACTERIAL COMPONENTS
188. Bodil Kavli: HUMAN URACIL-DNA GLYCOSYLASES FROM THE UNG GENE: STRUCTRUAL BASIS FOR SUBSTRATE SPECIFICITY AND REPAIR
189. Liv Thommesen: MOLECULAR MECHANISMS INVOLVED IN TNF- AND GASTRIN-MEDIATED GENE REGULATION
190. Turid Lingaas Holmen: SMOKING AND HEALTH IN ADOLESCENCE; THE NORD-TRØNDELAG HEALTH STUDY, 1995-97
191. Øyvind Hjertner: MULTIPLE MYELOMA: INTERACTIONS BETWEEN MALIGNANT PLASMA CELLS AND THE BONE MICROENVIRONMENT
192. Asbjørn Støylen: STRAIN RATE IMAGING OF THE LEFT VENTRICLE BY ULTRASOUND. FEASIBILITY, CLINICAL VALIDATION AND PHYSIOLOGICAL ASPECTS
193. Kristian Midthjell: DIABETES IN ADULTS IN NORD-TRØNDELAG. PUBLIC HEALTH ASPECTS OF DIABETES MELLITUS IN A LARGE, NON-SELECTED NORWEGIAN POPULATION.
194. Guanglin Cui: FUNCTIONAL ASPECTS OF THE ECL CELL IN RODENTS
195. Ulrik Wisløff: CARDIAC EFFECTS OF AEROBIC ENDURANCE TRAINING: HYPERTROPHY, CONTRACTILITY AND CALCUIM HANDLING IN NORMAL AND FAILING HEART
196. Øyvind Halaas: MECHANISMS OF IMMUNOMODULATION AND CELL-MEDIATED CYTOTOXICITY INDUCED BY BACTERIAL PRODUCTS
197. Tore Amundsen: PERFUSION MR IMAGING IN THE DIAGNOSIS OF PULMONARY EMBOLISM

URN:NBN:no-3463

198. Nanna Kurtze: THE SIGNIFICANCE OF ANXIETY AND DEPRESSION IN FATIQUE AND PATTERNS OF PAIN AMONG INDIVIDUALS DIAGNOSED WITH FIBROMYALGIA: RELATIONS WITH QUALITY OF LIFE, FUNCTIONAL DISABILITY, LIFESTYLE, EMPLOYMENT STATUS, CO-MORBIDITY AND GENDER
199. Tom Ivar Lund Nilsen: PROSPECTIVE STUDIES OF CANCER RISK IN NORD-TRØNDELAG: THE HUNT STUDY. Associations with anthropometric, socioeconomic, and lifestyle risk factors
200. Asta Kristine Håberg: A NEW APPROACH TO THE STUDY OF MIDDLE CEREBRAL ARTERY OCCLUSION IN THE RAT USING MAGNETIC RESONANCE TECHNIQUES

2002

201. Knut Jørgen Arntzen: PREGNANCY AND CYTOKINES
202. Henrik Døllner: INFLAMMATORY MEDIATORS IN PERINATAL INFECTIONS
203. Asta Bye: LOW FAT, LOW LACTOSE DIET USED AS PROPHYLACTIC TREATMENT OF ACUTE INTESTINAL REACTIONS DURING PELVIC RADIOTHERAPY. A PROSPECTIVE RANDOMISED STUDY.
204. Sylvester Moyo: STUDIES ON STREPTOCOCCUS AGALACTIAE (GROUP B STREPTOCOCCUS) SURFACE-ANCHORED MARKERS WITH EMPHASIS ON STRAINS AND HUMAN SERA FROM ZIMBABWE.
205. Knut Hagen: HEAD-HUNT: THE EPIDEMIOLOGY OF HEADACHE IN NORD-TRØNDELAG
206. Li Lixin: ON THE REGULATION AND ROLE OF UNCOUPLING PROTEIN-2 IN INSULIN PRODUCING ß-CELLS
207. Anne Hildur Henriksen: SYMPTOMS OF ALLERGY AND ASTHMA VERSUS MARKERS OF LOWER AIRWAY INFLAMMATION AMONG ADOLESCENTS
208. Egil Andreas Fors: NON-MALIGNANT PAIN IN RELATION TO PSYCHOLOGICAL AND ENVIRONTENTAL FACTORS. EXPERIENTAL AND CLINICAL STUDES OF PAIN WITH FOCUS ON FIBROMYALGIA
209. Pål Klepstad: MORPHINE FOR CANCER PAIN
210. Ingunn Bakke: MECHANISMS AND CONSEQUENCES OF PEROXISOME PROLIFERATOR-INDUCED HYPERFUNCTION OF THE RAT GASTRIN PRODUCING CELL
211. Ingrid Susann Gribbestad: MAGNETIC RESONANCE IMAGING AND SPECTROSCOPY OF BREAST CANCER
212. Rønnaug Astri Ødegård: PREECLAMPSIA – MATERNAL RISK FACTORS AND FETAL GROWTH
213. Johan Haux: STUDIES ON CYTOTOXICITY INDUCED BY HUMAN NATURAL KILLER CELLS AND DIGITOXIN
214. Turid Suzanne Berg-Nielsen: PARENTING PRACTICES AND MENTALLY DISORDERED ADOLESCENTS
215. Astrid Rydning: BLOOD FLOW AS A PROTECTIVE FACTOR FOR THE STOMACH MUCOSA. AN EXPERIMENTAL STUDY ON THE ROLE OF MAST CELLS AND SENSORY AFFERENT NEURONS

2003

216. Jan Pål Loennechen: HEART FAILURE AFTER MYOCARDIAL INFARCTION. Regional Differences, Myocyte Function, Gene Expression, and Response to Cariporide, Losartan, and Exercise Training.
217. Elisabeth Qvigstad: EFFECTS OF FATTY ACIDS AND OVER-STIMULATION ON INSULIN SECRETION IN MAN
218. Arne Åsberg: EPIDEMIOLOGICAL STUDIES IN HEREDITARY HEMOCHROMATOSIS: PREVALENCE, MORBIDITY AND BENEFIT OF SCREENING.
219. Johan Fredrik Skomsvoll: REPRODUCTIVE OUTCOME IN WOMEN WITH RHEUMATIC DISEASE. A population registry based study of the effects of inflammatory rheumatic disease and connective tissue disease on reproductive outcome in Norwegian women in 1967-1995.
220. Siv Mørkved: URINARY INCONTINENCE DURING PREGNANCY AND AFTER DELIVERY: EFFECT OF PELVIC FLOOR MUSCLE TRAINING IN PREVENTION AND TREATMENT
221. Marit S. Jordhøy: THE IMPACT OF COMPREHENSIVE PALLIATIVE CARE
222. Tom Christian Martinsen: HYPERGASTRINEMIA AND HYPOACIDITY IN RODENTS – CAUSES AND CONSEQUENCES
223. Solveig Tingulstad: CENTRALIZATION OF PRIMARY SURGERY FOR OVARAIN CANCER. FEASIBILITY AND IMPACT ON SURVIVAL

URN:NBN:no-3463

224. Haytham Eloqayli: METABOLIC CHANGES IN THE BRAIN CAUSED BY EPILEPTIC SEIZURES
225. Torunn Bruland: STUDIES OF EARLY RETROVIRUS-HOST INTERACTIONS – VIRAL DETERMINANTS FOR PATHOGENESIS AND THE INFLUENCE OF SEX ON THE SUSCEPTIBILITY TO FRIEND MURINE LEUKAEMIA VIRUS INFECTION
226. Torstein Hole: DOPPLER ECHOCARDIOGRAPHIC EVALUATION OF LEFT VENTRICULAR FUNCTION IN PATIENTS WITH ACUTE MYOCARDIAL INFARCTION
227. Vibeke Nossum: THE EFFECT OF VASCULAR BUBBLES ON ENDOTHELIAL FUNCTION
228. Sigurd Fasting: ROUTINE BASED RECORDING OF ADVERSE EVENTS DURING ANAESTHESIA – APPLICATION IN QUALITY IMPROVEMENT AND SAFETY
229. Solfrid Romundstad: EPIDEMIOLOGICAL STUDIES OF MICROALBUMINURIA. THE NORD-TRØNDELAG HEALTH STUDY 1995-97 (HUNT 2)
230. Geir Torheim: PROCESSING OF DYNAMIC DATA SETS IN MAGNETIC RESONANCE IMAGING
231. Catrine Ahlén: SKIN INFECTIONS IN OCCUPATIONAL SATURATION DIVERS IN THE NORTH SEA AND THE IMPACT OF THE ENVIRONMENT
232. Arnulf Langhammer: RESPIRATORY SYMPTOMS, LUNG FUNCTION AND BONE MINERAL DENSITY IN A COMPREHENSIVE POPULATION SURVEY. THE NORD-TRØNDELAG HEALTH STUDY 1995-97. THE BRONCHIAL OBSTRUCTION IN NORD-TRØNDELAG STUDY
233. Einar Kjelsås: EATING DISORDERS AND PHYSICAL ACTIVITY IN NON-CLINICAL SAMPLES
234. Arne Wibe: RECTAL CANCER TREATMENT IN NORWAY – STANDARDISATION OF SURGERY AND QUALITY ASSURANCE

2004

235. Eivind Witsø: BONE GRAFT AS AN ANTIBIOTIC CARRIER
236. Anne Mari Sund: DEVELOPMENT OF DEPRESSIVE SYMPTOMS IN EARLY ADOLESCENCE
237. Hallvard Lærum: EVALUATION OF ELECTRONIC MEDICAL RECORDS – A CLINICAL TASK PERSPECTIVE
238. Gustav Mikkelsen: ACCESSIBILITY OF INFORMATION IN ELECTRONIC PATIENT RECORDS; AN EVALUATION OF THE ROLE OF DATA QUALITY
239. Steinar Krokstad: SOCIOECONOMIC INEQUALITIES IN HEALTH AND DISABILITY. SOCIAL EPIDEMIOLOGY IN THE NORD-TRØNDELAG HEALTH STUDY (HUNT), NORWAY
240. Arne Kristian Myhre: NORMAL VARIATION IN ANOGENITAL ANATOMY AND MICROBIOLOGY IN NON-ABUSED PRESCHOOL CHILDREN
241. Ingunn Dybedal: NEGATIVE REGULATORS OF HEMATOPOIETEC STEM AND PROGENITOR CELLS
242. Beathe Sitter: TISSUE CHARACTERIZATION BY HIGH RESOLUTION MAGIC ANGLE SPINNING MR SPECTROSCOPY

URN:NBN:no-3463